Numerical simulations of sand dune morphodynamics and their application to the Mu Us Dune Field, China

By

Fei Ma

A dissertation submitted in partial fulfillment of
the requirements for the degree of
Doctor of Philosophy
(Geography)
at the
UNIVERSITY OF WISCONSIN-MADISON
2017

Date of final oral examination: 12/05/2017

The dissertation is approved by the following members of the Final Oral Committee:

Joseph A. Mason, Professor, Geography (Advisor)
John W. (Jack) Williams, Professor, Geography
James Burt, Professor, Geography
Erika Marín-Spiotta, Associate Professor, Geography
Mutlu Ozdogan, Associate Professor, Forestry and Environmental Studies

Abstract

Semi-arid landscapes are heavily influenced by climate change and human activities. Sand dunes in the Mu Us region, China experienced rapid stabilization during the past few decades, which is postulated to be a response to recent climate change (Xu et al., 2015) and land use change (Mason et al., 2008). With the information extracted from high-resolution Google Earth imagery and ASTER GDEM data and machine-learning models, I evaluated the relative importance of multiple environmental and anthropogenic variables for the recent changes in dune activity and vegetation cover. Spatial variation in climate variables contributed little, while elevation, human activities and vegetation spatial distribution played significant roles in both dune migration rate and vegetation cover change rate. To further visualize dune morphodynamic response to external forcings over time, I modified a Cellular Automaton (CA) model (Werner, 1995) and fit it to the Mu Us dune field by tuning model parameters (downwind transport jump unit, slab thickness, deposition probability, and erosion probability) . The model produced realistic barchans dune forms with only wind processes included, while parabolic dune forms were simulated with a combination of wind and anchoring vegetation. Through adjusting erosion probability (p_e), the model is capable of testing various wind and vegetation growth scenarios. With a linearly declining p_e, the vegetation integrated CA model was used to simulate the increase in precipitation in the late 1990s, and it produced stabilized parabolic dune forms that closely resemble those observed in the field. The successful simulation of realistic dune form changes also proves the CA model to be an effective research and educational tool for exploring interactions among climate, geomorphology and vegetation and predicting future trends of dune activity.

Acknowledgements

I would like to extend my sincere gratitude to my advisor, Professor Joe Mason, for his continued support for my PhD study, his guidance through the most challenging stages of this research, and his understanding, patience and motivation during the most difficult times of my graduate school. I grew significantly as a researcher as well as a person under his direction. I will miss sharing laughter and witty conversations with him in our geoscience field trips.

Besides my advisor, I would also like to thank the rest of my committee: Professor Jim Burt, Professor Erika Marín-Spiotta, Professor Mutlu Ozdogan, and Professor Jack Williams. I feel lucky to have received insightful comments and suggestions from these top notch researchers, and appreciate their hard questions which encourage me to think deeper and continue improving my research.

A very special thanks to Dr. Zhiwei Xu, a great friend from college and the most reliable and knowledgeable guide during my field work in Mu Us Dune Field in 2014. Without his help I probably would not have been able to find my way out of Mu Us!

I'm also grateful to the Department of Geography for funding this research through both the Leopold Geomorphology Graduate Research Award and the Trewartha Awards. The staff members provided unfailing assistance and support in my graduate course work and through the completion of this Phd research. I also appreciate the help and encouragement from members of the Mason lab (Kristy, Karen, Henry, Laura, Chase, and Mengyu) and colleagues from the Geography Department (Yue, Fei, Jing, Emily, Samuel).

Last but not least, I would like to thank my family- my husband Matt for being my biggest cheerleader and supporter in the past few years of dissertation writing, and my parents for always being there for me and interested in learning about my research (although they probably still have

not grasped what it is all about!). Thanks also to Robert, our son who will be born in a few weeks, for staying put until I finish my work; and our cats, Ozzie and Crash, for being great writing companions.

Contents

Abstract i
Acknowledgements ii
Introduction 1
Background 4
Climate, vegetation and sand dune activity 4
Cellular Automaton (CA) models and their application to aeolian systems 6
Research area and study sites 8
Climate data 10
Human activities 12
Chapter 1. Vegetation spatial patterns 14
Image processing 15
1.1. Study areas 16
1.2. Vegetation cover and elevation 22
1.3. Patchiness of vegetation 26
1.4. Nearest neighbor effect (Spatial autocorrelations) 28
Conclusions and Discussion 32
Chapter 2. Dune activity and regional vegetation change in response to environmental variables 34
1. Feature description and PCA analysis 36
Feature description 36
PCA analysis 39
2. Regression on dune down-wind migration rate 42
3. Regression on vegetation cover change rate 49
Conclusions and Discussion 55
Chapter 3. Cellular Automaton (CA) dune formation model 58
1. Model description 59
2. Model parameters 61
3. Sand flux 63
4. Experiments and Results 65
a. Original settings 66
b. Test model parameters 69
c. Modeling wind speed change in the Mu Us dune field 78

5. Web application 80
Conclusions and Discussion 81
Chapter 4. Vegetation integrated dune stabilization model 83
1. Current and proposed vegetation-integrated CA models 85
a. Elevation-based vegetation model 85
b. Growth function model 86
c. Dune slice-height model 92
2. Testing hypotheses on factors influencing vegetation stabilization of the dunes 101
a. Nearest neighbor effect 101
b. Effectiveness of windbreaking grids on top of dunes 103
Conclusions and Discussion 104
Conclusions 107
Reference 110

Introduction

Aeolian landforms and dune fields are distributed extensively across Earth's surface. Active (migrating) dunes pose challenges for infrastructure and farmland, and often serve as sand sources for dust storms (Qian et al., 2002). Arid ecosystems are particularly sensitive to global climate change (Schröter, D. et al, 2005), and past environmental change in dryland dune fields can often be linked to climate variation. For example, most Holocene dune activity in the central Great Plains is reported to coincide with frequent and severe drought (Miao et al., 2007). Some present dune fields are still responding to climate shifts from the past few hundred years (e.g., Hugenholtz and Wolfe 2005). GCM-based experiments suggest that significant dune reactivation driven by climate change can happen in three Kalahari dunefields by 2039 (Thomas et al., 2005). Understanding how dune activity responds to climate change can provide guidelines for socioeconomic adaptations.

Human activities also significantly affect dune activity. For example, the adoption of improved agricultural practices played a crucial role in reducing wind erosion activity and dust emissions on the Southern High Plains from 1961 to 2001 (Stout and Lee, 2003). A significant decrease in wind power in three dune fields in northern China produced limited response in terms of changes in dune mobility, which can be explained by human activities such as intense grazing (Mason et al., 2008). A bare, active sand dune in Israel was converted to a shrub-covered parabolic dune over the last 60 years due to changes in land use (Ardon et al., 2009). Historical dune activity in the Great Plains has been driven by a combined effect of both drought and land use practices (Muhs and Maat, 1993; Muhs S. A. Wolfe, 1999).

The availability of high-resolution remote sensing imagery has enhanced a range of geomorphic research, such as broad-scale analyses of dune patterns (Kocurek and Ewing, 2005) and migration rates (Yao et al., 2007). Availability of increasingly high-resolution elevation data, first through

sources such as ASTER GDEM and more recently through collection of LiDAR data, has improved three-dimensional analyses of the topographic variability of sand dunes (e.g. Hugenholtz and Barchyn, 2010). With information extracted from remote sensing images and DEM data, we can compare the relative importance of climate change and human forcings in recent dune activity, and identify the leading driver for changing activity in specific cases.

Empirical studies have shown that dune activity is controlled by wind power and vegetation cover: wind power determines sand transport capacity, while vegetation protects the sand surface from direct wind erosion and traps sand particles, thereby reducing wind velocity and sand available for transport (Yizhaq et al., 2007). While the presence of vegetation effectively reduces sand available for transport, sand movement and dune topography also affect vegetation growth and distribution (Brown, 1997; Lancaster and Baas, 1998; Mahowald et al., 2008). The complex feedback and interplay between vegetation growth and sand transport can drive the dune system between active and stabilized states; therefore the investigation of dune forms must take biologic processes into consideration (Hugenholtz and Wolfe, 2005).

Earlier quantitative studies of dunes focused on the movement of individual grains (e.g. Bagnold, 1941), or concentrated on measurements of wind flow and sand flux across single dunes (summarized by Knott and Warren, 1981). However, Werner (1995) developed a cellular automaton (CA) model that successfully simulates the morphology of four types of sand dunes without reference to small-scale grain-level processes. Despite the flexibility and potential of the CA model to be expanded to incorporate additional processes and questions, few studies have used it to test dune responses to climate change and human activities. Following Werner (1995), a series of subsequent studies (e.g. Baas, 2002; Nield and Baas, 2007; Pelletier et al., 2009) simulate the transition from barchan to parabolic dunes with the presence of vegetation. However, challenges remain with these models in simulating dune morphology changes in an actual dune field, and particularly in realistically representing effects of climate change and vegetation growth.

In this research, I aim to answer these questions:

1. **What is the relative magnitude of dune field response to climate and human activities?**

Chapter 1 focuses on spatial patterns of vegetation in the Mu Us dune field. It starts with a description of the study areas through Google Earth images and ASTER GDEMS, followed by a correlation analysis between vegetation cover and elevation. I also explore how vegetation patchiness relates with dune activity and spatial autocorrelation of vegetation cover. Chapter 2 builds on Chapter 1 and constructs machine learning models in order to predict the rates of recent (last 8-14 years) dune migration and vegetation cover change. The explanatory variables include climate, human and environmental aspects. Using machine learning models, the most important features in explaining response variables are selected: elevation, vegetation distribution, and human related variables.

2. **How do dune forms respond to climate change (especially wind strength)?**

In Chapter 3, I build a CA model following Werner (1995) and fit it to the Mu Us dune field. A range of model parameters are then modified to observe the response of dune morphology. Erosion probability is chosen to represent effects of changing wind speed.

3. **How do dune forms respond to vegetation growth? Can the recent stabilization and dune form changes in the Mu Us dune field be reproduced by a CA model? Can such a model be modified to test hypotheses on causes of recent dune stabilization?**

In Chapter 4, I propose a new model that adapts the Werner (1995) model and simulates the stabilization process of barchan dunes with the presence of vegetation. Verified by GE images and information presented in Chapter 1 and 2, the model produces realistic parabolic forms, and can be adjusted to simulate different scenarios, including the recent stabilization of the Mu Us dune field.

Background

Climate, vegetation and sand dune activity

Dune activity is often used as a "geo-indicator" of environmental changes. In southern Africa, for example, dune fields are likely to experience significant reactivation as a consequence of 21st century climate change (Thomas and Leason, 2005). Wind speed and precipitation are the main climate drivers for sediment transport and vegetation growth in dune stabilization and activation processes (Lancaster, 1988a; Hugenholtz and Wolfe, 2005a, 2005b; Tsoar, 2005; Yizhaq et al., 2007, 2009). For example, Lancaster (1988a) found that sand transport capacity is proportional to wind power (function of velocity cubed), and sand availability for transport is inversely proportional to vegetation cover, which is sensitive to precipitation. Past episodes of dune activity in Nebraska Sand Hills in late Holocene is correlated with dry conditions (Mason et al., 2004). Hugenholtz and Wolfe (2005) suggested that recent dune stabilization in the Canadian prairies is significantly correlated with decadal variations in moisture level and annual wind speed.

A popular index describing potential sand transport is Drift Potential (DP). DP is defined based on wind power above the threshold for entrainment (Fryberger and Dean, 1979):

$$DP = U^2(U-U_t)*t,$$

where U is average wind velocity at 10m height, U_t is threshold wind velocity, and t is the percentage of time wind in a particular velocity blew, as tabulated in a wind summary or calculated from actual wind measurements. DP is a scalar calculated using winds from all directions, and its units are conventionally given as vector units (VU, terminology of Fryberger and Dean, 1979). The DP for each wind rose segment can also be calculated, and used to compute a total vector, the resultant drift potential (RDP), with a direction (RDD, resultant drift direction) that indicates the net trend of sand drift and a magnitude indicating potential net drift in that direction. RDP/DP

(ratio of the magnitudes) is often used as an index for the directional variability of the wind drift. DP is often integrated in models to predict dune activities. For example, Yizhaq et al. (2007) proposed a model in which DP is used as the predominant control of dune mobility.

Vegetation also plays a critical rule in dune stabilization: it extracts momentum from the air flow, and increases the threshold shear velocity that is required to initiate and sustain transport (Wolfe and Nickling, 1993; Lancaster and Baas, 1998; Kuriyama et al., 2005), thereby reducing sand surface erosion. Recent studies on coastal dunes show that while sand supply determines dune formation time, dune size is strongly influenced by vegetation (Durán and Moore, 2013). In fact, vegetation cover change resulting from different grazing practices can sometimes have even more significant effects on dune activities than climate (Wang et al., 2006; Mason et al., 2008). Despite their importance in understanding the dune activation and stabilization processes, however, the surface characteristics of partly vegetated dunes remain poorly parameterized (Hugenholtz et al., 2012).

The mobility index M (Lancaster, 1988a) integrates both wind and vegetation factors, and is often used to predict dune mobility change in response to climate variations:

$$M = W/(P:PET)$$

where W is the percent of time wind is above the threshold velocity for sand transport, and P:PET is the ratio of precipitation to potential evapotranspiration, an index of moisture availability for plants. Lancaster's index M has been successfully applied in a wide range of environments (e.g. Muhs and Maat, 1993; Lancaster and Helm, 2000). However, the active state of some sand dunes is not consistent with this index: either these dunes exhibit higher levels of activity than is predicted by Lancaster's index M (Muhs S. A. Wolfe, 1999), or their activity responds to reduced M after a lag of years to centuries (Hugenholtz and Wolfe, 2005b; Mason et al., 2008). In particular, P:PET only explains a small portion of the decrease in active dune areas in Canadian prairies in the past several

decades; the dune response is actually superimposed on a longer-term trend towards stabilization since the 1700s. (Hugenholtz and Wolfe, 2005b). It is also common to find both active and fully stabilized dunes coexisting in the same small area where M value is essentially the same (Yizhaq et al., 2007). Across several dune fields of Northern China, both activation and stabilization were observed in different areas, though all these areas were affected by a wind power decrease since the 1970s, while effective moisture remained approximately the same (Mason et al., 2008).

The heterogeneity of dune field activity under the same climate regime suggests that non-climate related local factors, such as human activities, distance to ground water, etc. can also affect dune stabilization processes. These factors' relative importance as controls of dune activity in comparison to climate and vegetation cover is still poorly understood for most dune fields.

Cellular Automaton (CA) models and their application to aeolian systems

Given the observational and computational limitations, it has been a longstanding challenge to quantitatively interpret and model processes of dune field evolution over space and time. Many dune fields exhibit regular patterns, indicating that they may have evolved through a process of self-organization (Werner, 1995; Kocurek and Ewing, 2005). As far as applications to natural systems are concerned, stochastic rules often provide a better analogy to the system than deterministic ones, given that nonlinear complexity is a characteristic of real-world landscapes (Phillips, 2003). Moreover, compared with continuum models (representing flowing air and mobile sand as continuous materials, e.g. Duran and Herrmann, 2006; Yizhaq et al., 2007, 2009), discrete CA models (e.g. Werner, 1995; Baas, 2002; Nield and Baas, 2007) can more easily incorporate ecological and geomorphological aspects (Fonstad, 2006).

CA models have been developed to simulate self-organization of active (unvegetated) dunes (Werner, 1995) as well as vegetated ones (e.g. Baas, 2002; Nield and Baas, 2007). Through random

entrainment, the Werner (1995) model first generates local relief from a flat bed covered with a layer of sand, and randomly selects a cell where sand is to be picked up by wind (eroded). In the deposition step, the dune topography (dune height, spacing, slope, etc.) is enhanced by a feedback mechanism through shadow zones downwind of each developing dune and avalanching when dune slopes exceed the angle of repose (30°). Werner's CA dune model (1995) is the foundation for a series of publications; for example, addition of vegetation (e.g., Nield and Baas, 2007; Pelletier, 2009; Baas and Nield, 2010), shear stress parameterizations (e.g., Narteau et al., 2009), wind tunnel validation with ripples (Hatano et al., 2004), bedform dynamics models (e.g., Werner and Kocurek, 1999), and exploration of dune field boundary conditions (Ewing and Kocurek, 2010), etc. The model is flexible and can represent any spatial or temporal dimension by redefinition of cell size and iteration duration (Nield and Baas, 2007).

These models represent a major advance in understanding dune morphodynamics, allowing for exploration of more complex relationships between climate and dune activities than is assumed when simple indicators such as P:PET and M are used. These CA models do not require complex airflow or sediment transport dynamics, yet successfully reproduce barchan, crescent, and linear dune forms. However, more work is needed to test whether these models can be useful interpretive and predictive tools for real dune landscapes with the presence of vegetation. Baas (2002) employed 'vegetation growth functions' to simulate vegetation response to burial but such functions are created by trial and error; Pelletier et al. (2009) used elevation to characterize vegetation distribution on dunes, yet dune forms generated by their model are somewhat different from those observed in the field.

Black and white aerial photographs have long been used to discriminate vegetation-covered and bare dune surfaces (e.g. Anthonsen et al., 1996; Gaylord and Stetler, 1994; Tsoar and Blumberg, 2002). Researchers often convert these photos to grey scale digital images before classification and analysis (Xu et al., 2015). In this study, high resolution Google Earth imagery is obtained and

converted to gray scale to analyze dune form changes in the stabilization process. Relative brightness (digital numbers) can reflect the surface conditions: high and low Digital Number (DN) values correspond to bare sand and vegetation respectively.

The increasing availability of high-resolution digital imagery and topographic data also enables efforts to characterize and quantify changes in dune morphology and verify numerical models. For example, Anthonsen et al. (1996) converted a series of hardcopy topographic maps (1887-1977) and aerial photos (1945-1992) into digital data to measure changes in vegetation cover as well as sand erosion and deposition on dunes. Xu et al. (2015) used high-resolution Google Earth images to examine trends and morphology changes of dune stabilization in the Mu Us dune field. Barchyn and Hugenholtz (2015) tested their hypothesis of dune field activity using multi-temporal topographic images, and estimated the relation between slipface deposition rates and vegetation deposition tolerance in stabilizing dunes. These advances in the application of imaging technologies make it possible not only to use actual dune field morphology to validate modeling efforts, but also to construct models using features extracted from these images. In this research, key non-climate related features (e.g. vegetation distribution, vegetation cover percentage, etc.) will be extracted from Google Earth satellite images for data analysis (Chapter 1 and 2) and for model validations (Chapter 3 and 4).

Research area and study sites

The Mu Us dune field is located in semi-arid north-central China. On average, dunes moved 1.3-4.7 meters per year in this region over the past few decades (Xu et al., 2015). Stations near the Mu Us dunes indicate a range of mean annual precipitation of 260-450mm, decreasing from southeast to northwest; and mean annual temperature of 6-9°C (Mason et al., 2008). An elevation map of Mu Us

dune field was generated using ASTER GDEM data with a spatial resolution of 30m by 27m. Elevation is higher in the NW of the dune field than the SE (Figure 1).

Many parts of the Mu Us dune field experienced rapid stabilization during 1980-2000, in some cases since the 1970s, possibly because of the combined effect of climate change (especially decreased wind strength) and land use change (Mason et al., 2008; Xu et al., 2015). A long-term trend of stabilization started in some marginal regions since the 1950s, and the trend became more evident since the 1970s (Mason et al., 2008; Runnström, 2003; Wang et al., 2005; Wu and Ci, 2002; Xu et al., 2015). Xu et al. (2015) described changes in vegetation cover and dune morphology in this area using high-resolution Google Earth images, and proposed conceptual models of vegetated dune morphodynamics during stabilization.

The ongoing stabilization of the Mu Us dune field, especially rapid since 1990, provides an opportunity to test the machine learning methods and CA model approach in simulating changes in dune forms in response to climate change and human activities. Knowledge on how dunes respond to trajectories of climate variables and land use will be valuable in assessing environmental and socioeconomic impacts from global warming and human activities in arid regions.

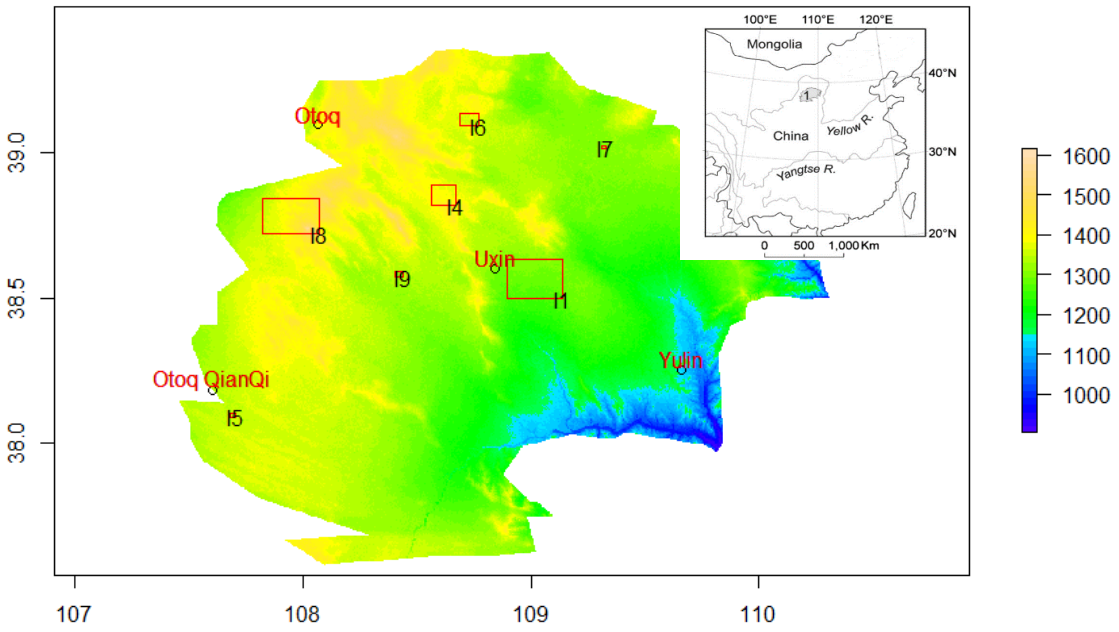

Figure 1 DEM of Mu Us dune field; Inset: location of MU Us (labeled as '1') in the map (adapted from Mason et al., 2008)

In summer 2014, I did reconnaissance field work in the Mu Us dune field to observe dune forms and vegetation species in different areas of the field. Seven sites were selected based on availability and quality of historical satellite images from Google Earth (Figure 1). Photos from the field work were combined with the satellite images to get a better understanding of vegetation cover and spatial distribution.

Climate data

Climate data for 1991 to 2012 from five weather stations was retrieved from the Global Summary of the Day dataset provided by the U.S. National Climatic Data Center (NCDC) (https://www.ncdc.noaa.gov/). Annual precipitation, mean temperature and potential evapotranspiration were calculated following Thornthwaite (1948). Smooth curves were fitted to data points using the LOESS method (Local Polynomial Regression Fitting) (Figure 2).

Dune migration follows the dominant wind direction, from northwest to southeast. Here I used 6 m/s at 10 m (following Fryberger and Dean, 1979) as the threshold for sand movement, with the result expressed in Vector Units (VU). Through the last two decades, DP has been gradually decreasing in the Mu Us region (Figure 2). A severe drought occurred in 1999 as reflected by low effective moisture (P:PET), accompanied by a low precipitation and high temperature (Figure 2).

In the Mu Us dune field, while stabilization began earlier in some areas, the general trend toward greater stability only became apparent after the year 2000, well after most of the decrease in wind power during the 1980s (Xu et al., 2015). It is possible that a lag exists between the climate and dune response; and Mu Us desert is sooner to respond compared with other dune fields in northern China (Mason et al., 2008). Climate data is integrated into multivariate models simulating the spatial variation of dune migration rate and vegetation spatial cover change rate (Chapter 2). To simulate the time required for dune stabilization and to understand how wind drift affects dune activities, a CA model will be developed and verified using data from Mu Us dune field (Chapter 3) and expanded to test vegetation effects (Chapter 4).

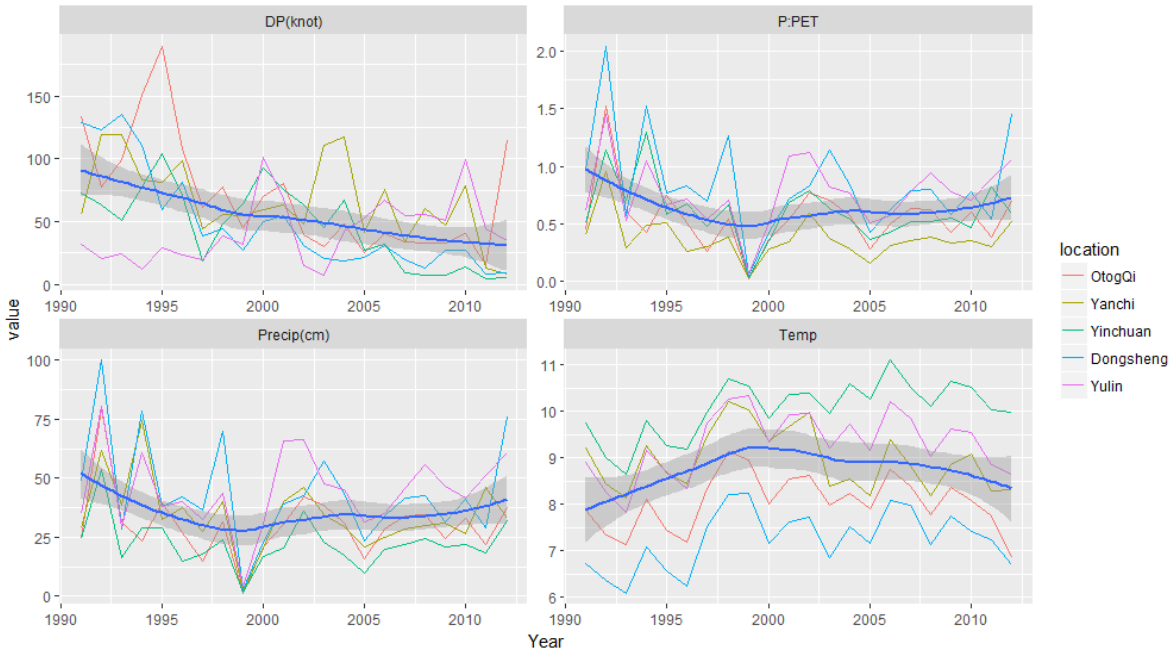

Figure 2 Climate of Mu Us Dune Field in the past 20 years

Each climate data point is the average value over a year. The gray ribbons with blue lines in the middle are the smoothed curves for the actual values of climate variables to show the general trends with time

Human activities

According to Mason et al. (2008) and Xu et al. (2015), while reduced wind strength is likely the most significant contributor to the recent widespread stabilization in the Mu Us dune field, changes in land use could also have favored stabilization in some areas. In the past few decades, the Mu Us dune field saw one of the most extensive efforts in dune stabilization in the world. Dune fixation efforts usually take place in interdune areas near small villages or towns, places where dune migration can threaten nearby houses or structures. Low flat interdune areas are preferred for artificial stabilization efforts because of their organic-rich soil, thick grass and easy-to-access shallow groundwater (Xu et al., 2015). "Checkerboards" of straw or sticks, or rows of vegetation (such as *Caragana microphylla*, *Sabina vulgaris* and *Artemisia ordosica*), are often used to stabilize the dunes through increasing surface roughness and decreasing sand transport (Xu et al., 2015).

These artificial stabilization methods proved to be very effective: some dunes were fixed immediately with their morphology “frozen” in-situ.

Aside from artificial stabilization, livestock grazing is another major form of human activity in Mu Us dune field. It has been strictly regulated over the past few decades. Over-grazing is banned and heavily penalized, and nomadic pastoralism is encouraged with government incentives (based on personal discussion with local herders). Active grazing was only observed in the southwest area of the dune field based on observations made in summer 2014. Given that destruction of the vegetation canopy by grazing can result in a significant increase in the near-surface wind velocity (Wiggs et al., 1994), these vegetation preservation measures further help with dune stabilization. The grazing impact on dune stabilization can be at least partly reflected by distance to and size of nearby villages or farmland. Together with density of artificial wind-breaking ‘grids’ of shrubs or vertical sticks, they are listed as ‘human’ factors in the machine learning model in Chapter 2. The location effect of these grids on barchan dunes will be tested using the CA model in Chapter 4.

Chapter 1. Vegetation spatial patterns

Vegetation spatial patterns and how they change in response to environmental conditions provide important information for modeling dune activity. Past research showed that vegetation cover has more influence on dune activity than wind speed (Muhs and Maat, 1993; Muhs et al., 1995; Hugenholtz and Wolfe, 2005b). Dune responses to vegetation can also be very fast. For example, the height of dunes at Jockey Ridge, North Carolina, went from increasing to decreasing soon after an increase in interdune vegetation density caused by human activities (Mitasova et al., 2005).

Vegetation distribution on dunes is affected by multiple factors, amongst which climate and human disturbance are the most obvious. However, elevation often has an inverse relationship with vegetation cover (Pelletier et al., 2009; Xu et al., 2015), because lower areas are closer to water table, or experience less wind erosion compared with higher elevations. If this inverse relationship with elevation is present in the Mu Us dune field, it should be incorporated into modeling of dunes, if possible.

Using a vegetation integrated CA model, Kéfi et al. (2007) found that vegetation patch sizes and their count can be indicative of dune activity. They follow an inverse power law relationship in a stable dune field, which can be explained by local positive interactions such as seed dispersal and local facilitation. Under disturbance such as overgrazing, Kéfi et al. found that vegetation patches and their count diverge from this relationship. This kind of neighborhood effect also could be taken into consideration when constructing a dune morphology model with vegetation; however, it is important to test whether the patch size-count relationship identified by Kéfi is associated with dune stability in the Mu Us study area.

In this chapter, I aim to quantitatively describe current vegetation spatial patterns and dune activity and conduct simple univariate analysis, to lay the groundwork for modeling and predictions on change in vegetation distribution and dune activity with time in upcoming chapters. As part of this analysis, relationships between elevation and vegetation cover are investigated, along with vegetation patchiness. I used Google Earth images to quantitatively assess vegetation spatial patterns in the Mu Us dune field, and obtained data that will be used to assist these modeling efforts.

This chapter starts with a description of vegetation cover and dune activity in each study area (Section 1.1). I sampled 1000 random sites in each area and modeled the relationship between vegetation cover and elevation using linear regression (Section 1.2). Relationships between size of vegetation patches and their count is explored in Section 1.3. Variograms are then generated to analyze vegetation spatial autocorrelation and its directional effect (Section 1.4). This analysis was supplemented with field observations.

Image processing

To study the change in vegetation cover, I obtained pairs of Google Earth images for seven study sites, each pair ranging from 7 to 10 years apart. These images were taken in summer months, which eliminates the noise caused by snow. Due to the intermittent availability of cloudless satellite data, these areas are not of the same size; yet they are distributed across the entire Mu Us dune field. To prepare these images for analysis, I converted them to grayscale and adjusted their brightness, then performed georeferencing.

These images were converted to grayscale through the 'Luma' method, which uses a linear function on RGB components to approximate luminance. Specifically, the new DN value is calculated by

$$DN = .3*Red + .59*Green +. 11*Blue$$

Where 'Red', 'Green' and 'Blue' refer to values of corresponding bands. The brightness of a pair of images was then adjusted by setting their controlled point digital number to the same value using the curve tool in the GIMP software. Specifically, a new maximum DN value (DN_{max}) was calculated based on DN values of control points from a pair of images (B1 and B2) as below:

$$DN_{max} = (256 * (B1 + 1))/(B2 + 1) - 1$$

The new maximum DN value for image 2 was then reset as DN_{max} instead of 255.

Georeferencing of each image was performed by referring to ground control points using Google Earth (fixed local features such as road intersections, houses, etc.).

Misclassification of large dunes can be caused by varied spatial illumination on complex dune surfaces. As a result, it is difficult to decide whether the difference in brightness is caused by topography or illumination. Levin et al. (2004) showed that one can separate slope and aspect of sand dunes from shading using two Landsat images with different sun zenith and azimuth angles (one image acquired in winter and the other in summer, for example). Since Google Earth images used in the study are obtained from summer and with limited shadows, the spatial illumination problem is neglected, which may result in some misclassification of vegetation as shadows, or vice versa.

1.1. Study areas

Area I1 is located near the town of Uxin and has experienced significant vegetation growth from 1999 to 2010 (negative change in DN predominates over positive change). Many dunes in this area have formed or are forming parabolic shapes and starting to stabilize (Figure 3a). Site I4 also went through significant re-vegetation and stabilization.

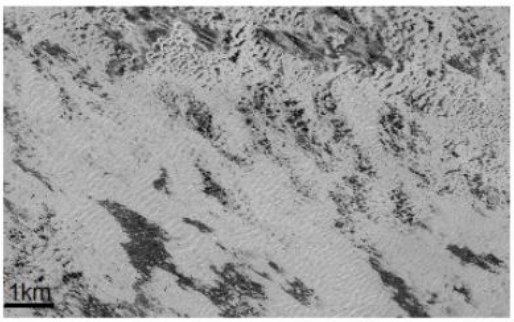

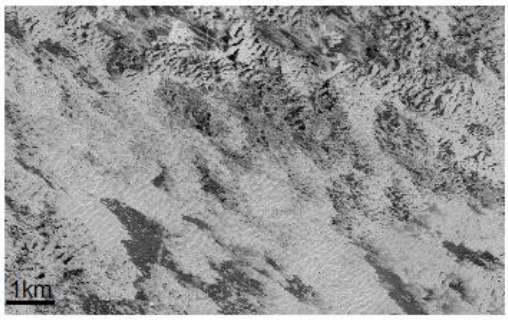

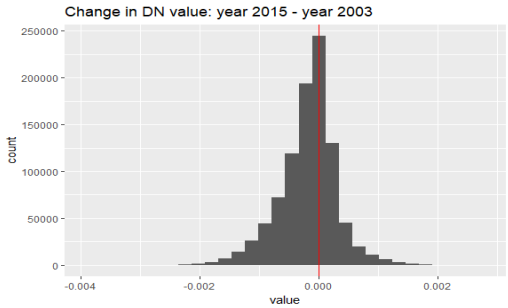

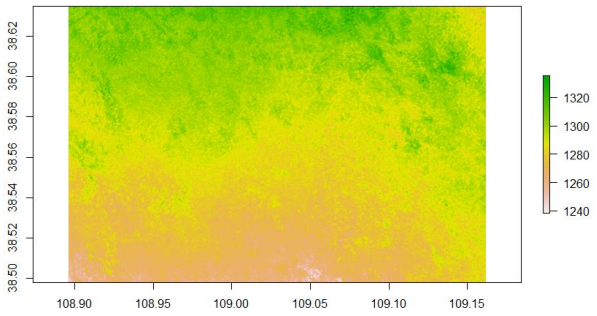

Area I1

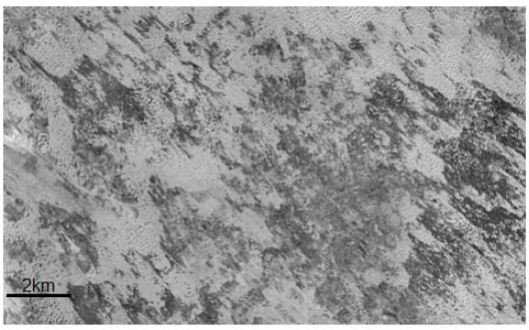

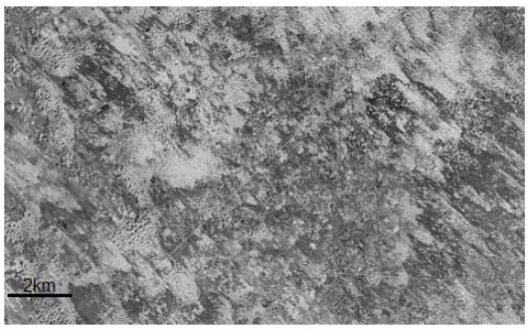

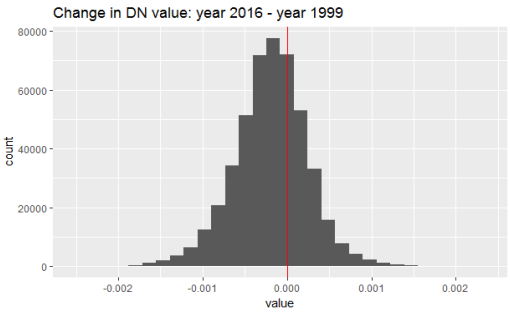

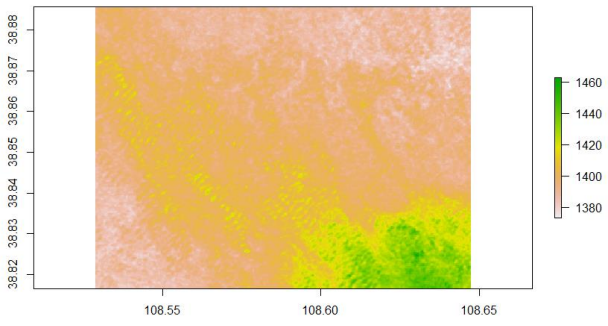

Area I4

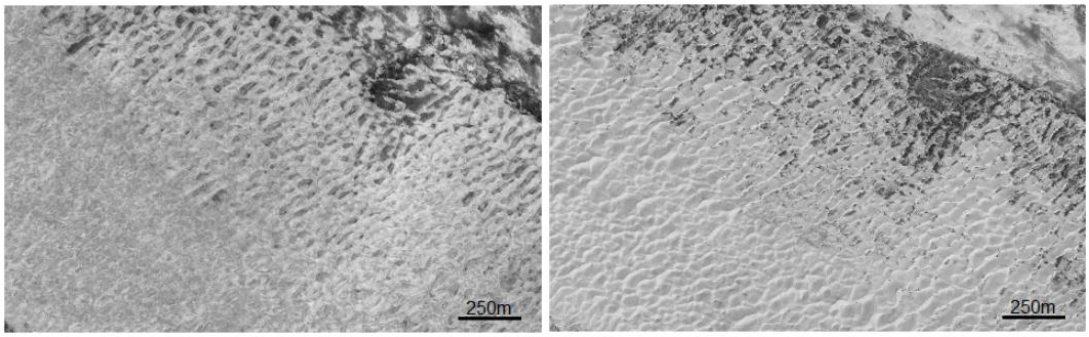

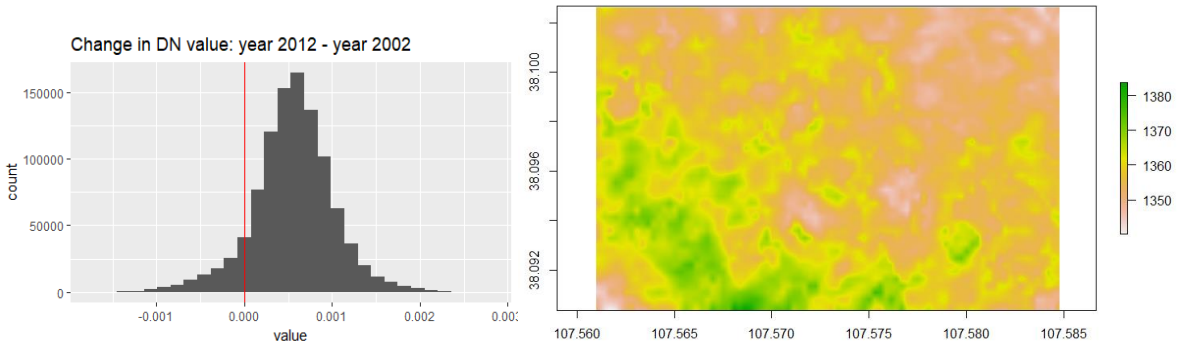

Area I5

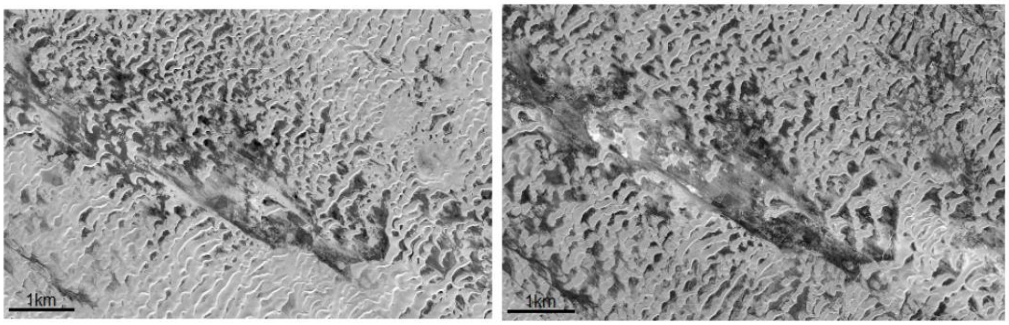

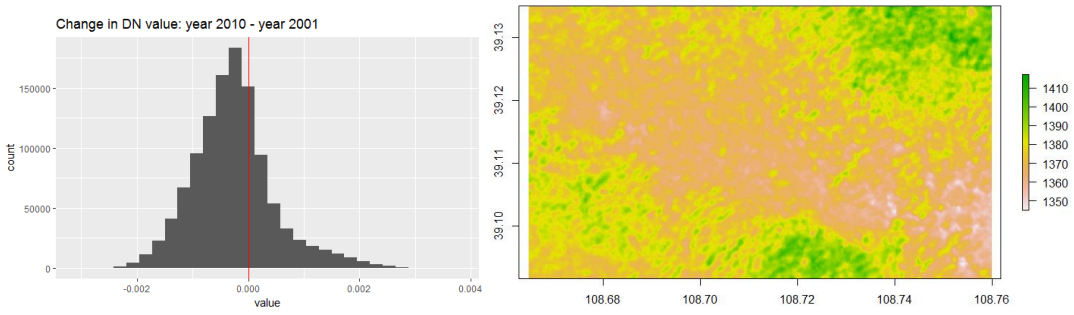

Area I6

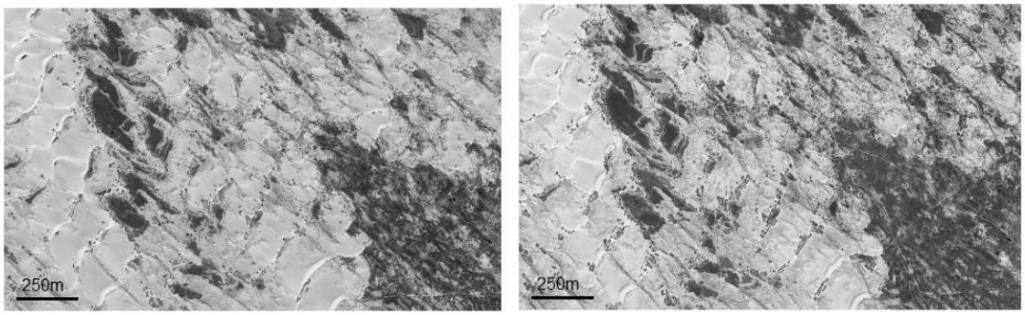

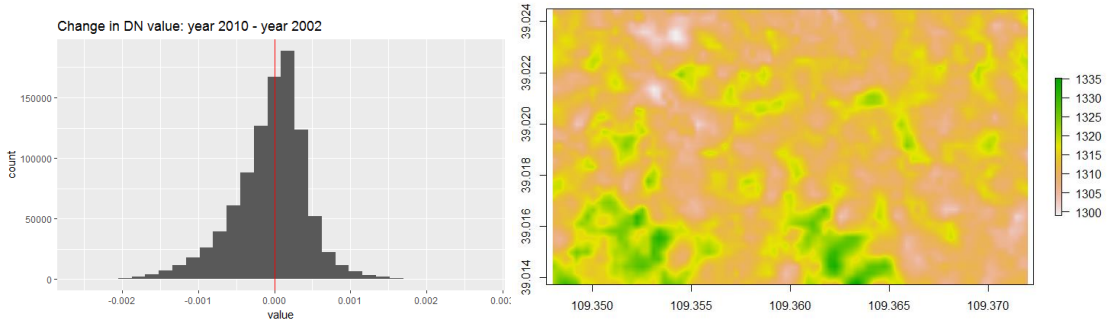

Area I7

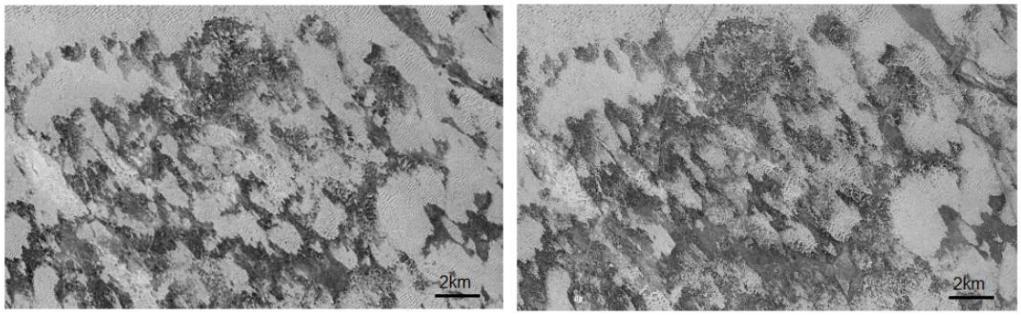

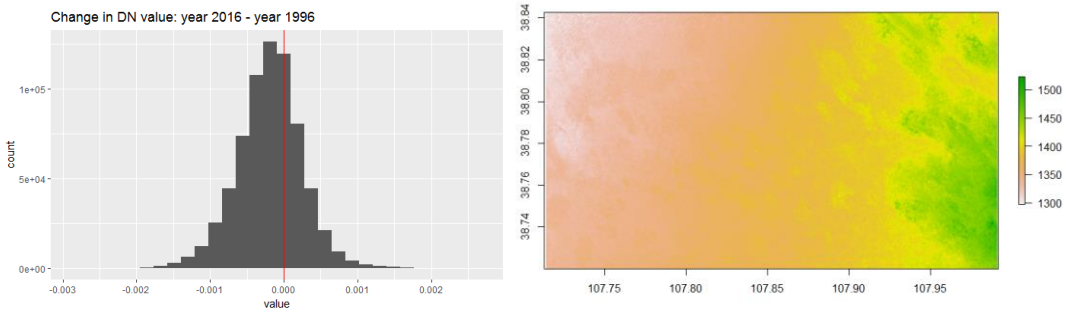

Area I8

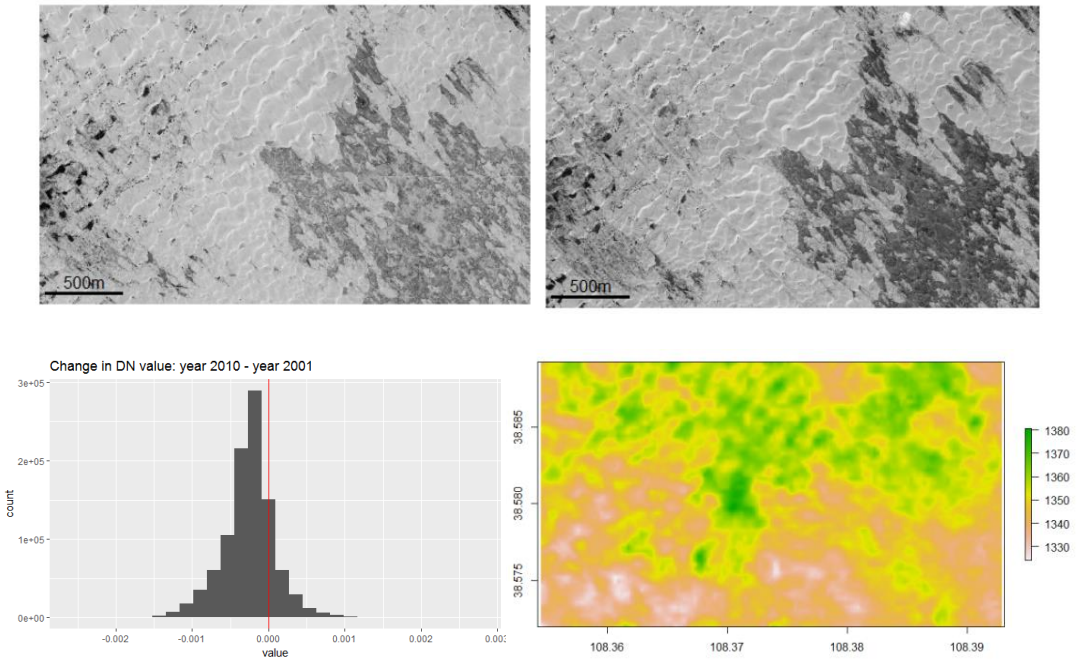

Area I9

Figure 3 Grey scale images from Google Earth, change in DN values, and DEM based on Aster GDEM data for each study area

North is toward top. Image source: Google™ Earth, Aster GDEM

Area I5 is located in the southwest corner of Mu Us dune field, close to the town Otoq Qianqi. In 2002, vegetation was concentrated in the northeast corner of the study area, where elevation is lower compared with the southwest side. From the 2012 image, sand dunes expanded in the northeast corner of this region, which is close to the county road and can be heavily influenced by human activities such to sheep herding, as is observed in the field (Figure 4b). In fact, the straight line separating the unvegetated northeast corner and the rest of the area may be a fence line. Area I5 is the only study area found with an overall decrease in vegetation cover and reactivation of sand dunes. This can be correlated with a large increase in livestock numbers in this area from 2000 to 2005 (Xu et al., 2017, unpublished).

Vegetation growth occurred in most parts of area I6 between year 2001 and 2010 as shown in the histogram of DN value change. Vegetation pixels are found along SW-NE direction in the middle of

the plot, highly correlated with the elevation pattern of this area. This correlation will be further explored in section 2.

Area I7 is close to the town of Tuke, where lush vegetation is observed in lower interdune areas. Tall bushes as high as 2m are found on lee side and the top of dunes. No signs of man-made grids were spotted.

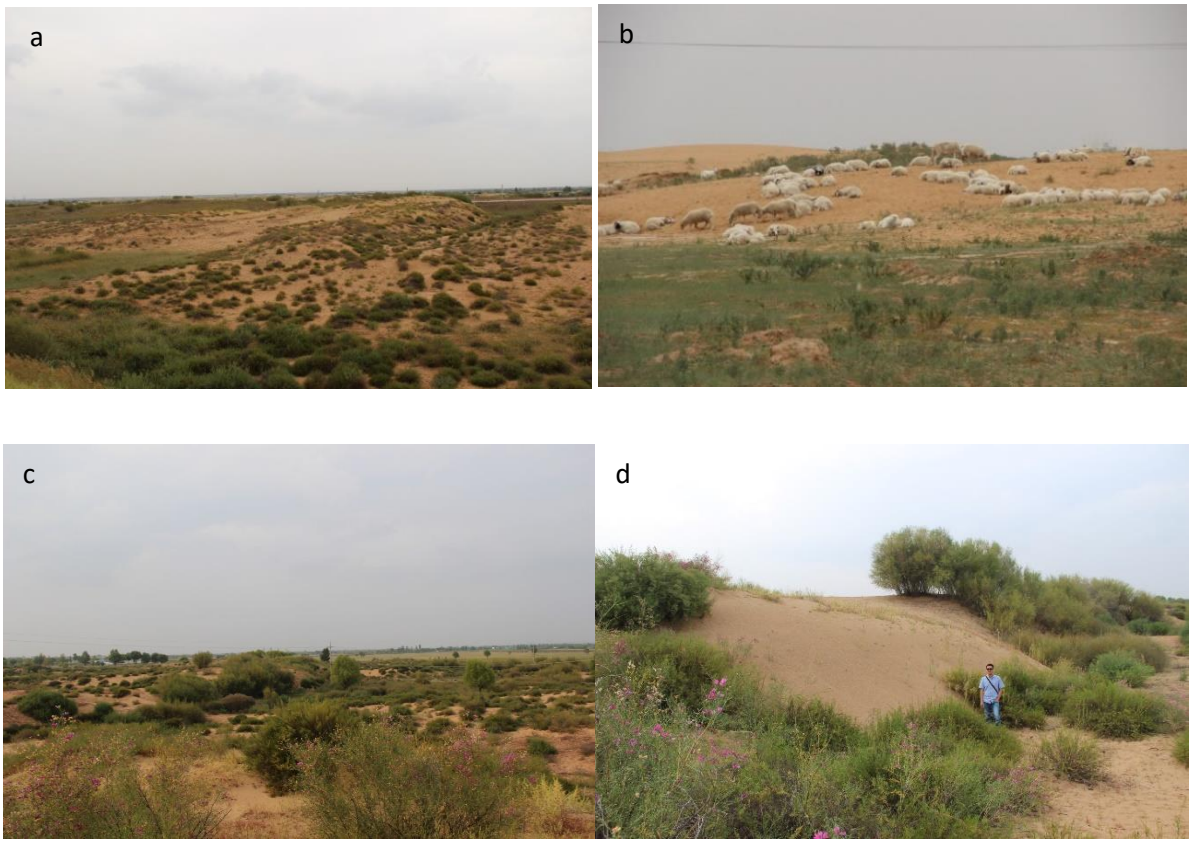

Figure 4 Field observations of some research areas (a-d: I1, I5, I7, I7)

Area I8 is located on the northwest corner of Mu Us desert, where few man-made structures can be identified from satellite images. Image resolution is lower compared with other sites. Located in the center of Mu US, area I9 doesn't have many man-made structures nearby either. Areas covered by vegetation (most of the southeast side and small portion of the southwest side) correspond to lower elevation on the map.

In summary, vegetation declined in the past two decades in local areas in the western Mu Us dune field, while most of the field experienced vegetation increase. This agrees with previous research that found dunes are stabilizing in the eastern Mu Us since the 1970s, while dune mobility increased in the west (Wang et al., 2005; Mason et al., 2008; Xu et al., 2017, unpublished).

1.2. Vegetation cover and elevation

Although an inverse correlation between elevation and vegetation exists in some areas of Mu Us dune field (Xu et al., 2015), vegetation cover does not show a clear trend with elevation across the entire Mu Us dune field (Figure 5). In fact, the correlation between vegetation cover and elevation is low for most study areas, with an absolute value ranging from 0.067 to 0.315 (Table 1).

This low correlation may be related to the varying water table level of these study areas. To evaluate that possibility, relative elevation was used to approximate the height difference between a location and local water table level, using the elevation of a cell above or below its neighbors.

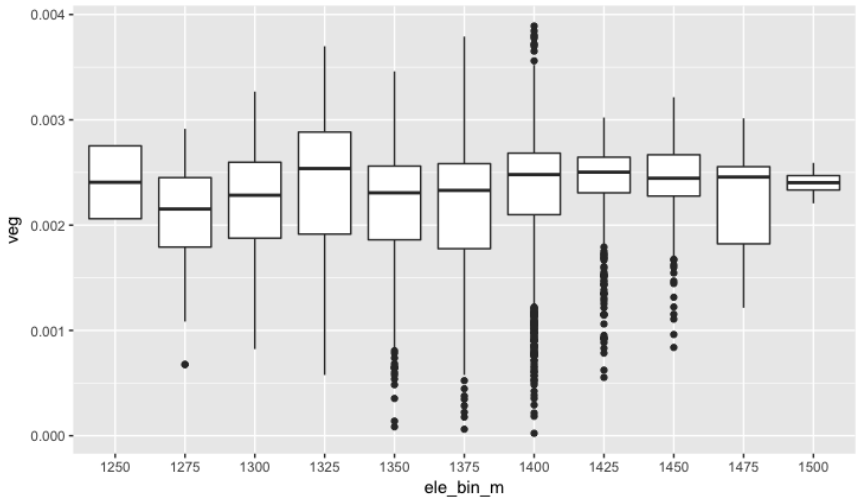

Figure 5 Boxplot of vegetation cover with elevation for the whole Mu Us dune field

Relative elevation (RE) of a focal cell i is calculated as:

$$RE_i = Z_i - \min_{dij<x}(Z_j)$$

where Z_i is the elevation value of the focal cell, $\min_{dij<x}(Z_j)$ is the minimum elevation of all adjacent cells Z_j where the distance between the focal and adjacent cells (d_{ij}) is less than x. Here I used range values calculated from variogram (Table 2) as an estimate for larger areas (for example, 500m for area I1 and I8) and trial and error to estimate d_{ij} for smaller areas. The correlation coefficient between relative elevation and vegetation cover is calculated for each area (Corr_RE), and for sand dunes only (Corr_RE_sand, defined as areas of top 10% of DN values) respectively (Table 1). Relative elevation depicts local landscapes in more detail as dune crestlines are shown much more clearly in RE images than in the original maps of elevation (Figure 6).

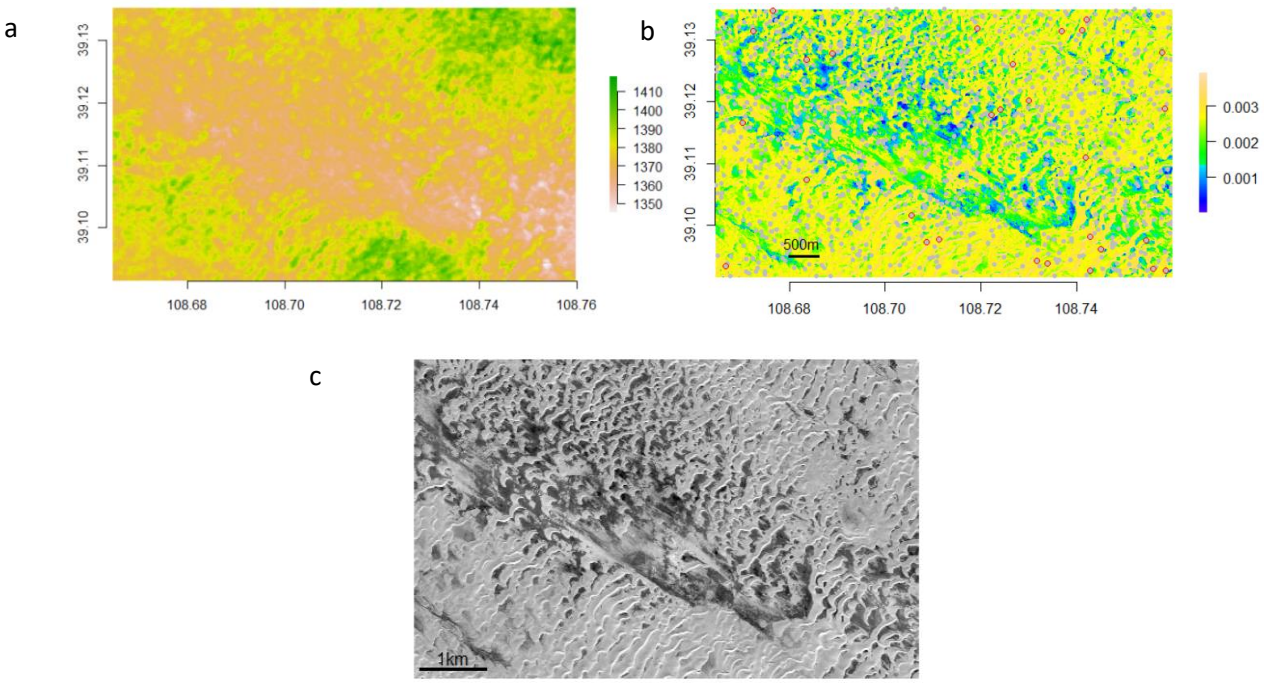

Area I6

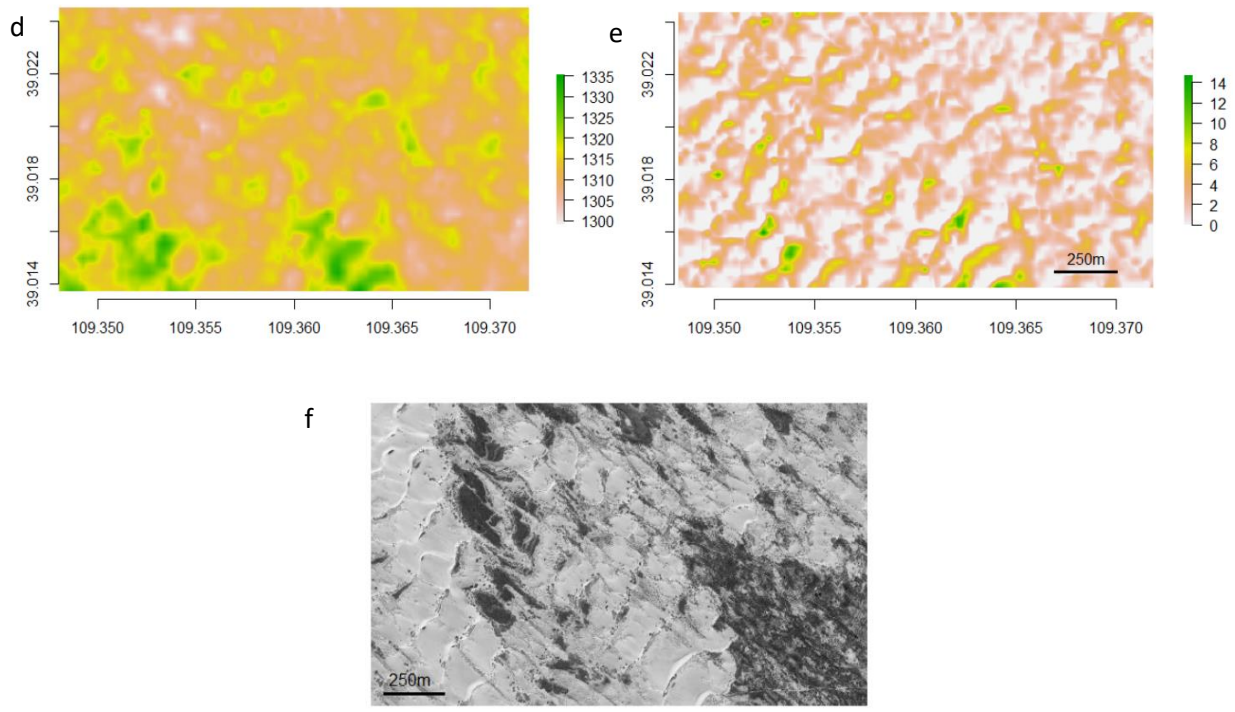

Area I7

Figure 6 Absolute (a, d) and relative elevation (or local relief, b, e) of Area I6 and Area I7

North is toward top. Image source: Google™ Earth, Aster GDEM

Using samples randomly selected from relative elevation maps (shown as red circles in Figure 7a.), correlation coefficients between elevation and DN are positive though low for all study areas (Table 1). RE and RE sand are not significantly correlated with DN for most study areas; however, the correlation is stronger for area I4 (0.365, p value of 0.001, Table 1Table 1). In area I4 (Figure 7b and c), DN increases (i.e. vegetation cover decreases) as both absolute elevation and RE sand increase, and the correlation is stronger with RE sand.

Table 1 Sizes and vegetation-elevation correlation coefficient for each study area in Mu Us dune field

*(Correlation coefficients are calculated using Pearson method and are unitless. Size of areas is measured directly on Google Earth using rectangular tool. I use * to suggest significant level: **: < 0.01; *: <0.1)*

Area	*Size(km^2)*	*Corr_original*	*Corr_RE*	*Corr_RE_sand*	*Corr_RE_sand_pval*
I1	350	0.149	-0.016	-0.044	0.822
I4	78	0.194	0.047	0.365	0.001**
I5	2.89	0.172	-0.010	-0.023	0.851
I6	38.8	0.315	0.049	0.065	0.797
I7	2.49	0.295	0.001	0.335	0.094*
I8	326	0.067	0.031	-0.052	0.804
I9	6.32	0.179	0.103	0.032	0.843

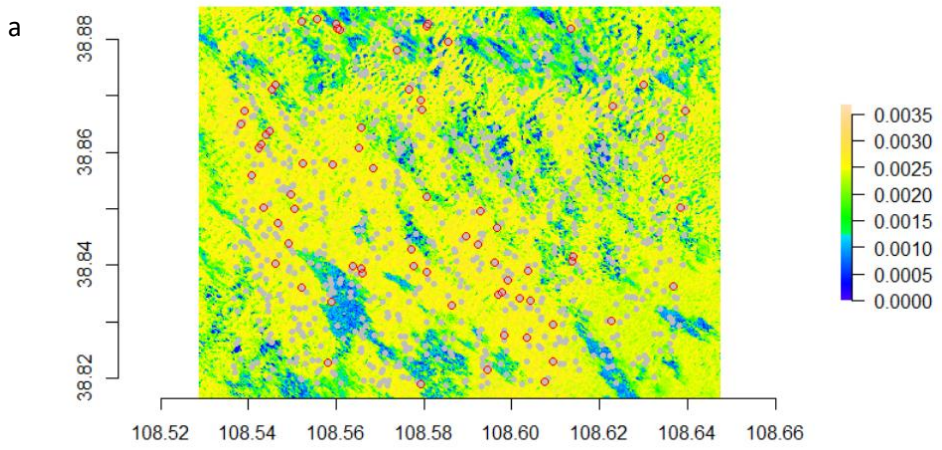

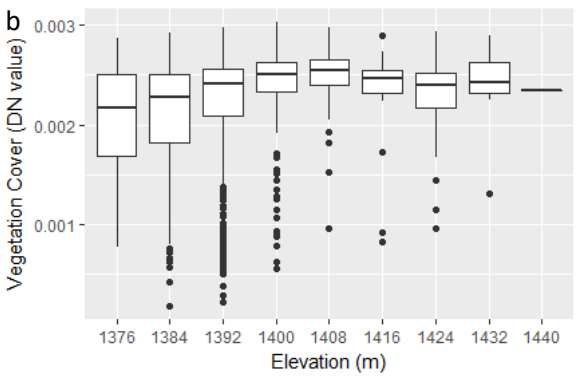

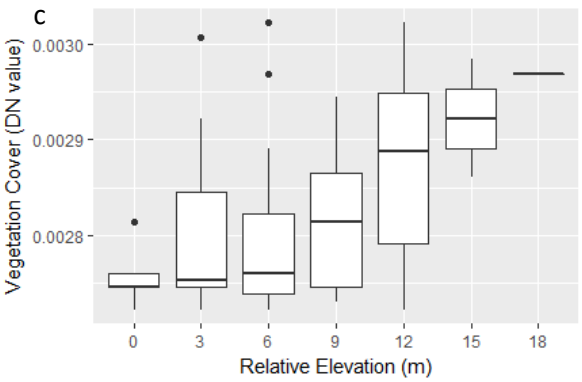

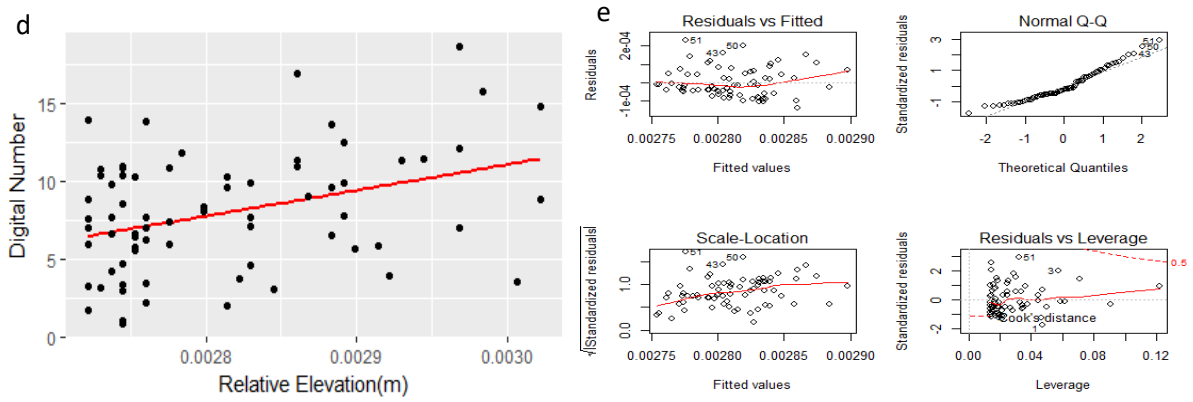

Figure 7 Correlation between relative elevation (x-axis) and DN value (y-axis)

Vegetation cover map showing samples points (grey dots) and sand dune samples (red circles; upper 10% in pixel brightness of grey dots) for Area I4 (a); Correlation between elevation (b) and relative elevation (c) and DN value (y-axis) of Area 4 for sand pixels (DN value in the upper 10%); Linear regression shows fit between vegetation cover and elevation (d); Diagnostic plots (e) show that the data is normally distributed, as evidenced by the linear pattern in QQ plot; The scale-location plot shows no homoscedasticity within the dataset; No outliers are spotted in the leverage plot. Sample size: 200; p-value: 0.09

1.3. Patchiness of vegetation

Dune field vegetation is often found to be distributed in patches, due to availability of shade, water, nutrients and lower wind drift (Maestre and Cortina, 2005). In the study areas of the Mu Us dune field Moran's I (defined below) is close to 1, suggesting positive spatial correlations (Table 2).

$$I = \frac{\frac{N}{S_0}\sum_i \sum_j W_{ij} Z_i Z_j}{\sum_i Z_i^2}$$

Where Z_i is the difference between variable of interest and the mean, and W_{ij} is the matrix of weights that is 3x3 ("Queen's case") with '0' in the center surrounded by '1's. Vegetation tends to expand from near existing patches rather than colonizing new sites randomly, because Moran's I for the difference between two images is also close to 1 (Table 2).

Table 2 Moran's I in Mu Us study areas

Area	*Size(km2)*	*Moran's I (before)*	*Moran's I (after)*	*Moran's I (after - before)*	*Range(m)*
I1	350	0.861	0.748	0.651	463.3663
I4	78	0.873	0.855	0.611	158.9648
I5	2.89	0.912	0.867	0.853	82.05746
I6	38.8	0.915	0.902	0.862	371.667
I7	2.49	0.923	0.914	0.633	400.0374
I8	326	0.919	0.856	0.699	513.9414
I9	6.32	0.889	0.921	0.755	199.9997

To estimate patch sizes, I first randomly sampled latitudinal lines from each study area, then calculated length of vegetation pixels (defined as DN value < 0.0025) that intersect with these lines. Size of a patch is represented by the distance on a transecting line that is completely covered by vegetation. The patch count histograms are generated based on patch size, which is then used to create patch count – patch size graph on log scales (Figure 8).

Model simulations (Kéfi et al., 2007) show that areas with low grazing pressure, characterized by strong local positive interactions and a large proportion of local seed dispersal, often have an inverse power law relationship in patch-size distribution. When the strength of local positive interactions is decreased, as with heavier grazing, this distribution would deviate from a straight line on power law plot. In the Mu Us Dune field, size and number of vegetation patches follow an inverse power-law correlation relationship (Figure 8), suggesting that grazing pressure is low according to Kéfi et al. (2007). However, vegetation cover of Area I5 decreased, possibly because of grazing pressure, while it increased in I9 (Section 1.1). This suggests that the patch size-number relationship emphasized by Kéfi et al. may have limited predictive power in identifying areas where

the dune field is becoming more active because of disturbance such as grazing pressure. Instead, there is a need for a multivariate analysis relating dune activity and vegetation cover to factors including human disturbance, as described in Chapter 2.

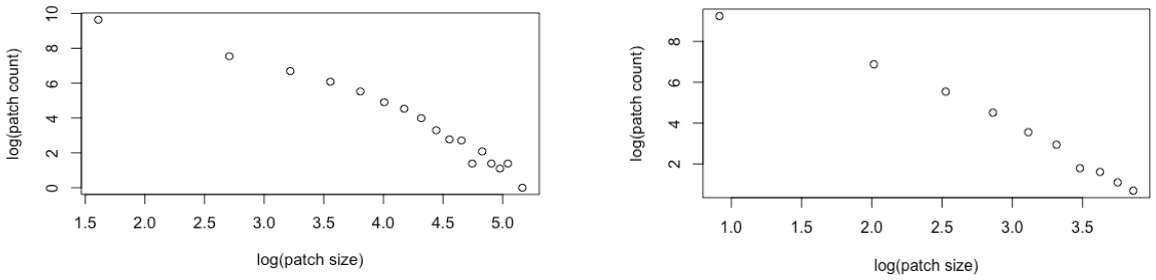

Figure 8 Vegetation patch size distribution using Area I9 (left) and Area I5 (right) as examples

1.4. Nearest neighbor effect (Spatial autocorrelations)

To further quantify vegetation spatial autocorrelations, I calculated semi-variance values and plotted variograms for pairs of vegetation sample points. Semi-variance values usually increase with distance between pairs of points, since sites that are closer are more similar in a variable or process (Z_x) than those that are further apart. Semi-variance is calculated as half the average squared difference between points $Z(x_i)$ and $Z(x_i+h)$:

$$\gamma(h) = \frac{1}{2N}\sum_{i=1}^{N}[Z(x_i) - Z(x_i + h)]^2$$

where N denotes the number of pairs of observations $Z(x_i)$ and $Z(x_i+h)$ with location x_i and x_i+h; h is the distance between these two points (Matheron, 1963).

A variogram is characterized by the range, sill and nugget. The distances between data pairs at which semi-variance values are calculated are called lags. Range is the lag value at which variogram starts to level off. It represents the distance over which data are no longer correlated. Sill is the

variogram value corresponding to the range and represents the total variation. The nugget, the y intercept of the variogram, shows the extent of random, unexplained variation within the data. Range value is of particular interest to the study, since it reflects the distance within which spatial autocorrelation is maintained, and sample points within range distance are therefore considered nearest neighbors.

Geostatistical methods require data to be normally distributed and stationary (mean and standard deviation values do not change with location). Most research areas in Mu Us Dune field have DN value distributions roughly following a normal distribution based on their bell-shaped histogram and linear QQ plot (e.g. Area I4, Figure 7).

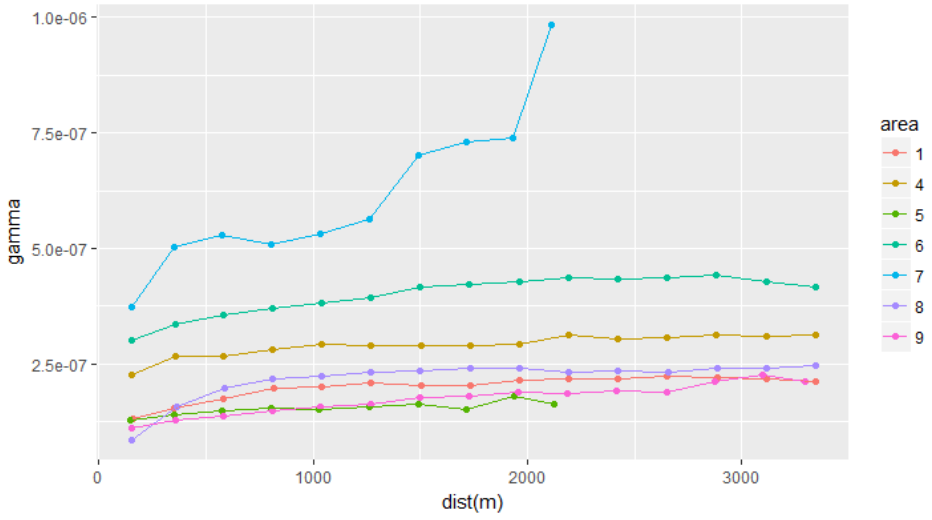

Figure 9 Vegetation variograms of study areas

Range values for all study areas were estimated after fitting these semi-variograms to a distribution (e.g. spherical, exponential, etc.) (Table 2). Vegetation variograms calculated along E-W direction are presented in Figure 9. The larger study areas (I1, I8) have a range value of about 500m (Figure 9, Table 2), which will be used as the 'nearest neighbor' distance for these areas in later chapters. Area I7 does not show a clear semi-variogram pattern, possibly because of its small size.

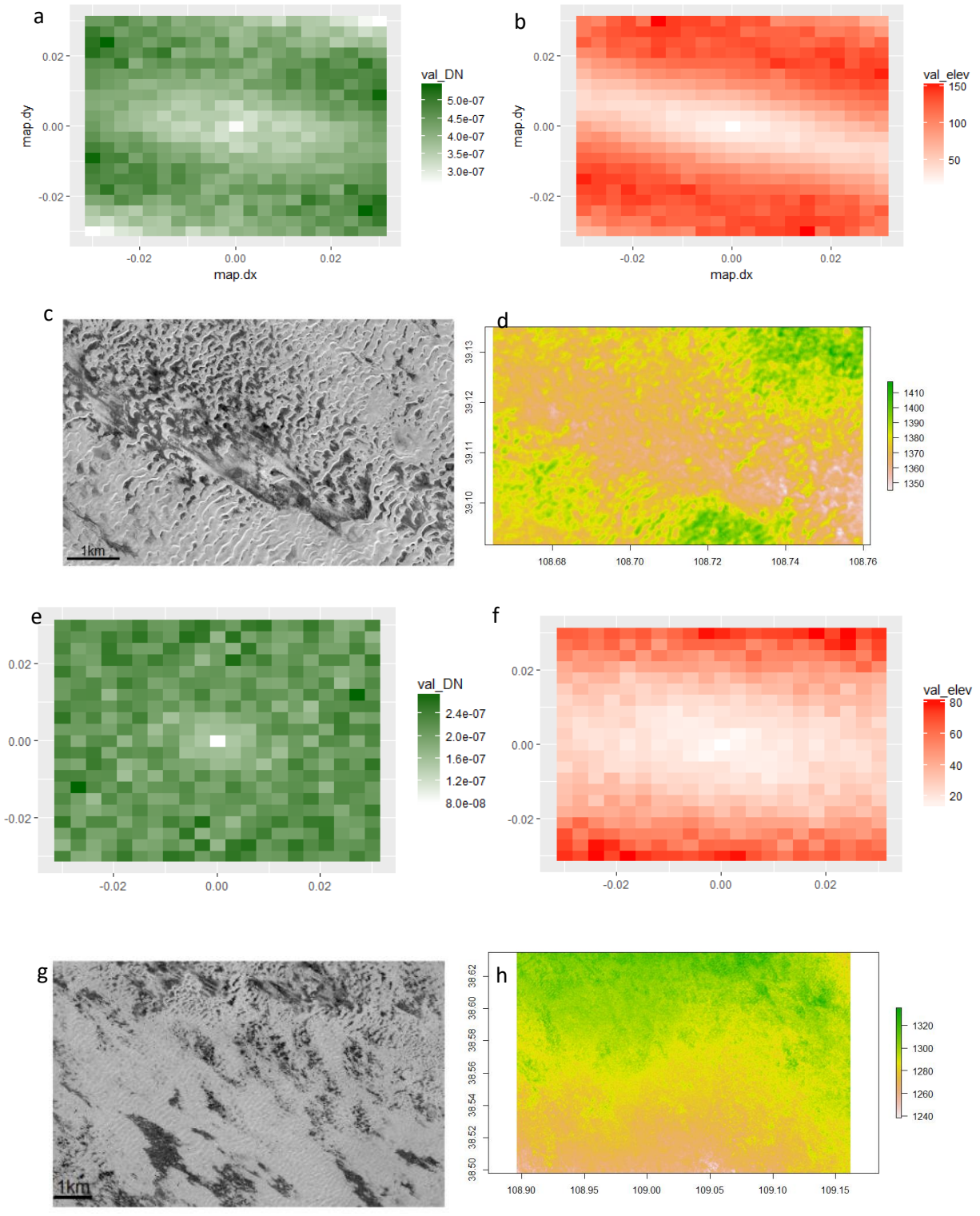

Figure 10 Analysis of the anisotropy of spatial autocorrelation for vegetation cover and elevation in Area I6 (a-d) and Area I11 (e-h). Panels a, b, e, and f are variogram maps, explained in the text. Panels c and g are grayscale images portraying vegetation coverage (dark = vegetation); panels d and h show elevation (m above sea level). For area I6 (a-d), vegetation (a and c) and

elevation (b and d) both demonstrate anisotropy. A transect along 145°N shows high spatial continuity along that direction (with the longest range) in both vegetation and elevation for Area I6. Vegetation in Area I1 (e to h) shows isotropy while elevation demonstrates anisotropy with the largest range along x-axis. North is toward top. Image source: Google™ Earth, Aster GDEM

Directional dependence of vegetation distribution can provide further insights on its controlling factors. Anisotropy or isotropy can be demonstrated by variogram maps (or "Anisotropic Semivariance Surfaces"), portraying the semivariance contribution of each pair of points with h distance apart along all directions (each map cell represents a specific distance and direction, plotted relative to the map center) (Figure 10). A transect line in any direction from the center to the margins of the variogram map is equivalent to the variogram in that direction. Less variation in color along a certain direction suggests that the range value in that direction is large (e.g. NW-SE direction in Figure 10 a and b), which is a sign of anisotropy; otherwise the range value is roughly the same along all directions and data would be characterized by isotropy. From the variogram maps of area I6 (Figure 10 a-d), vegetation is anisotropic and has the largest range along NW-SE. Elevation is anisotropic too with the largest range in the same direction, suggesting the correlation between vegetation and elevation in this area. In addition, the RDD (i.e. resultant direction of potential sand transport) for the Mu Us dune field is also generally NW-SE, consistent with the dune migration direction (Mason et al., 2008); therefore the pattern of anisotropy in I6 suggests a link with the direction of sand transport and the resulting dune forms. For area I1 (Figure 10 e to h), however, vegetation has no directional effect while elevation shows anisotropy, another piece of evidence that elevation alone cannot always explain vegetation distribution patterns.

Conclusions and Discussion

In general, the study areas display the increase of vegetation cover previously reported for the Mu Us dune field (Xu et al., 2015), though to varying degrees. Area I5, in the western part of the dune field, is a exception, with bare sand clearly increasing.

Simple correlation analysis provides only very limited evidence for the relationship between vegetation cover and elevation (or more local, relative elevation) that was proposed in earlier research on dune fields. The conditions that have been proposed to explain this relationship—greater wind exposure on high points of the landscape and a shallow water table in low areas—should apply in the Mu Us dune field, but possibly other controls on vegetation distribution are also important. It is unclear why a correlation between vegetation cover and relative elevation of sand emerges in study area I4, but not the others.

In contrast, the analyses in this chapter do indicate patchiness and spatial autocorrelation of vegetation that may reflect effects of seed dispersal and local facilitation of plant growth through sheltering and greater nutrient availability. This information quantitatively confirms earlier speculation about vegetation patchiness and spatial autocorrelation in this dune field (Xu et al., 2015), and should be incorporated into modeling of vegetated dune behavior, if possible. The range value typical for variograms of the larger study areas (~500 m) is also useful as an indicator of the scale of neighbor effects to consider in modeling. The analysis demonstrates that elevation can be an influential factor in vegetation spatial patterns, but it is not the sole deciding factor. The relationship between vegetation patch size and number, suggested by Kéfi et al. (2007) as an indicator for distinguishing stable dune field landscapes with low grazing pressure from those affected by higher disturbance levels, does not appear to be useful for this purpose in the Mu Us dune field. The anisotropy of spatial autocorrelation suggests effects of wind and sand transport directions in some study areas, but not others, also a new observation worth further study.

In the next chapter, I will take a multivariate approach and build models to relate recent dune migration and vegetation cover changes over time with multiple factors (including climatic variables, elevation, and variables representing human impacts).

Chapter 2. Dune activity and regional vegetation change in response to environmental variables

As discussed in the Introduction and Chapter 1, a range of factors can affect dune activity. Their relative importance in the dune stabilization process, however, has rarely been analyzed quantitatively. Bullard et al. (1995) carried out a detailed statistical analysis of dune patterns, mapping and classifying linear dune patterns using aerial photographs. However, they did not study their response to environmental variables. Wang et al. (2005) performed principal component analysis (PCA) to compare human and climate influence on dune activity; yet they only used survey data from cities on the fringe of the dune field in their model while leaving the vast area in the middle of dune field unstudied. Baas and Nield (2010, 2007) employed PCA on blowout forms using state variables derived from simulation results of their Discrete Ecogeomorphic Aeolian Landscapes (DECAL) model. They then constructed a phase graph demonstrating 11 dune categories. However, their model simulates blowouts rather than the stabilization process of barchan dunes. Moreover, these generated dune types are based on model simulations instead of actual dune fields.

The inherent complexity of the sand dune stabilization process and the availability of high resolution satellite images have led to the use of machine learning methods as a viable alternative to physical modeling approaches. Decadal-scale morphology changes (such as dune migration and size changes) can be observed and measured from high resolution, multi-temporal imagery freely available from Google™ Earth (Hugenholtz et al., 2012). Though limited by the availability of a long-term, historic (over 100 years) record of satellite images, we can use segments of the long-term dune stabilization process from satellite images to build and test models, thereby reconciling the scale discrepancies between model and observations.

In this chapter, I use features measured directly from Google Earth (GE) satellite images as explanatory variables to model rates of dune migration (Section 2.2) and vegetation cover change (Section 2.3). These features are described and grouped into categories using PCA in Section 2.1. Dune migration rate and rate of vegetation cover change rate calculated for each sample (a pair of images), and the explanatory variables represent conditions at the time of the first image of each pair (except for Moran's I, where both initial and final values were considered as explanatory variables). As a consequence, the analyses in this chapter deal with spatial variation of dune migration rate and vegetation cover change across the dune field, in response to spatially varying environmental factors.

Two patches of sand dunes are selected from each of the seven study areas in the Mu Us dune field based on image quality and availability. A pair of images of each patch were obtained from two years (ranging from 8 to 14 years apart). From each patch, five dunes were randomly selected, and features were extracted from the earlier image. Dune migration rate was estimated by the position change of each individual sand dune crest line averaged by number of years between the pair of images. Using the same imaging processing approach as described in Chapter 1, pixel brightness (DN value) was used to represent vegetation cover, after adjusting the brightness of the images to match control point DN values. Vegetation cover change rate was calculated at patch level by dividing average pixel brightness (DN value) change with number of years between the pair of images. All analysis was conducted in R.

1. Feature description and PCA analysis

Feature description

Climate factors such as temperature and precipitation can clearly influence vegetation growth, and ratio of precipitation to potential evapotranspiration (P:PET) is often used to estimate effective moisture, i.e., moisture available to dune-stabilizing plants (Lancaster, 1988a). Wind data from 1991 to 2012 obtained from the NCDC was used to calculate DP (see Background for methods), which affects the susceptibility of vegetation to disturbance (Yizhaq et al., 2007). Climate variables of a sand patch of a certain year were approximated using data from the closest weather station.

Bagnold (1941) indicated that migration speed of dunes is inversely correlated with their height. In the model by Duran and Herrmann (2006), dune size is essential in determining fixation index:

$$\theta = Q / (V^{1/3} V_v)$$

where Q is sediment flux, V is barchan volume, and V_v is vertical vegetation growth rate. If $\theta > 0.5$ then barchan dunes remain mobile because vegetation growth does not keep up with sediment flux, otherwise they are stabilized by vegetation. The equation used implies that larger dunes will stabilize at lower vegetation growth rates and/or higher sediment fluxes.

Barchyn and Hugenholtz (2012) also pointed out that larger transverse dunes stabilize more quickly than smaller, wider spaced barchan dunes because of their lower speed. To estimate dune size (or volume) from satellite images, researchers have used Lee Face Length (LFL) since the lee face has a narrow range of slope angles and thus this length is closely related to maximum dune height (Xu et al., 2015). Here I used largest length in the wind-parallel direction (dune width) instead of LFL as a closer estimate for dune sizes, since the latter represents a very small distance that is difficult to measure accurately from some of the satellite images used for this analysis.

Xu et al. (2015) found that vegetation growth decreases with the increase in elevation in Mu Us dune field, possibly due to the influence of increasing depth to the water table. In their numeric model of dune activities, Pelletier et al. (2009) used elevation to approximate surface roughness, which is inversely correlated with sediment flux.

Human activities, such as farming, herding, and planting wind-breaking grids can also change vegetation cover and surface roughness. These activities can be observed in the field, such as planted trees (Figure 11a), embedded wind-breaking grids of sticks or shrubs, and fences (Figure 11b) to prevent animals from grazing in certain areas. The buried poles from fences (Figure 11b) suggest dune migration. These wind-breaking grids are evident as straight, dotted lines on sand dunes in satellite images (Figure 11c).

In this chapter, as in Chapter 1, elevation is obtained from Aster GDEM; note that this is not local, relative elevation related to height on a dune, but instead reflects broader variation in elevation across the dune field that is mainly related to topography of the sub-dune surface. Vegetation related features (such as distance to nearest vegetation patch) are measured directly from GE images for use as explanatory variables.

The grid density is estimated from satellite images with a value between 0 and 1. Other human activity metrics such as distance to closest man-made structures (water body, villages, etc.) can also be measured directly from satellite images.

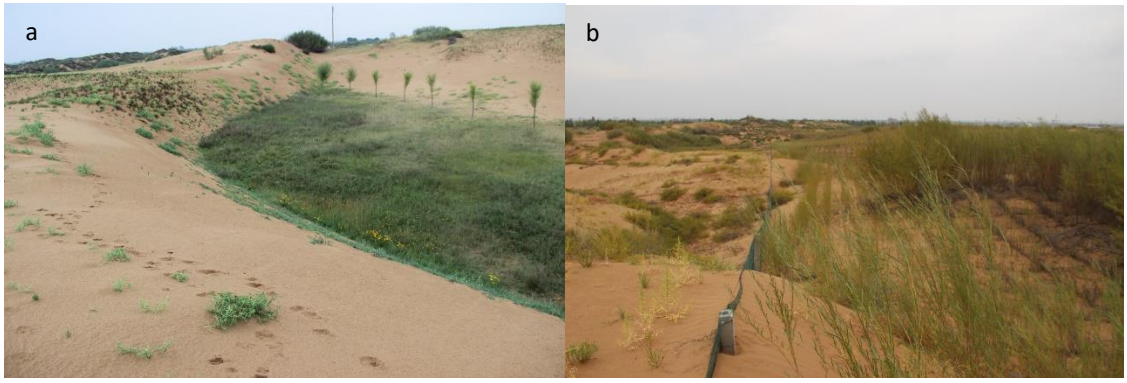

c 

Figure 11 Human activities observed in the field and from satellite images (Area I1)

Human planted trees (a), observed fence and grids from the field (b) and parabolic dunes and grids observed from Google Earth (c) North is toward top. Image source: Google™ Earth

All features that are included in the analysis are summarized in Table 3.

Table 3 Explanatory variable description for dune migration speed (range of variation: 0-7.3m/year)

Category	*Explanatory variables*	*Values description*	*Range of variation*
Non-human	Elevation/ESL	Retrieved from Aster DEM data	1282-1482m
	Dune size (dune width)	Measured using Ruler tool on GE	20.9-176.0m
	Drift Potential	Value from nearby station, NCDC	15-111(knot)
	Average temperature	Value from nearby station, NCDC	7.72-9.96(°C)
	Effective moisture (P/PET)	Value from nearby station, NCDC	0.38-1.12
	DN value of pixels (up and down wind direction)	Value measured on grey scale images	33-215
	Size of closest vegetation patch up and down wind direction	Measured using Polygon tool on GE	0-29070m^2
	Size of nearest vegetation patches	Measured using Polygon tool on GE	5580 -1.2*$10^6$$m^2$
	distance of vegetation patches nearby	Measured using Ruler tool on GE	0-2213m
	Initial Moran's I	Measured from GE images	0.803-0.973

	End Moran's I	Measured from GE images	0.850-0.963
Human	Distance to nearest village/city/farmland	Measured using Ruler tool on GE	562-7447m
	Size of nearest village/city/farmland	Measured using Polygon tool on GE	760-1.5*$10^7$$m^2$
	Distance to nearest waterbody <2km	Measured using Ruler tool on GE	0, 1
	Grid density on a sand dune	DN value measured on GE	0-0.93

PCA analysis

To further group the two categories of features listed in Table 3 into several subcategories (such as climate or vegetation), and gain a better understanding of the amount of variation for each subcategory, I used PCA to convert these variables into uncorrelated Principal Components (PCs). Each PC can be characterized by its leading variables. PCs are also used in place of actual features in the models in section 2.2 and 2.3 to identify the leading dimension (climate, vegetation, or human) contributing to dune migration rate and vegetation cover changes.

Using R packages FactoMineR and factoextra, I created a scree plot (Figure 12a) that shows the importance of PCs, where the first 6 PCs explain 80.8% of the variation.

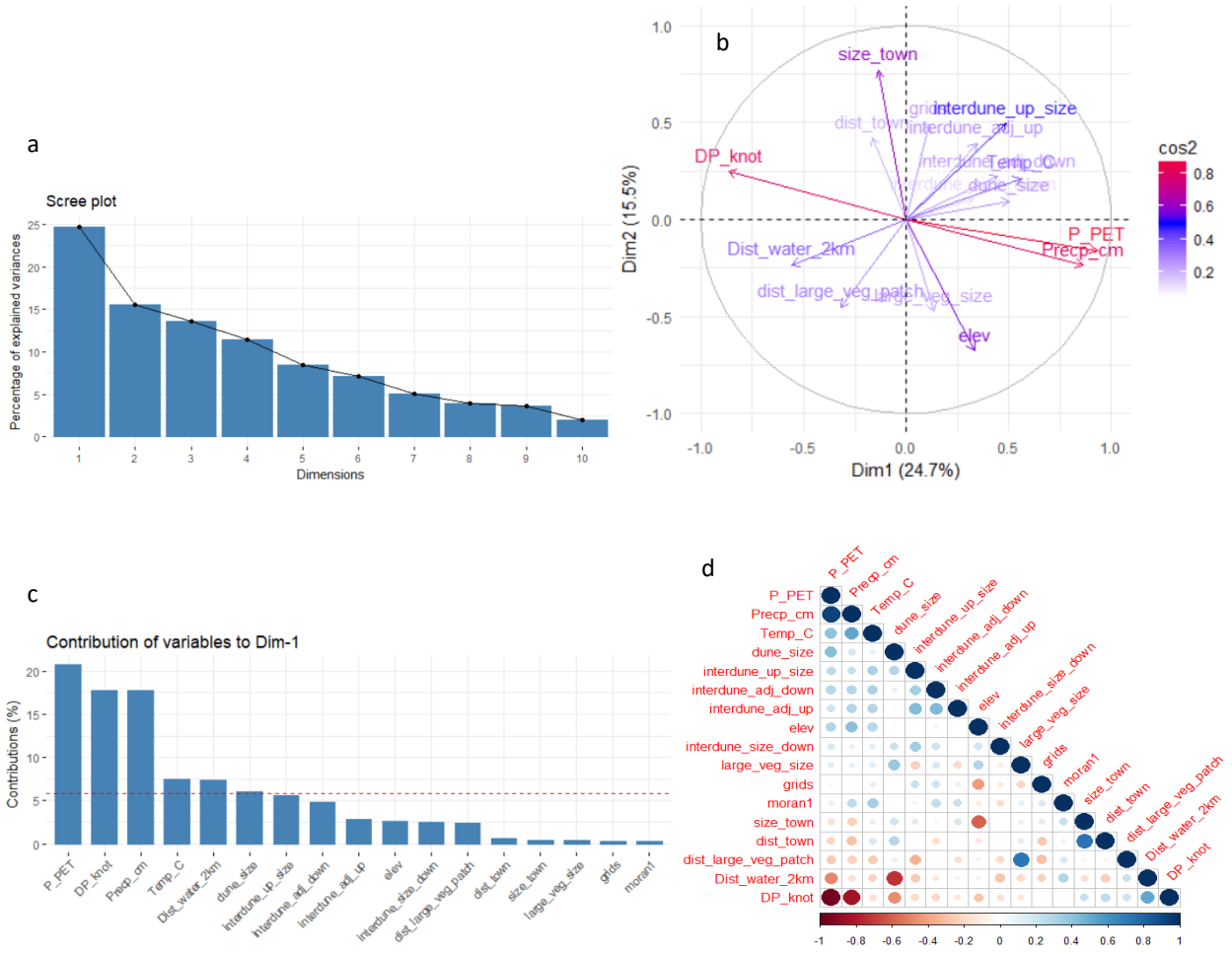

Figure 12 Scree plot (a); Variable factor map showing variable contributions (cos^2) to the first two dimensions (b); Bar graph showing variable contribution to PC1 (red dashed line suggests expected contribution: 6.67% = 100%/15 variables, where variables with values above the line are considered major contributor to PC1 (c); Correlation ('normalized' variance ranging between -1 to 1) between variables (d)

Each variable can be plotted in the component space using their loadings (correlation between a variable and a PC) as coordinates. An ordination plot (Figure 12b) projects all variables onto the first two PCs. Variables that are close to each other in the graph are more correlated to each other, such as P/PET and precipitation. Vector length indicates the correlation between variable and the first two principal components. The most important variables that explain the first PC are P/PET,

Precipitation, and DP (Figure 12c and Table 4); size of nearest town and elevation are leading variables for the second PC (Table 4).

Table 4 Contribution of variables to each PC

	Dim.1	*Dim.2*	*Dim.3*	*Dim.4*	*Dim.5*
elev	0.1099	0.4569	0.0018	0.0024	0.2473
grids	0.0126	0.2407	0.0699	0.0038	0.3929
interdune_adj_up	0.1180	0.1536	0.0977	0.1575	0.0394
interdune_up_size	0.2378	0.2445	0.0232	0.0030	0.0390
interdune_adj_down	0.2008	0.0497	0.0107	0.1702	0.0203
interdune_size_down	0.1077	0.0104	0.0056	0.1206	0.2122
dist_large_veg_patch	0.0995	0.2034	0.2269	0.2285	0.0370
large_veg_size	0.0177	0.2230	0.4146	0.1717	0.0319
Dist_water_2km	0.3099	0.0545	0.2884	0.1932	0.0405
dist_town	0.0265	0.1770	0.4633	0.0096	0.1848
size_town	0.0183	0.5922	0.1865	0.0305	0.0034
dune_size	0.2527	0.0090	0.4769	0.0306	0.0198
DP_knot	0.7462	0.0602	0.0020	0.0322	0.0430
P_PET	0.8721	0.0256	0.0001	0.0014	0.0171
Precp_cm	0.7456	0.0556	0.0442	0.0384	0.0002
Temp_C	0.3139	0.0450	0.0001	0.1439	0.1003
moran1	0.0124	0.0369	0.0053	0.5979	0.0098

PC3 is heavily influenced by dune size and distance to large human establishments (Table 4). PC4 is mainly affected by vegetation distribution (Moran's I). PC5 is led by man-made wind breaking grids and elevation. In all, the climate component (PC1) has the largest variation amongst all PCs. Most other PCs have mixed effects from vegetation and human activities.

2. Regression on dune down-wind migration rate

In this section, I will investigate the factors controlling the rates of dunes' down-wind migration in the study areas, during the short periods of time represented by the paired images. To quantify dune movement, researchers have measured the distance between two lines representing the position of dunes successively in time (Gay, 1999; Bailey and Bristow, 2004). Edges of slipfaces and brink lines are often used as representations of dune positions (e.g., coastal dunes of Oregon, Hunter et al., 1983, coastal dunes of Brazil, Jimenez et al., 1999 and Levin et al., 2009). In this research, I adopted the same method and used the average value of multiple measurements between crest lines as dune migration distance. The migration rates and all features are standardized by subtracting the mean value from them and dividing the remainder with the standard deviation.

Environmental and human activity related features (Table 4) are employed as explanatory variables for modeling dune migration rates. Due to the high dimensional component of the data set as well as the multi-collinearity of the variables (Figure 12d), I compared three models: Random Forest, Multivariate least squares and Support Vector Machines (SVM), and evaluated their goodness of fit using Mean Squared Error (MSE).

Random Forest

Random Forest (RF) is a non-parametric, decision tree-based classification or regression model first proposed by Breiman (2001). RF constructs an ensemble of trees using a bagging method, while randomizing the growth of each tree; it then computes mean prediction of all individual trees. Random Forest overcomes the overfitting problem of the plain decision tree method (Breiman,

2001). It has been applied in the prediction of tree species distributions under current and future climate scenarios (Prasad et al., 2006), the prediction of soil organic matter in Inner Mongolia of north China (Wiesmeier et al., 2011), and land cover classifications (Rodriguez-Galiano et al., 2012).

The importance of a variable in RF regression is measured by the 'Gini index', the residual sum of squares (suggesting 'node impurities') from splitting on this variable, which is then averaged over all trees. This importance ranking can be used to filter out irrelevant features or to identify top contributors. Using RF, for example, Wiesmeier et al. (2011) showed that land use, RSG and geology are the most important variables influencing SOC storage. Given that some of these variables are correlated (especially climate related variables; Figure 12d), I used a conditional permutation importance measure as suggested by (Strobl et al., 2008), which is implemented in the R 'party' package. RF models were built on training data set that is composed of a random sample of 70% of original dataset with randomization seed set at 1000 for reproducibility. The number of trees (ntree) is set at 25 when MSE is lowest for ntree from 1 to 100 (Figure 13a). Using the test dataset (the remaining 30% of original data), the model predictions shows good predictability in the actual migration rate values, with an MSE = 0.376 $(m/y)^2$ (Figure 13b).

Stability in variable importance increases with increasing dimension and decreasing samples in the dataset (Wang et al., 2016). To cope with the variation in Gini index and MSE each time the model is run, I ran the RF model 20 times and calculated the average Gini value. From Figure 13c, elevation is the most significant feature based on Gini index, followed by size of nearest town. The most important signals did not change when the randomization seed was set at different values, echoing

previous research which found that the most important features are more stable than the less significant ones in model iterations (Wang et al., 2016).

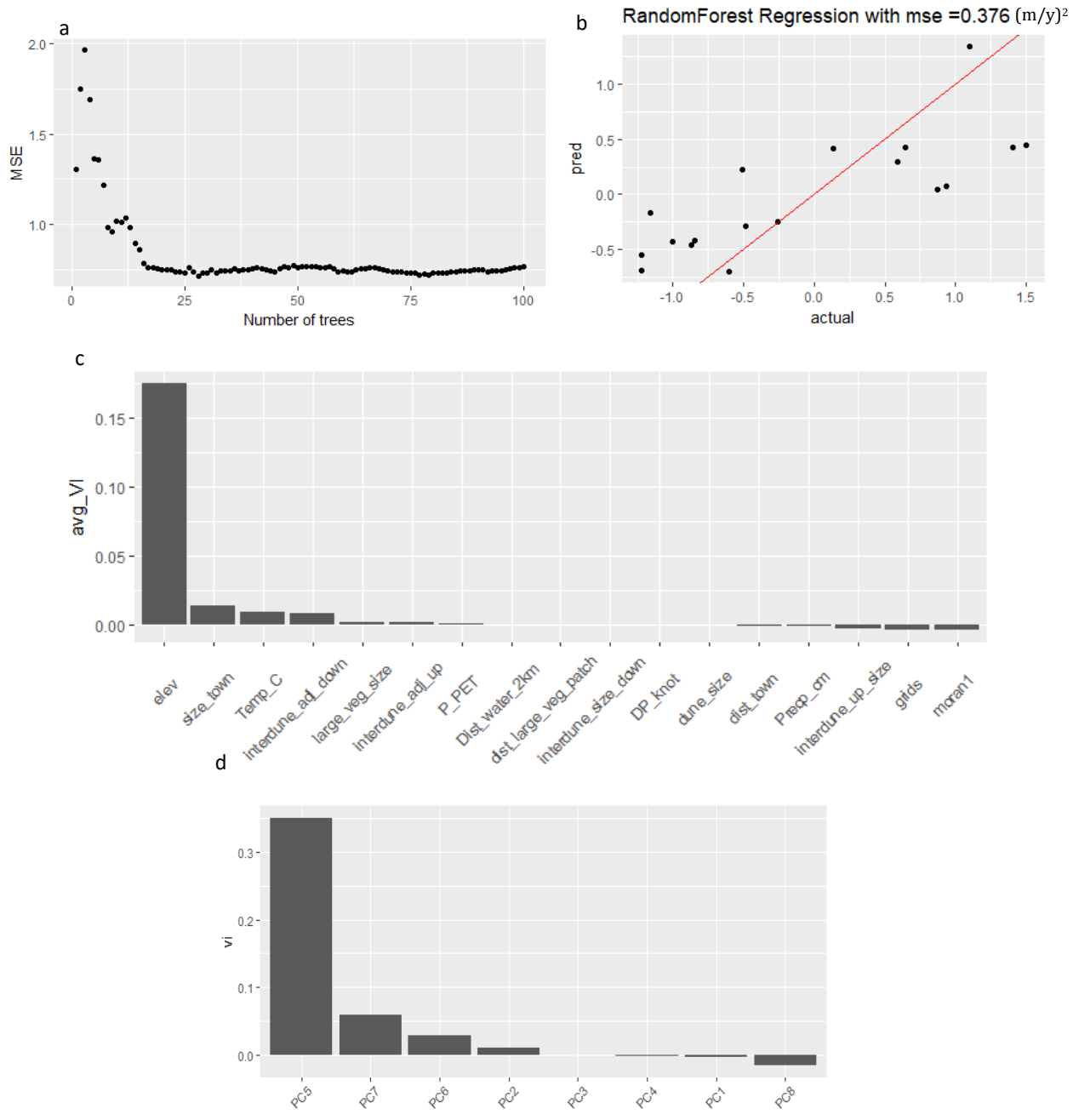

Figure 13 Results from RF analyses of dune migration rates: change in MSE with number of trees (a), Linear correlation between Random Forest prediction and the standardized dune migration rate (b), Variable Importance with features (c), Variable importance with PCs (d)

Using the top eight PCs as explanatory variables for dune migration rate, PC5 (the elevation and grid component) is shown to be the most significant component (Figure 13d), agreeing with the result reported by the RF model using the original features (Figure 13c). Despite its large influence on the PCA ordination (Section 2.1), the climate component (PC1) is not very influential on dune migration rates.

SVM

Support Vector Machine (SVM) is also a popular model used for both regression and classification problems. It has robust performance on sparse and noisy data, and has been applied in remote sensing research (Mountrakis et al., 2011), land cover and land use analysis (e.g., classification based on ASTER image of Koh Tao in Thailand, Szuster et al., 2011), or even extraterrestrial image analysis (e.g., the detection of Martian sand dunes, Bandeira et al., 2011). SVM is implemented by constructing a hyperplane in a high-dimensional space. For classification, the best hyperplane is selected when data points of its nearest classes have the largest distance from it. SVM can also be used to solve regression problems through the introduction of loss functions. For non-linear classification, hyperplanes need to be projected to higher dimensions for better fit, where non-linear kernels can be used, such as Polynomial and Exponential Radial Basis Function (RBF).

After tuning the parameters through a bootstrap resampling method, I selected the optimal model with the smallest RMSE. These parameters used in the model were: degree = 3, scale = 0.1 and C = 0.25. I chose the Polynomial Kernel, which had best performance when compared with other popular kernels such as Linear and RBF. MSE is calculated as 0.219 $(m/y)^2$, smaller than MSE of Random Forest model (Figure 14). The most important variables suggested by SVM method are similar to the ones identified by Random Forest, with elevation still being the top contributor to changes in dune migration rate.

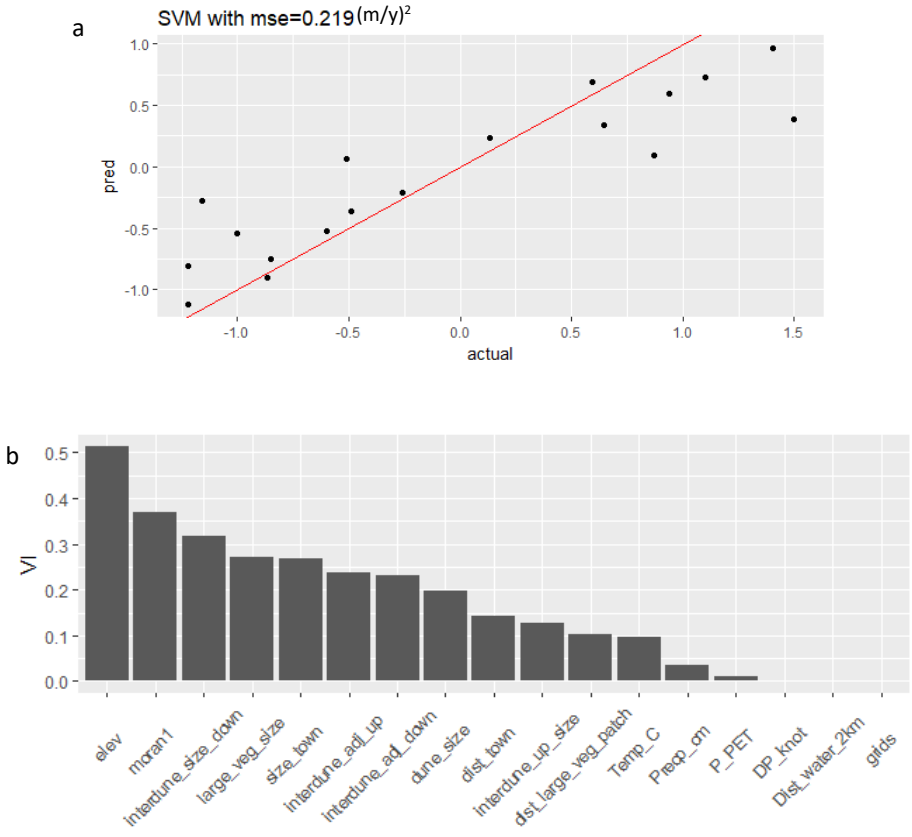

Figure 14 Linear correlation between SVM prediction and the standardized dune migration rate (a); Variable importance with all features

To explore the direction and scale of dune migration rate change with variations in the most important variables generated from SVM, I built a Multivariate Linear Regression model (MLR) model using these variables (elevation, downwind interdune vegetation patch size, initial Moran's I value, and largest vegetation patch size and size of town):

$$migration\_rate \sim elev + interdune\_size\_down + moran1 + large\_veg\_size + size\_town$$

The diagnostic plots (Figure 15) show that the data are roughly normally distributed, characterized by homoscedasticity and without highly influential outliers.

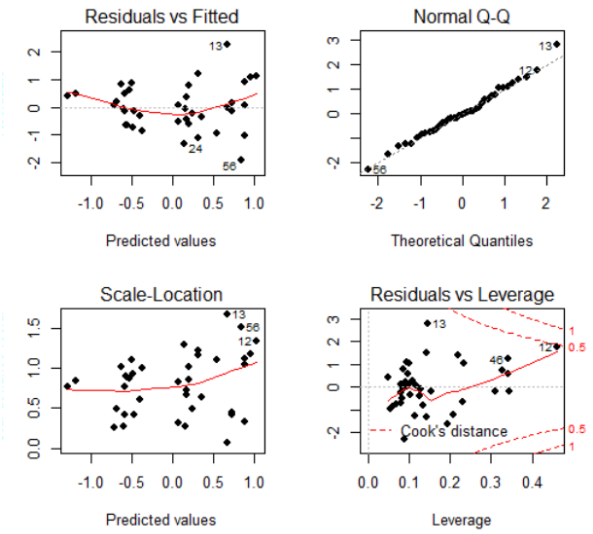

Figure 15 The fit and diagnostic of Multivariate Linear Model

Using a stepwise method, a new model was selected based on the lowest AIC (103.63) with a MSE of 0.605$(m/y)^2$, with a power of 0.7 at significant level of 0.1. In this model, elevation has the highest contribution (Table 5a), agreeing with variable importance rankings generated from RF and SVM models. The coefficient column suggests that the higher the elevation is, and the smaller vegetation patches are, the faster dunes migrate in the Mu Us study areas.

Table 5 ANOVA on factors related with dune migration rate

a. Starting with selected features (elev, interdune_size_down, moran1, large_veg_size, size_town)

	Estimate	*Standard Error*	*t value*	*Pr(>|t|)*	
(Intercept)	-0.01871m/y	0.13839	-0.135	0.89322	
elev	0.61885y^{-1}	0.14818	4.176	0.00018	***
large_veg_size	-0.36217 $(m*y)^{-1}$	0.15517	-2.334	0.02529	*

b. Starting with all features

	Estimate	*Standard Error*	*t value*	*Pr(>|t|)*	
(Intercept)	0.005236m/y	0.122508	0.043	0.96621	
interdune_adj_up	-0.60626$(m*y)^{-1}$	0.164389	-3.688	0.000964	***
large_veg_size	-0.98239$(m*y)^{-1}$	0.195216	-5.032	2.54E-05	***
Dist_water_2km	-6.50361$(y)^{-1}$	1.522014	-4.273	0.000201	***
dist_town	-0.39031$(y)^{-1}$	0.287685	-1.357	0.185704	
size_town	0.433145$(m*y)^{-1}$	0.323924	1.337	0.191926	
dune_size	0.363133$(y)^{-1}$	0.225235	1.612	0.118125	
DP_knot	-12.2998m/(y*knot)	3.116032	-3.947	0.000484	***
P_PET	-32.9779m/y	7.624521	-4.325	0.000175	***
Precp_cm	19.39062$(y/100)^{-1}$	4.241998	4.571	8.95E-05	***
moran1	0.679949m/y	0.267091	2.546	0.016694	*

Significance level: 0.001 '**' 0.01 '*' 0.05 '.'

For comparison, I also built a model that starts with all 17 features and is trimmed down to 10 using AIC through stepwise selection. The result in Table 5b is very different from Table 5a. For example, elevation is no longer amongst the most significant features. This can be attributed to the small sample size of the dataset, since the power of the current 17-feature model is only 0.5 at significant level of 0.1. To increase the power to 0.8 at the same significant level, at least 104 samples will be required.

In summary, models generally agree that elevation is the leading factor in determining dune migration speed. This can be related with locally greater exposure to strong winds at higher elevations, not reflected by the DP from weather stations used in these models. Nearby vegetation patch size also plays important roles (Table 5a), since larger vegetation patches are likely more

effective than smaller ones in trapping sand and limiting supply to downwind dunes. SVM had the best performance of all three models while MLR had the worst, which can potentially be improved by adding more sample points.

3. Regression on vegetation cover change rate

To predict vegetation cover change rate, Yizhaq et al. (2007) proposed a continuum model that is comprised of three parts, which are respectively: vegetation growth (including resource competition and growth), sand movement effect on vegetation, and wind drag on vegetation:

$$\frac{dv}{dt} = \alpha(v + \eta)\left(1 - \frac{v}{v_{\max}}\right) - \varepsilon \,\mathrm{DP}\,\theta(v_c - v)v - \gamma\,\mathrm{DP}^{2/3}\,v$$

where v is the vegetation cover; v_{max} = 1, representing completely vegetated dunes; θ is a random vegetation growth factor; v_c is a critical vegetation cover above which sand transport decreases; $\theta(v_c\text{-}v)$ =1 when $v<v_c$, and 0 otherwise; $DP^{2/3}$ represents wind drag on vegetation. However, the model neglects local features (such as local patches of vegetation) and moisture.

As a viable alternative, statistical models have been developed to predict vegetation cover types using environmental variables as well as vegetation spatial distribution information (Franklin, 1995; Miller and Franklin, 2002). Miller and Franklin (2002) built GLM and tree-based classification models to predict the presence of vegetation species using predictors such as precipitation, elevation, etc. However, studies on predicting vegetation cover change rate in dune fields are scarce.

In this section, the spatial variation of yearly vegetation cover change of dune patches is treated as the response variable. A positive, rapid increase in vegetation cover suggests fast stabilization, while a negative value represents land degradation or dune activation. Explanatory variables are

slightly different than those used in Chapter 2.2, with values averaged over the area of each vegetation patch (Table 6). These variables still cover climate, human and environmental aspects. To simplify the model, I assumed that vegetation is in temporary equilibrium with the environment following Guisan and Theurillat (2000).

Table 6 Explanatory variables for vegetation cover change rate (range: $-7*10^{-5}$ – $6*10^{-5}$/year)

Category	***X- variables***	***Values description***	***Range of variation***
Non-human	Elevation	Retrieved from Aster DEM data	1283-1407m
	Drift Potential	Value from nearby station, NCDC	15-111knot
	Average temperature	Value from nearby station, NCDC	7.72-9.96°C
	Effective moisture (P/PET)	Value from nearby station, NCDC	0.38-1.12
	Size of largest vegetation patches nearby	Measured using Polygon tool on GE	1398-7.2*$10^7$$m^2$
	distance of largest vegetation patches nearby	Measured using Ruler tool on GE	0-6404m
	Initial Moran's I	Initial spatial pattern of vegetation distribution	0.80-0.97
	Distance to nearest village/city/farmland	Measured using Ruler tool on GE	550-7447m
Human	Distance to nearest waterbody <2km	Measured using Ruler tool on GE	0, 1
	Size of nearest village/city/farmland	Measured using Polygon tool on GE	760-3.2*$10^7$$m^2$
	Grid density on dune	DN value measured on GE	0-0.616

Similarly as in Section 2.1, I decomposed the variables using PCA. PC1, PC2 and PC3 are related to climate, human and vegetation spatial distribution respectively (Table 7). The first five PCs explain 81.6% of the total variation (Figure 16a). From the variable factor map, drift potential and precipitation are major factors explaining the climate component (Figure 16b).

Table 7 Principal Components of variables explaining vegetation cover change rate

	Dim.1	*Dim.2*	*Dim.3*	*Dim.4*	*Dim.5*
elev	0.424	10.332	26.722	6.916	3.649
grids	3.894	15.497	12.655	1.448	8.578
dist_large_veg	21.038	2.616	13.169	3.011	8.111
size_large_veg	8.613	12.464	10.249	6.248	0.465
dist_town	4.186	0.006	1.439	20.124	42.655
size_town	3.510	24.541	0.060	8.897	8.440
DP	21.929	15.588	2.373	4.738	7.132
prec	28.323	5.948	14.055	0.073	0.046
temp	7.861	10.833	6.463	21.178	3.275
moran1	0.222	2.175	12.814	27.368	17.649

With these top five principal components as inputs, I used Random Forest methods to identify the major contributor to vegetation cover change rate. The random forest regression on vegetation cover change rate using these five PCs shows that the human dimension (PC2) is the most important factor, while the climate dimension (PC1) only ranks 4th amongst all PCs (Figure 16c).

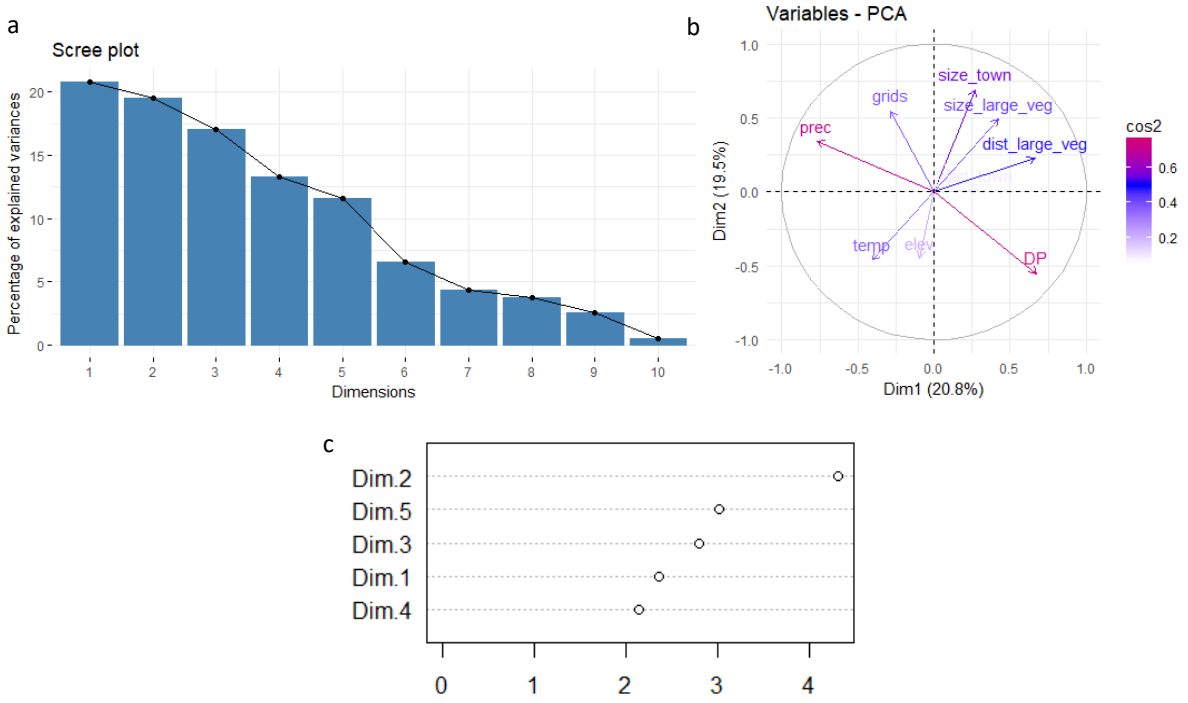

Figure 16 Scree plot (a) and variable factor map (b) of variables explaining vegetation cover change rate after PCA; PC variable importance in explaining vegetation cover change rate (c)

Random Forest and Multivariate Regression are not suitable for this analysis. Instability in variable importance generated by Random Forest models increases with decreasing sample size, and the power of Multivariate Regression would be only 0.3 for significant level = 0.1 with our dataset, much smaller than 0.7 in the Multivariate Regression model in Chapter 2.2 (Table 5a). With that background, I chose SVM model to predict vegetation growth rate.

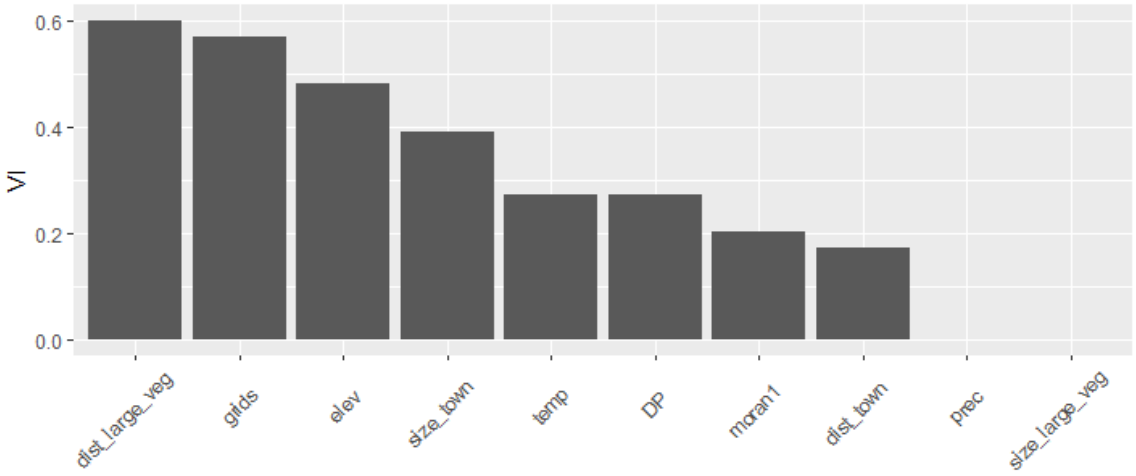

Figure 17 Variable importance in explaining vegetation cover change in patches

The prediction using SVM yields an MSE of 0.965 $(m/y)^2$. Comparing these ten features, distance to largest vegetation patch, grid density, elevation and size to nearest town play the most significant roles in determining vegetation cover change rate (Figure 17). This is coherent with the importance ranking of PCs, where the largest contribution comes from the human dimension.

To understand how vegetation cover change responds to the four most important variables, I performed sensitivity analysis. Specifically, I adjusted values of these variables in the test data by adding 1 standard deviation, 2 standard deviation, substracting 1 standard deviation, 2 standard deviation to their original values, and predicting their corresponding vegetation cover change rates using the SVM model trained with original data. From Figure 18, the vegetation cover change is most sensitive to grid density and elevation.

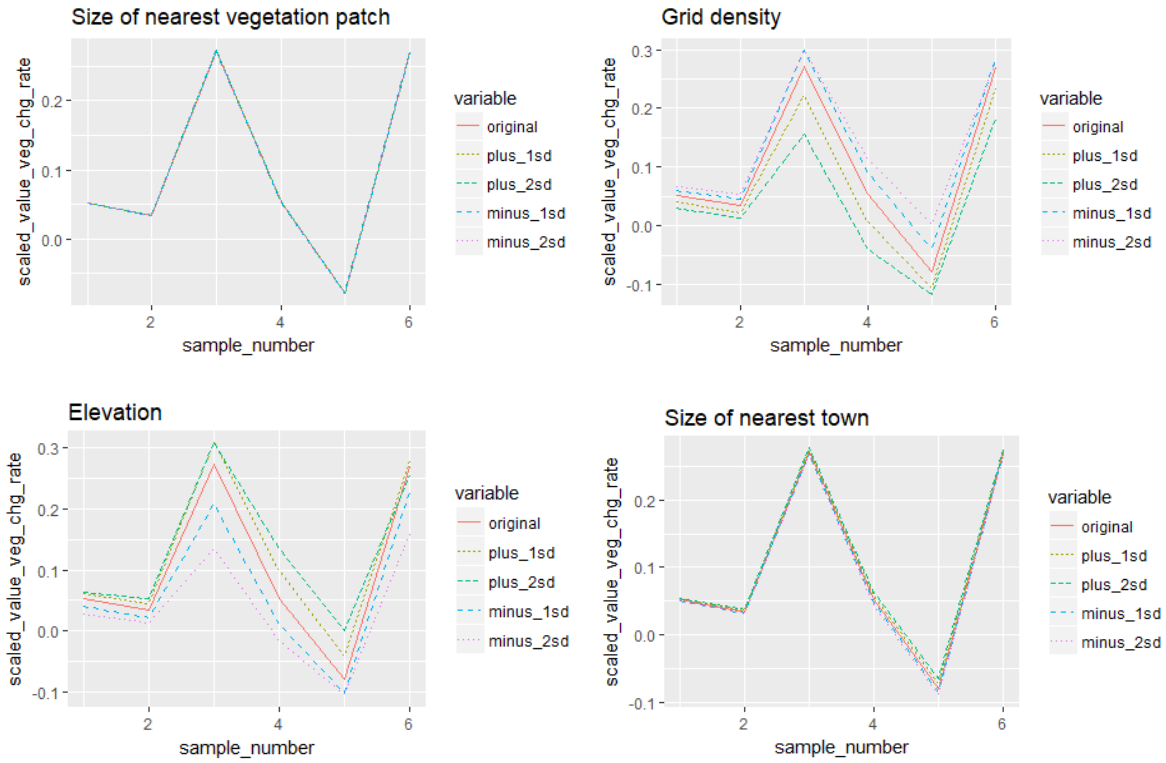

Figure 18 Sensitivity analysis on top features generated by SVM

X axis refers to sample points in the test dataset

To sum up, size of nearest vegetation patch, grid density, elevation, and size of nearest town are the most important factors in determining vegetation cover change rate based on SVM simulations. This change rate is most sensitive to the density of wind breaking grids and elevation among these top factors. SVM model on original features and RF model on PCs both suggest that human activities have stronger influence on vegetation growth than spatial climate variation in Mu Us dune field. Constructing grids is an effective practice in encouraging vegetation growth. The location effect of these man-made grids will be explored in Chapter 4 using vegetation integrated CA model.

Conclusions and Discussion

The analyses presented here provide interesting and potentially important insights on current environmental changes in the Mu Us dune field. These insights represent a new contribution resulting from the application of machine learning methods to data retrieved from Google Earth images, an approach rarely undertaken in past research on dune field geomorphology. The good fit as demonstrated by low MSE values shows that the models developed here can be effective tools in evaluating the importance of factors contributing to spatial variations of environmental variables.

The importance of elevation and variables related to vegetation patterns and human activity as predictors of current rates of dune migration and vegetation change is especially noteworthy. These results may at first appear to conflict with previous interpretations of recent change in the dune field, in which expanding vegetation cover and stabilization has been related mainly to decreased DP since the 1970s, and possibly also to higher temperature and a longer growing season (Xu et al., 2015).

The analyses in this chapter do not actually test that hypotheses, however. The major drop in DP at stations in and around the dune field occurred prior to 2000, and DP has been at relatively low levels since then, although with interannual variation (see Introduction). Xu et al. (2015) emphasize that if the current stabilization of the dune field is driven by reduced DP, it must be a lagged response, since only limited stabilization was found by Mason et al. (2008) using imagery up to about 2003. The significant upward trend of temperature before 2000 is also not evident in the years covered by this chapter's analyses. The climate variables used as predictors here are those of the first images, so they would not reflect current trends even if they were present. Instead, the climate variables in this analysis largely represent spatial variation across the dune field, which is substantial but apparently is not an important factor in determining spatial variation of dune migration rates and vegetation change.

With that background, the results presented here can be interpreted as follows: In the present environment of generally stable dune fields (with some local exceptions), elevation emerges as one of the most important factors influencing the migration rate of still active dunes and the local rate of vegetation change. As noted earlier, this can be explained as an effect of greater wind exposure at higher elevations, although greater depth to the water table may also play a role. The importance of variables representing vegetation patchiness (Moran's I), adjacent interdune sizes, and vegetation patch size in prediction of migration rate suggest that local vegetation distribution represents limitations on overall sand flux across the landscape that influence dune migration. For vegetation change, both elevation and the presence of grids are important factors, not surprisingly. The size of nearby towns is important for both dune migration and vegetation change, probably because of greater human disturbance of many kinds near towns.

Overall, these results emphasize the importance of non-climatic factors as controls of local dune activity and vegetation change in the Mu Us dune field, even if overall stabilization is occurring in response to climate change. These factors include more or less permanent topographic effects as well as dynamic effects of human activity and the expansion of vegetation from existing patches.

Admittedly, the methodology presented in this chapter is not without limitations. Satellite images provide an intuitive way for studying environmental changes of dune fields. However, data accuracy can be affected by several factors in the process of data collection and image processing. First, defining dune boundaries can be highly subjective. The task of assigning points, lines or polygons to represent dune features is often up to the decision of observers, making results difficult to reproduce (Hugenholtz and Barchyn, 2010; Hugenholtz et al., 2012). The GeoVisual tool launched by Descartes lab[1] uses neural networks to recognize objects (such as airport runways, wind turbines and sand dunes) and detect similarities on maps based on Landsat 8 or NAIP Aerial

[1] search.descarteslabs.com

Images. However, their visual search tool is not applicable to this research since it lacks historical images. In addition, dune forms can change significantly through time; therefore the task of identifying the same sand dune in a later image can only be completed with the knowledge of both its position and shape. This can make automatic detection using machine learning very challenging. As a result, the number of sample points is limited since the human sampling and classification process is slow. Second, the selection of study areas is subject to the availability of clear and cloudless images, therefore dune patches are not randomly distributed. However, these areas cover most of central, west and north of Mu Us dune field, where the variation in vegetation cover, climate, elevation, etc. is sufficiently large. Third, there are issues related to the use of DN to estimate vegetation change. After the conversion from RGB to gray scale, I adjusted the brightness of about half the images since the light varies between images taken at different times. In this study, I selected control points on bare sand (that is not in the shade) from a pair of images, and assigned these control points the same DN value, thereby aligning the brightness of both images to the same scale. However, other reasons can potentially explain the difference in brightness of the control points, such as early vegetation colonization that might appear slightly darker than bare sand.

Chapter 3. Cellular Automaton (CA) dune formation model

Wind is the primary discriminator in dune pattern formation. Lancaster (1995) found broad agreement between theoretical and observed relationships of wind regime and dune forms. Wind speed and direction are the two aspects of its effect on dune forms. For example, barchan dunes are formed under unidirectional wind, and linear dunes are often shaped by two wind streams at a high angle to each other. The complexity of dune forms reflects in part the complexity of wind regimes: dune dynamics respond not only to regional wind patterns, but also to interactions between dune morphology and secondary local flow regimes (Livingstone et al., 2007). In addition, dune patterns formed can be complicated due to the time required for dunes to respond to rapid climate change (Kocurek and Ewing, 2005).

Despite the well-documented complexity of the processes influencing dune morphology, Werner (1995) successfully produced barchan, linear and star dune forms using a CA model of sand transport, without directly addressing the internal dynamics and nonlinear feedback mechanisms in sand dune formation process. To simulate sand transport by winds from varying directions, the Werner model defines a slab displacement along varying directions. Nield and Baas (2007) pointed out that this method is restricted by overall length of displacement and proposed a simple alternative of rotating the cell grid, but their method is restricted by edge effects. Modeling transport and dune form evolution resulting from bimodal or multimodal wind directions remains a challenge to be solved (Nield and Baas, 2007). In this research, I focus on dunes formed under unidirectional winds. Unidirectional winds not only dominate the Mu Us dune field, but also many other parts of the world. For example, in North American Great Plains, unidirectional wind regimes dominates over 180,000 km^2 of dune fields (Halfen and Johnson, 2013). Researchers estimated that

migrating crescent dunes formed under unidirectional wind occupy about half of the total area of desert dune fields (Wasson and Hyde, 1983).

The goal of this chapter was to construct a dune morphology model to simulate major changes in wind strength, such as the decrease that occurred in northern China since the 1970s. I first built a generic model simulating the formation of barchan dunes following Werner (1995). Then I set the model space to reflect the temporal and spatial scales appropriate to the study areas, and adjusted different model parameters to observe how they affect the output dune forms. The parameter that best describes the effect of wind strength changes was then selected.

1. Model description

The Werner (1995) model emulates a closed system with no external sediment source, and the initial state consists of randomly generated patches of sand. The sand initially in those patches represents the maximum volume of sand within the model space that is available to supply transport and dune construction. Sand transport is represented by movement of sand "slabs". One or more slabs sit on a non-erodible flat base. Sand movement involves selection of each grid cell in random order; if slabs are present at the selected cell, the top slab is removed and transported downwind a certain distance. Deposition of this sand slab is subject to a random process. If a random number (between 0 and 1) generated is smaller than deposition probability (p_d), then the height of the sand at such location will increase by one slab thickness. If not deposited, the slab will move downwind and the process is repeated. Bare destination cells are assigned lower p_d values, to reflect the increased saltation distance on rock or other hard surfaces (Bagnold, 1941). In most models, the p_d value is 0.6 for sand-covered surfaces, and 0.4 for bare surfaces (e.g. Werner, 1995; Barchyn and Hugenholtz, 2012). If the destination cell is in a shadow zone, however, the slab will be automatically deposited (p_d =1). Shadow zone refers to the areas on the lee side of the dune that are

shielded from wind erosion, defined by a line from the dune crest to the ground surface at an angle of 15° from horizontal (Figure 19a). The angle in surface elevation constructed between a center cell and its adjacent cells cannot exceed 30°[2] (angle of repose), otherwise a sand slab is brought from the neighbor to the center cell ('avalanching'). If there is more than one slope that exceeds the angle of repose, the model picks the direction with steepest angle and performs the avalanche routine. The process repeats until the angle is below 30° (Figure 19a). The model implemented in this paper can be reflected by the flow chart in Figure 19b.

The model I constructed starts with one layer of sand evenly distributed on the lattice. In each iteration, a function going through each cell and decide whether erode or not randomly: if a randomly generated value is smaller than the preset erosion probability (p_e), then the top slab in that cell is picked up; otherwise the function moves on to the next cell. The difference between this setting and the original Werner (1995) one is that a cell will not be selected multiple times in one iteration in this model, which more realistically reflects the actual wind-sand interactions. Once a sand slab is picked up, it goes through the erosion – transport – deposition process as described above.

Cellular automata (CA) are discrete in time, space and state. In this section, a cellular automaton (A) is defined by a lattice (L) of 100m by 100m, a state space (Q) for sand, a neighborhood window (d) in Rook's case, where four closest cells in N, S, E, W directions surrounding a center cell are considered its 'neighbors', and a local transition function (f) (Adamatzky, 1994).

A = <L, Q, d, f>

[2] 30° is a low estimate of the angle of repose, which is typically 33° or 34°

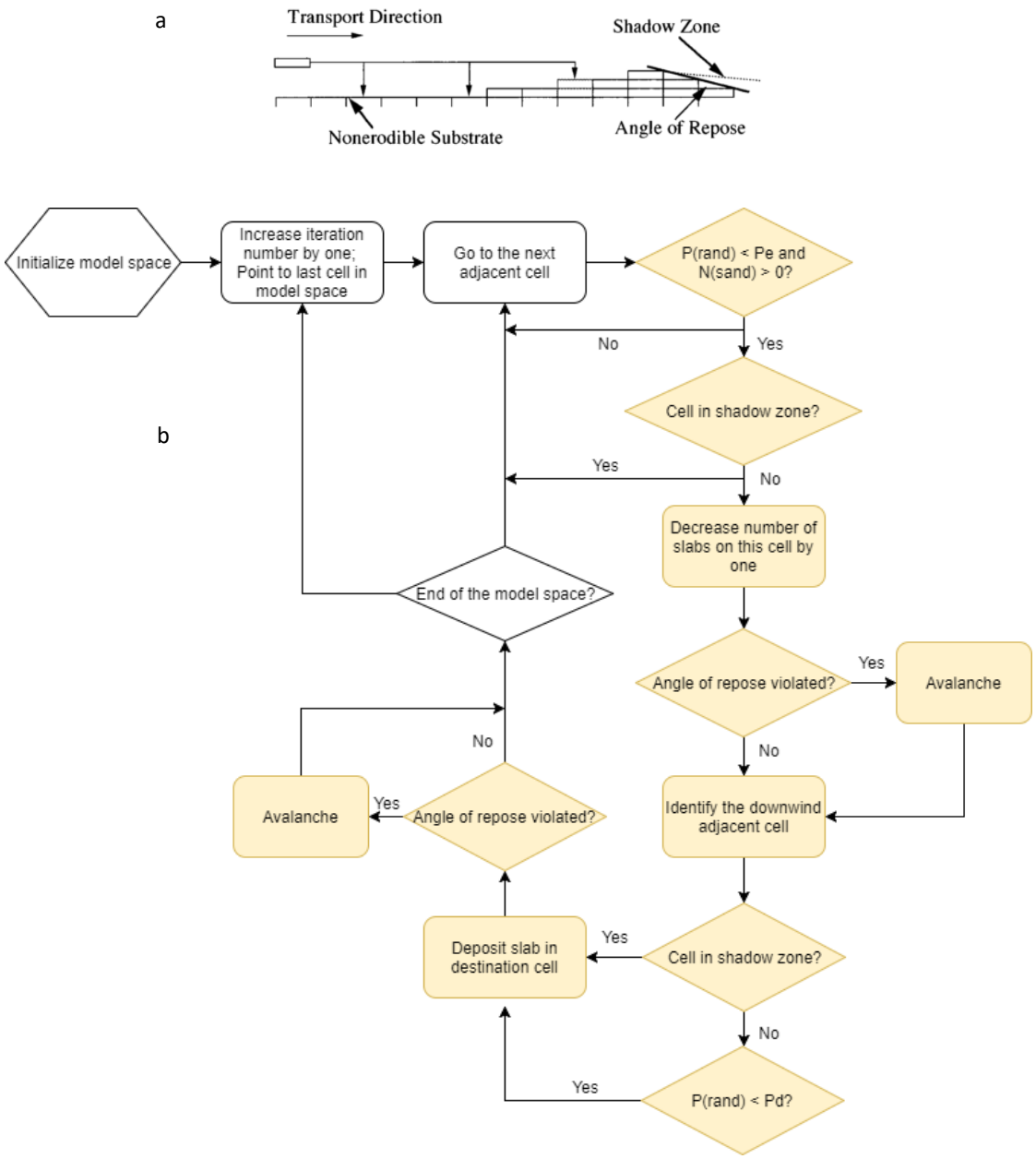

Figure 19 Side view of Werner's dune transport model (a, Werner, 1995); Flow chart of the model in the current research (b)

Yellow color in the flow chart indicates processes that happen to one sand slab

2. Model parameters

The parameters and concepts that are key to the CA model are briefly described below:

Deposition (settlement) probability: Deposition probability for sandy surfaces (p_s) is usually set at higher values than that for bedrock (p_n) to reflect differences in momentum absorption (Bagnold, 1941). Most workers have set $p_s = 0.6$ and $p_n = 0.4$ following Werner (1995). Both p_s and p_n are set to 1 in shadow zones. Slabs move along the wind direction unless they are transported by avalanching to enforce angle of repose.

Erosion probability: p_e was first introduced to the original Werner (1995) model by Baas (2002) to reflect the interaction between vegetation and sand transport.

Deposition jump unit: Number of cells that a sand slab moves downwind each time it is picked up or deflected. Most workers used d=1m (length of the side of a cell), which is more realistic distance at the dune scale than at ripple scale (Eastwood et al., 2011). Nield and Baas (2007) pointed out that increasing d has a similar effect as diluting the model space along the wind direction.

Shadow zone: Sand slabs that are transported downwind into a shadow zone will be deposited immediately. The shadow zone angle is set at 15° following most studies (Werner, 1995; Baas, 2002; Nield and Baas, 2007). Barchyn and Hugenholtz (2012b) found that this value affects maximum height of formed dunes.

Slab thickness: Number of slabs (h) picked up by wind in each iteration. It represents the amount of sediment available for transport; increasing h can increase the size of resultant dunes and change their shapes (Nield and Baas, 2007).

Dynamic/Periodic boundary: The 100m by 100m model space in this research has periodic boundaries along the y axis. That is, slabs that fall off the boundary (x=101m) are brought back to x=0m. This ensures that the model space does not have external sand sources; that is, no sand enters or leaves the system during model runs.

Avalanche: Avalanching refers to the procedure of moving neighboring slabs downhill to ensure that the angle of repose remains less than 30°. The algorithm assesses angle of repose between the 4 nearest neighbors of a given cell (N, S, E, and W; Rook's case). If there is more than one slope that exceeds the angle of repose, the model picks the directions with the steepest angle to perform the avalanche routine. Researchers believe that avalanching is one of the key controlling factors on the forms of dunes, regardless of their scales (Vandewalle and Galam, 1999; Werner, 1995). Avalanche frequency has been used to measure dune mobility in an iteration as an indicator for dune form stability (Nield and Baas, 2007).

Number of iterations: The number of iterations taken to stabilize dunes. This parameter can be associated with number of years according to time and distance measured from remote sensing images or other local records.

EST (Equivalent Sediment Thickness): The parameter that represents EST in the model is initial thickness (h_0) if the sand is distributed as a sheet of uniform thickness, or average initial thickness if the model starts with sand distributed in patches. Dune fields with greater EST typically form transverse dunes (high RDP/DP, that is, unimodal winds) or star dunes (low RDP/DP, multimodal winds), while sand sheets with thinner EST eventually converge into barchan dunes (high RDP/DP) or longitudinal dunes (low RDP/DP, bimodal winds) (Wasson and Hyde, 1983). Because of the dynamic boundary setting in the model, EST remains the same throughout all iterations.

3. Sand flux

Sand flux (m^3/s) q is defined as

$q = Q/t$,

where Q is the volume of sand transported along x direction within time t. In essence, Q is number of slabs times the volume of each slab (1*1*h, where h is the slab thickness). A fraction (p_d) of all slabs will travel one unit distance (d); another fraction of sand slabs ($(1- p_d)* p_d$) will travel 2d; and so on. The expected distance (D) that any sand slab travels is

$$E(D) = d*(1+2(1- p_d) + 3(1- p_d)^2 + \dots n(1- p_d)^{n-1}) \longrightarrow d/ p_d^2, \text{ as } n \longrightarrow \infty$$

Since I have a large number (10,000) of sand slabs to start with, this approximation is reasonable. For a vertical window of length L and height h perpendicular to wind direction, the expected sand volume transported is:

$$E(Q)= L*h* p_e * p_d *d / p^2_d = L*h* p_e *d/ p_d$$

Where h is the thickness of each sand slab; L is the length of each slab, which is defined as 1m here. p_e is the erosion probability at the start of a transportation cycle. Pd is the deposition probability at the destination cell. Both Pe and Pd can vary depending on the condition of this cell (bare sand, vegetated, ground). The expected (average) sand flux is therefore

$$E(q) = E(Q/t) = L*h* p_e *d/(p_d *t) = (L*h)*(p_e / p_d)*d/t \quad (1)$$

This is consistent with the form of volumetric flow rate defined as q = A * v where A is the area of plane cross-section, and v is the sand transport velocity. From equation (1), average sand flux is directly related with number of units a slab is transported downwind in each jump (d); thickness of sand slabs (h); deposition probability (p_d); erosion probability (pe). These variables will be adjusted independently in Section 3.4 to assess their effects on dune forms produced by the CA model. Equation (1) also shows that q has nothing to do with the initial thickness of sand sheet (h_0).

4. Experiments and Results

In this section, a simulated Mu Us dune form is created from a flat bed based on a modified CA model, where some model parameters are adjusted according to information extracted from Google Earth Images to reflect local conditions. This Mu Us dune model is then used to test hypothetical scenarios, such as the drop of wind speed sufficient to lower DP by about 150 VU between 1980 and1995 in this area (Xu et al., 2015).

Researchers have tuned parameters in Werner (1995) model to fit it to their research area. For example, Pelletier et al., (2009) adjusted d and p_s to 5 pixels and 0.5 respectively to emulate dune forms at Jockey's Ridge, NC. However, very few researchers have thoroughly tested effects of varying model parameters and used the results to justify selection of particular values for simulating dune processes in a given area. In this section, I will test six model parameters from equation (1) and examine their effects on dune forms and sand transport by adjusting their values. These parameters are: number of units a slab is transported downwind in each jump (d); thickness of sand slabs (h); deposition probability (p_d); erosion probability (p_e), and initial thickness of sand slabs (h0).

Dune size and spacing increase with wind speed and sand transport rates (Wilson, 1972); the relation between dune height and spacing can be approximated by a power function (Lancaster, 1988b). It is difficult to quantitatively compare fully active dune forms in the Mu Us dune field before the large change of DP that occurred since the 1970s; older Landsat images have low resolution and US spy satellite photos provide limited coverage and are difficult to georeference. However, it appears that there have not been major changes in the basic form of the active crescentic dunes in this area. Therefore a parameter that adequately represents wind speed will be one that, when changed, allows dunes to change their height and spacing but does not alter their basic form.

a. Original settings

The original settings generally follow Werner (1995), but start with a flat sheet of sand of 1m thickness over the 100m by 100m field. The model forms dunes that merge and grow in size until a steady state is reached. Baas (2002), Pelletier et al. (2009) and Barchyn and Hugenholtz (2012) initiated their models with similar settings. After dune forms are established, they migrate downwind steadily while maintaining their forms.

Three parameters are generated during the model runtime to quantitatively describe the process: maximum height of dunes, avalanche frequency (number of avalanches in each iteration), and number of slabs crossing the border in each iteration. Maximum height of dunes is an indicator of largest dune size: for a given height, the size of dune is restricted because of angle of repose. It also reflects dune migration rate, which is inversely proportional to dune height (assuming sand transport rates are independent of dune height) (Bagnold, 1941). Frequency of avalanches is used as a measure of dune mobility (Nield and Baas, 2007). The number of sand slabs crossing the border approximates sand flux q. All these parameters are recorded every cycle, which is composed of 100 iterations in the original setting; each iteration is an erosion-deposition process for each randomly picked cell. All these parameters can potentially indicate the 'steady state' of active dunes.

From the model output, dune migration rate stabilizes after about 30 cycles when both maximum dune height and avalanche frequency start to flatten out (Figure 20). The maximum number of slabs crossing the model border occurs in the beginning of the simulation when the model is 'tuning up'. The cyclic pattern after about 20 cycles reflects the alternation between formed dune hills and inter-dune plains that are crossing the border (Figure 20d).

Since dune migration speed is inversely related with dune size (Werner, 1995), smaller barchan dunes eventually catch up with larger ones (Figure 20 cycle 30 to cycle 40). In this case maximum height started to level off after about 30 cycles, when crescentic dunes collided and merged into two major crescentic ridges. These crescentic ridges did not break into barchan dunes after they formed, consistent with Werner (1995). This suggests that the 'attractor' of the CA model can be the number of dune-crest terminations (Werner, 1995), and the final stage of all simulations could be some form of crescentic ridges. Later experiments in this chapter will focus on the process that leads to a stable dune form (i.e., little change in form or size, not stabilized by vegetation), with a stable avalanching frequency.

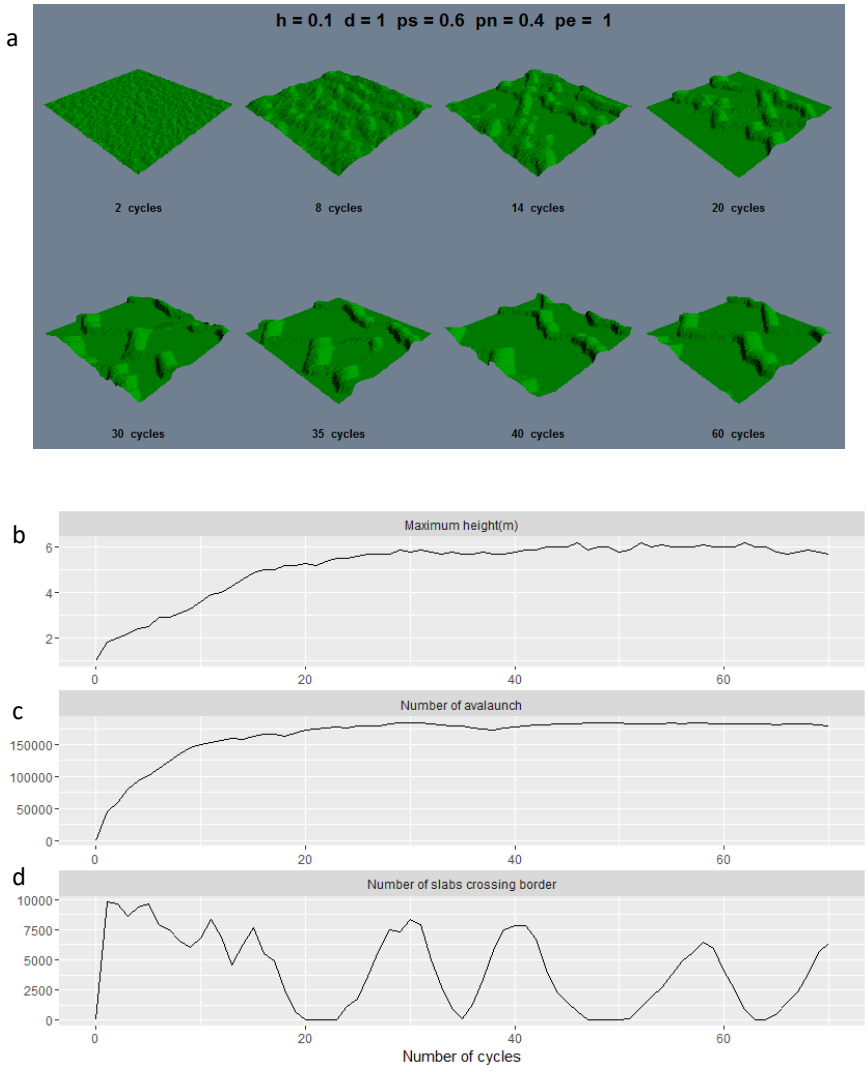

Figure 20 Simulation results using CA model with original settings

Slab thickness (h) = 0.1m, slab transport jump (d) = 1m, deposition probability on sandy surface (p_s) of 0.6, on non-sand surface (pn) = 0.4, erosion probability = 1. One cycle is defined as 100 iterations. a: dune forms; b: maximum height with time; c. avalanche frequency with time; d. number of slabs crossing border with time

To fit the model space to the actual dune field, I used the average dune migration speed calculated from satellite images, 3m/y (Chapter 2.2), which is close to the estimate of Xu et al. (2015). The actual value depends on a range of factors such as size of dune and vegetation growth rate (Duran and Herrmann, 2006; Xu et al., 2015). In the current simulation, dunes migrate at about 8m per 100 iterations after dunes are formed. Therefore 100 iterations represent 2.67 years, i.e. one year's time equates to approximately 38 iterations for Mu Us dune field. This is comparable to other research areas, such as a coastal dune field in Brazil where a yearly cycle of 50 iterations is applied (Baas and Nield, 2010). This calibration can be used to estimate the time scale of dune form evolution, for example in Figure 20b, the dune forms become stable at around 30 *100/38 = 78 years. However, at this the stable stage, the dunes are 20 - 50m in length along the migration direction (Figure 20a), which is about one third the size of most active dunes in the Mu Us study areas (50-150m) based on the measurements from Google Earth images (Chapter 2). The stable maximum height reached after 30 cycles (Figure 20b) also implies a lee face length at the low end of those reported by Xu et al. (2015). This discrepancy needs further investigation. It may be resolvable by simply changing the assumed spatial scale so that one grid cell is 3 by 3 m, in which case one year = 12.5 iterations, which is considerably fewer than estimated for other dune fields with similar models. The original spatial scale (1 by 1 m grid) and estimated time scale (38 iterations per year) is used below in this chapter and Chapter 4; using the adjusted scale would not change most conclusions other than those on the timescale of changing dune forms.

b. Test model parameters

To simulate dropping wind speed in Mu Us dune field, I will modify parameters in this model and examine how dune forms will respond. Though decreasing time span of transport (t) or increasing slab length (L) can both increase q based on equation (1), these values will not be modified since they set the temporal and spatial scales of the model: 38 iterations corresponds to one year, and the model space is equivalent to a 100m by 100m field with a unit size of 1m by 1m.

1. Downwind transport jump unit (d)

This section investigates how increasing sand slab downwind migration jump unit (d) may affect dune forms. This value cannot be decreased below d=1m, used in the initial settings, but higher values were tested to see if changing d can be used to represent wind speed changes in general. Using (d) to 2m while keeping everything else the same, barchan dunes still formed, though much larger in size (Fig. 3b); when d=3m (not shown), 4m or 8m, dune forms become obscured with reduced slopes on the slip faces. In fact, in order for realistic barchan dunes to form, the value of d cannot be larger than 2m. The number of slabs crossing the border is roughly proportional to the value of d. In addition, the size of the dunes decreases as d increases.

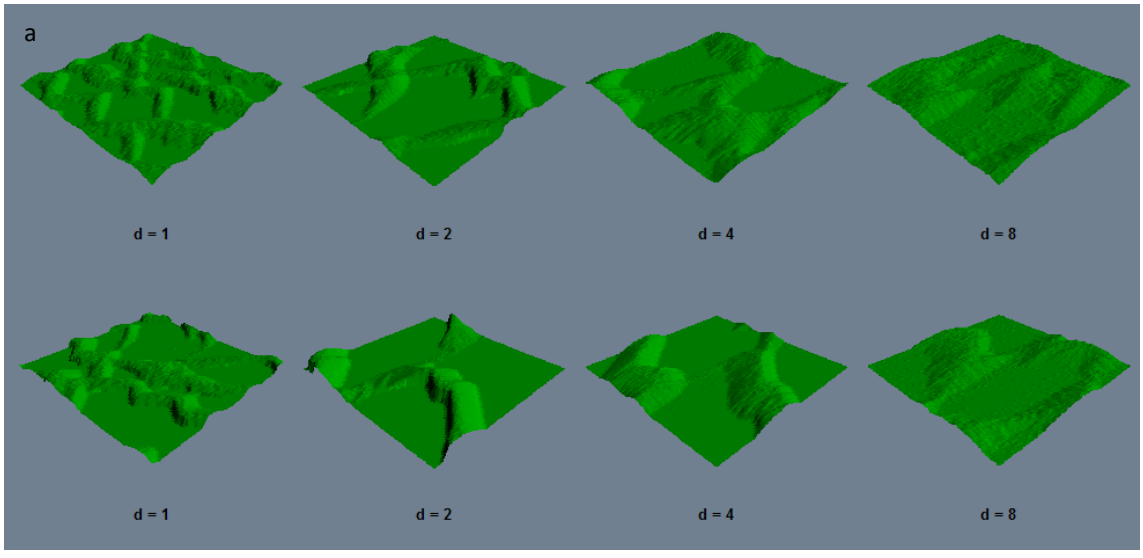

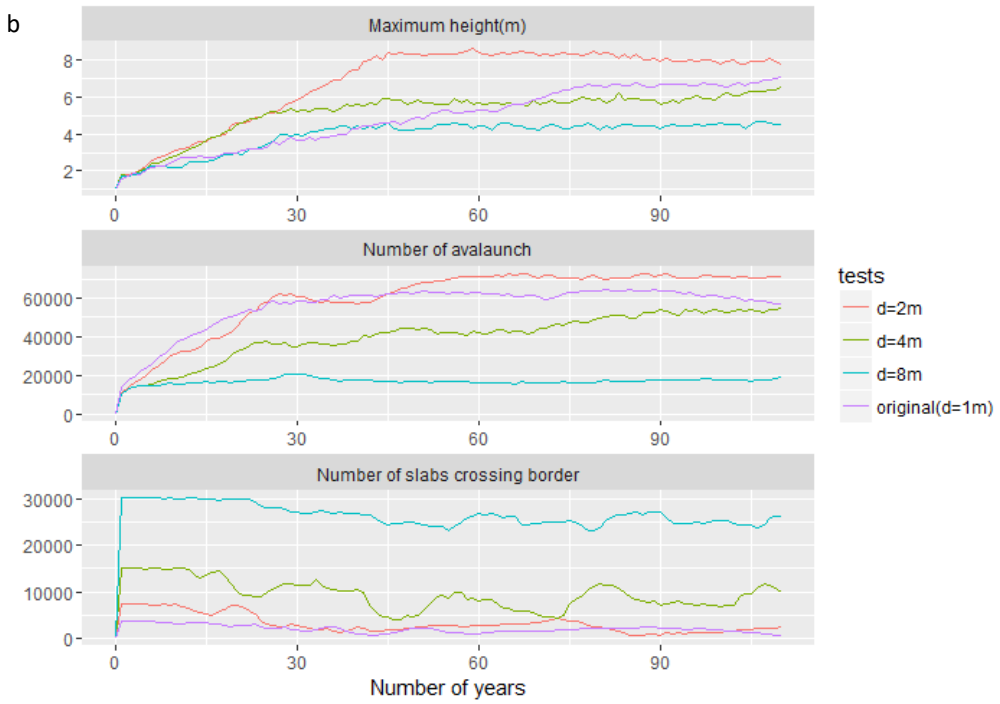

Figure 21 Dune forms with modified downwind transport jump unit

a. (first row: after 20 years; second row: after 50 years) adjusting d; b. statistics of model results

In a word, d cannot be used to simulate wind effect since its value can only be set at 1m or 2m, because realistic dunes are not formed with larger values.

2. Slab thickness (h)

Baas (2002) and Nield and Baas (2007) simulated changes in wind power through modifying the number of slabs that are picked up in each cycle. Based on equation (1), h*L is the volumetric component in q. L is not a parameter to be modified, since the model is built on 1m by 1m grids and increasing L is equivalent to enlarging the field size that the model lattice represents. However, slab thickness h does not have such restrictions and can be any value.

Test results (Figure 22) show that compared with the original settings, it takes longer for dunes to reach a stable form when slab thickness decreases. For h = 0.08m and 0.11m, barchan dunes still

emerged after 30-40 years. Average number of avalanches is close to the value with the original settings, and maximum height of dunes is close as well. No dune structure can be observed, however, when h is as high as 0.13m.

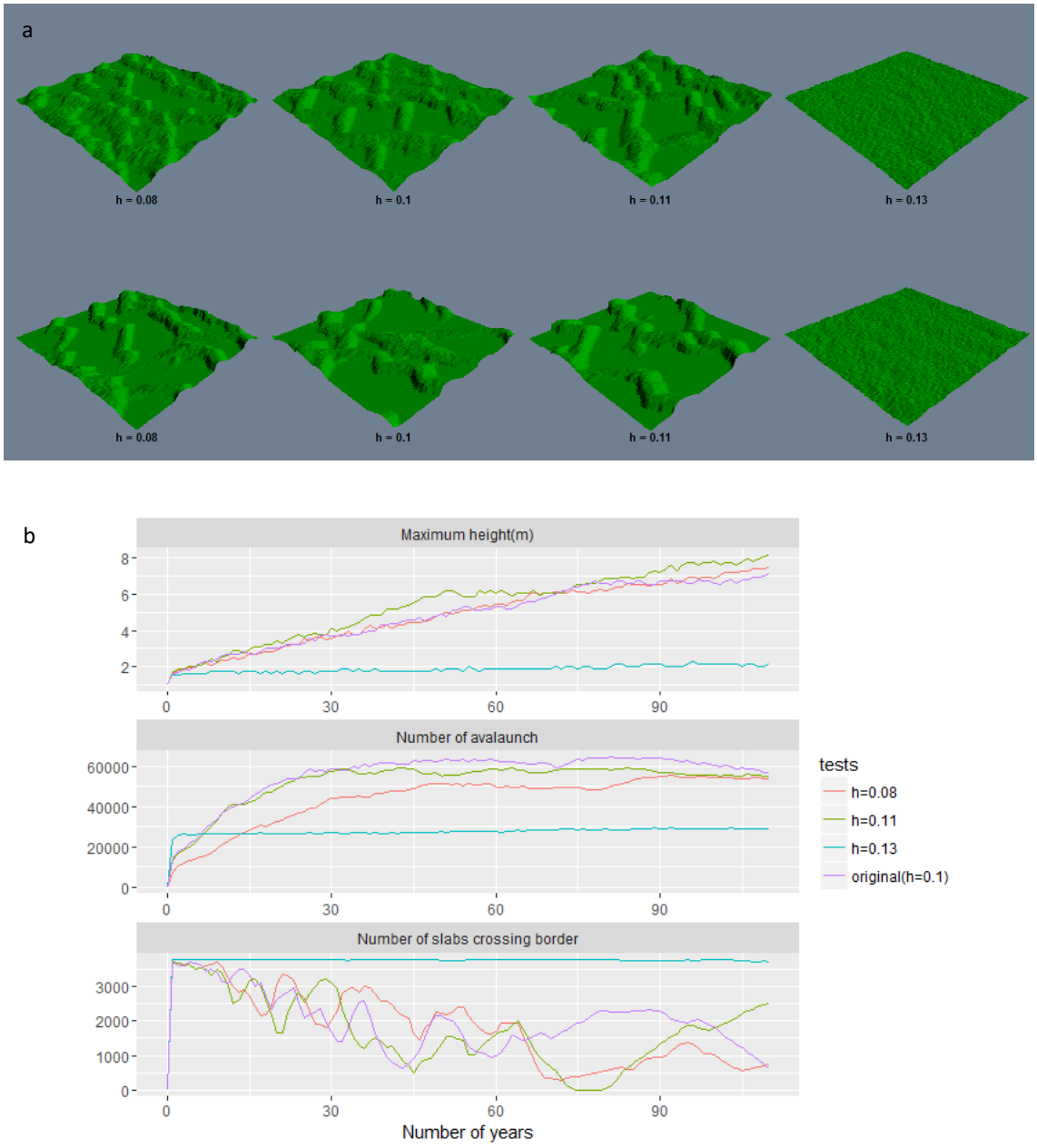

Figure 22 Dune forms with modified slab thickness h

a: first row: after 20 years; second row: after 50 years; b. statistics of model results

From the simulations, no dune forms can be observed when slab thickness is set to be larger than 0.12m or smaller than 0.06m (not shown). Even when starting from established dune forms, the landscape can be obscured after 1 or 2 years if h is outside of the 0.06 - 0.12m range. The figure on number of slabs crossing the border shows a cyclic pattern with an increasing period, suggesting that large dunes are formed with expanding space in between.

Nield and Baas (2007) reported the relationship between dune speed and shear velocity using Sharp's ripple speed equation (1963). Assuming a roughness length of 0.2mm, speed c follows:

$$C = 1.96*10^{-3}U_* - 7.78*10^{-4} \quad (2)$$

Where U_* is the shear velocity.

Bagnold's transport equation (1941) links transport rate q to a range of shear velocities u_*:

$$q = C \frac{\rho}{g} \sqrt{\frac{d}{D}} u_*^3 \quad (3)$$

The velocity component of equation (1) u can be written as

$$u = q/h \quad (4)$$

Where u is the slab transport velocity. C/q should be in proportion to u/q. Assuming a sediment grain size of d =0.3 and sand bulk density of 1600kg/m^3, with (2), (3), (4), and the fact that c/q ~ u/q = 1/h, h should range from 0.077 to 0.13m (after Nield and Baas, 2007), which is consistent with the present model simulation (0.06 - 0.12m).

Overall, one can adjust h as long as its value falls within the range of 0.06-0.12m (these experiments) or 0.077 - 0.13m (based on the analysis of Nield and Baas, 2007). The barchan dunes generated by different h values converge in maximum height, instead of having various sizes according to wind speed, however. In addition, this appropriate range of variation of h is relatively small, limiting its utility in representing large changes in wind speed.

3. Deposition probability (ps and pn)

Deposition probability at sites without sand slabs is often set to be lower than at those covered by sand, because of lower rebound saltation possibility on sandy surfaces (Bagnold, 1941; Werner, 1995; Nield and Baas, 2007). However, dune shapes still form when p_s and p_n are the same value (Fig. 4a). With a lower p_d (0.4/0.2), it takes less time (55 years) than the original settings for dune forms to stabilize (78 years). When p_d is set to higher values (0.8/0.6), formed dunes have smaller slopes on the lee side and demonstrate a different form compared with p_d with lower values. With deposition probability increasing, avalanching frequency decreases.

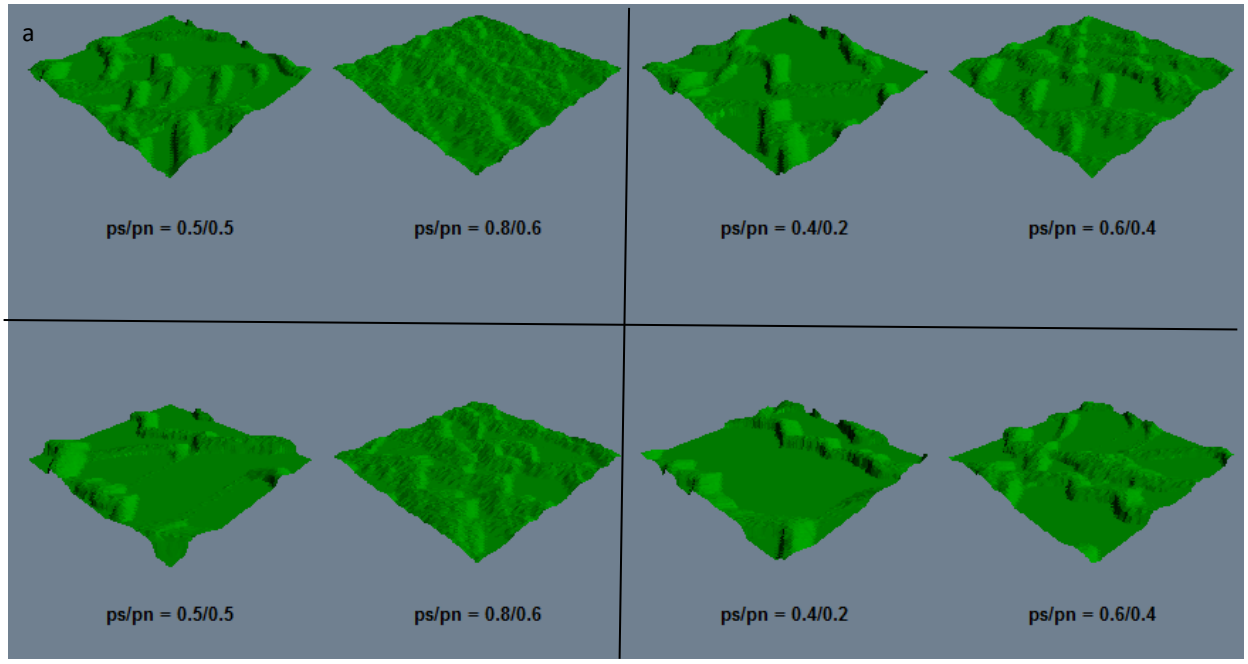

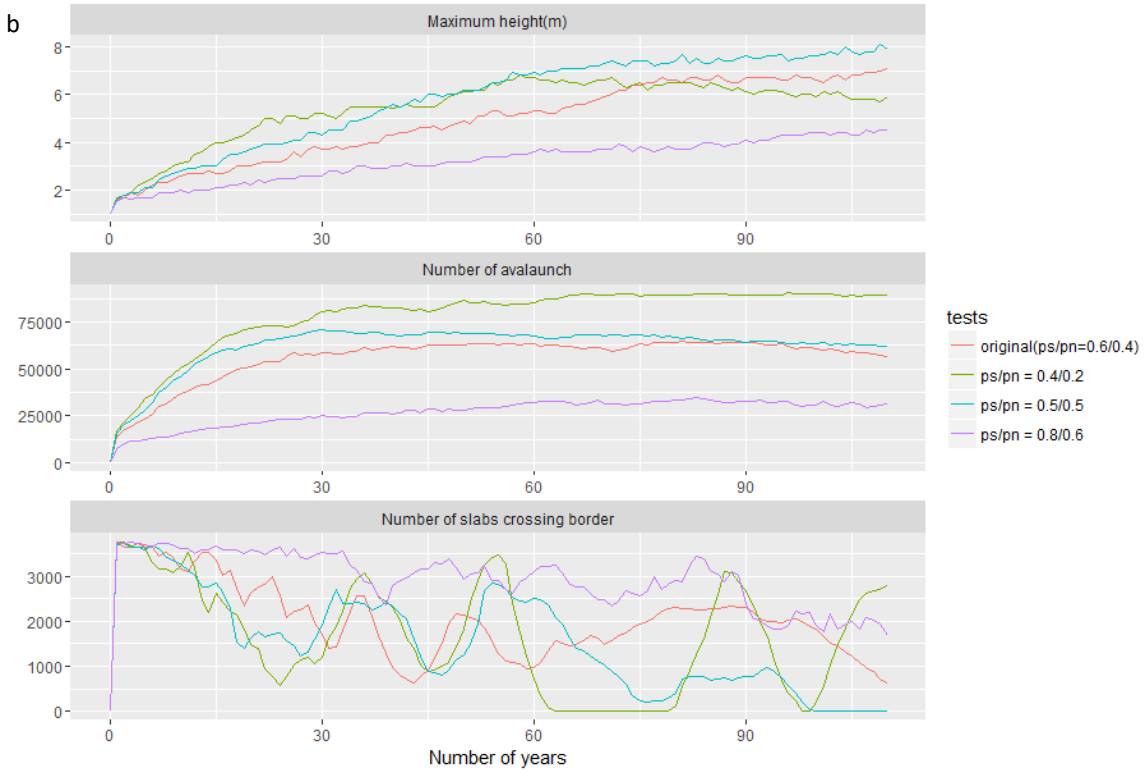

Figure 23 Dune forms with adjusted deposition probability p_d

a. first row: after 20 years; second row: after 50 years; b. statistics of model results

Based on the model output, p_d is not an ideal candidate for the simulation of wind effect, since similar changes in dune forms (Figure 23; especially when p_d is larger) have not been observed in the Mu Us dune field following a large drop in DP.

4. Erosion probability (pe)

In general, the higher p_e is, the larger the size of the dunes that will form. Dune spacing also becomes larger. However, the basic form of the dunes does not change as much as when p_d is changed. It takes longer for the dunes to form in the small p_e setting (p_e = 0.2), which is reasonable since the chance that slabs will be picked up is smaller than in a high p_e setting.

The response of the three parameters (maximum height, number of avalanches, and number of slabs crossing the border) is similar to that from the test on deposition probability (Figure 23).

a

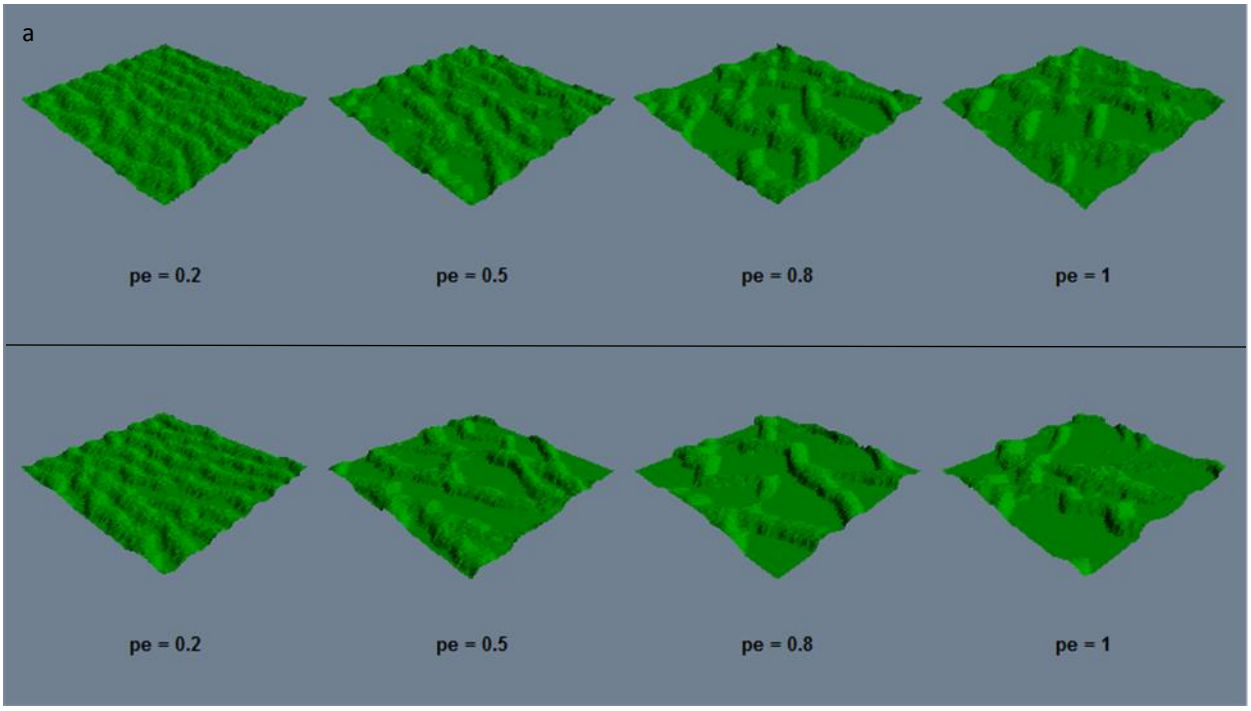
pe = 0.2
pe = 0.5
pe = 0.8
pe = 1
pe = 0.2
pe = 0.5
pe = 0.8
pe = 1

b

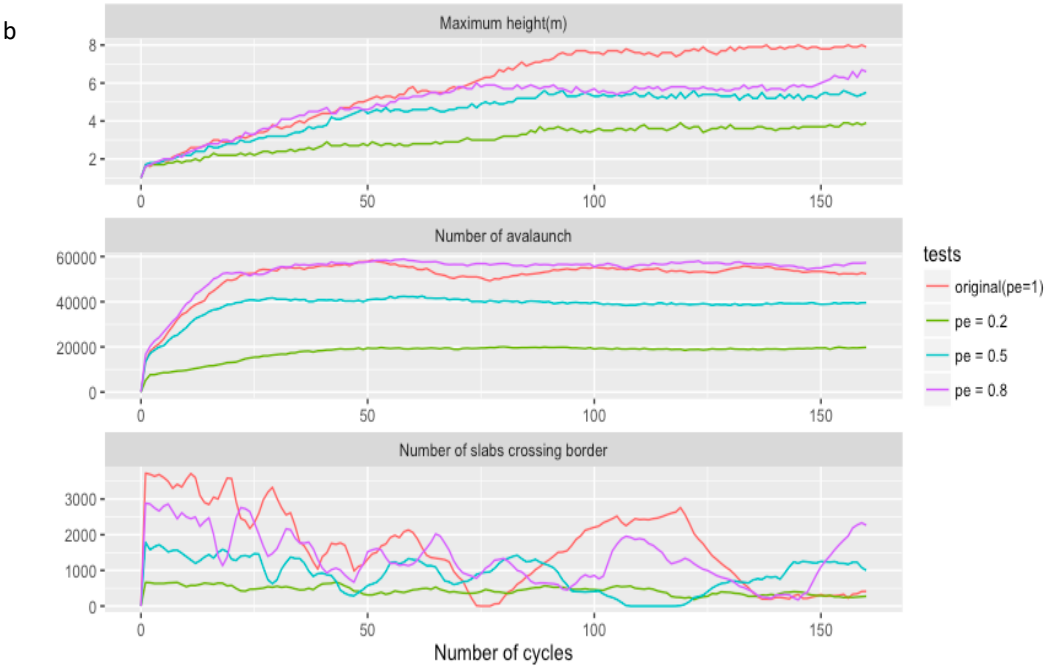
Maximum height(m)
Number of avalaunch
Number of slabs crossing border
Number of cycles
tests
original(pe=1)
pe = 0.2
pe = 0.5
pe = 0.8

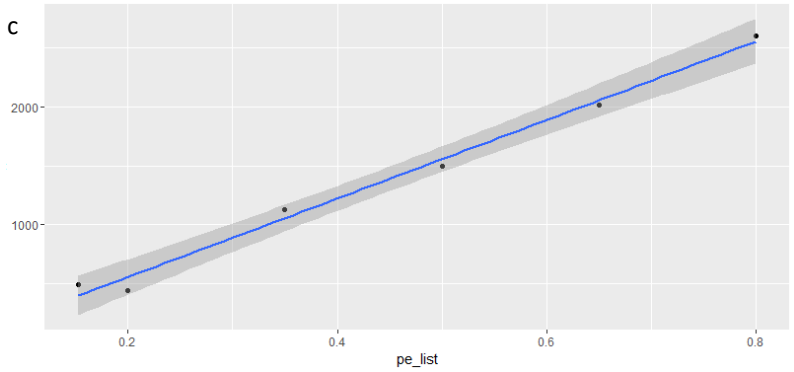

Figure 24 Dune forms with adjusted erosion probability p_e

a. first row: after 20 years; second row: after 50 years; b. statistics of model results; c. linear relationship between number of sand slabs passing a cross section per unit time and value of p_e *used in tests (0.15, 0.2, 0.35, 0.5, 0.65, 0.8, 1)*

p_e and number of sand slabs transport rate roughly follow a linear relationship: $N = -111.33 + 3333.41 * p_e$, with $R^2 = 0.99$, p-value <0.001 (Figure 24).

The experiments above show that the number of avalanches can serve as an indicator of the 'steady state' of dunes (Nield and Baas, 2007); dune height however, often reaches a stable state well after the number of avalanches (Pelletier et al., 2009).

5. Increase initial sand supply (EST, h_0)

Directly linked with sand supply, EST is not an option for simulating effects of increased wind speed because sand supply can vary independently of wind speed (e.g. greater exposure of a sand source because of vegetation or geomorphic processes). However, one can verify the effect of additional sand supply on the resultant dune forms. Typically, dune fields with greater EST form transverse dunes, while those with smaller EST become dominate barchan dunes in a unidirectional wind regime (Wasson and Hyde, 1983; Bishop et al., 2002). With an EST of h_0, the average sand flux for a random 100m by 100m plot in Mu Us dune field is:

$q = 100m^* h_0 * c * p_e$

Therefore increasing h_0 contributes to an increase in sand flux.

Barchan dunes are formed with 1m as initial sand sheet thickness (Figure 20a). As shown in Figure 25 top panel, crescentic ridges are formed with a larger initial sand sheet thickness (2m and 5m). With a rising EST, dune size increases while interdune distance decreases. This observation agrees with findings of (Barchyn and Hugenholtz, (2012). In addition, with an initial sand layer less than 1m, barchan dunes are still formed (Figure 25 bottom panel).

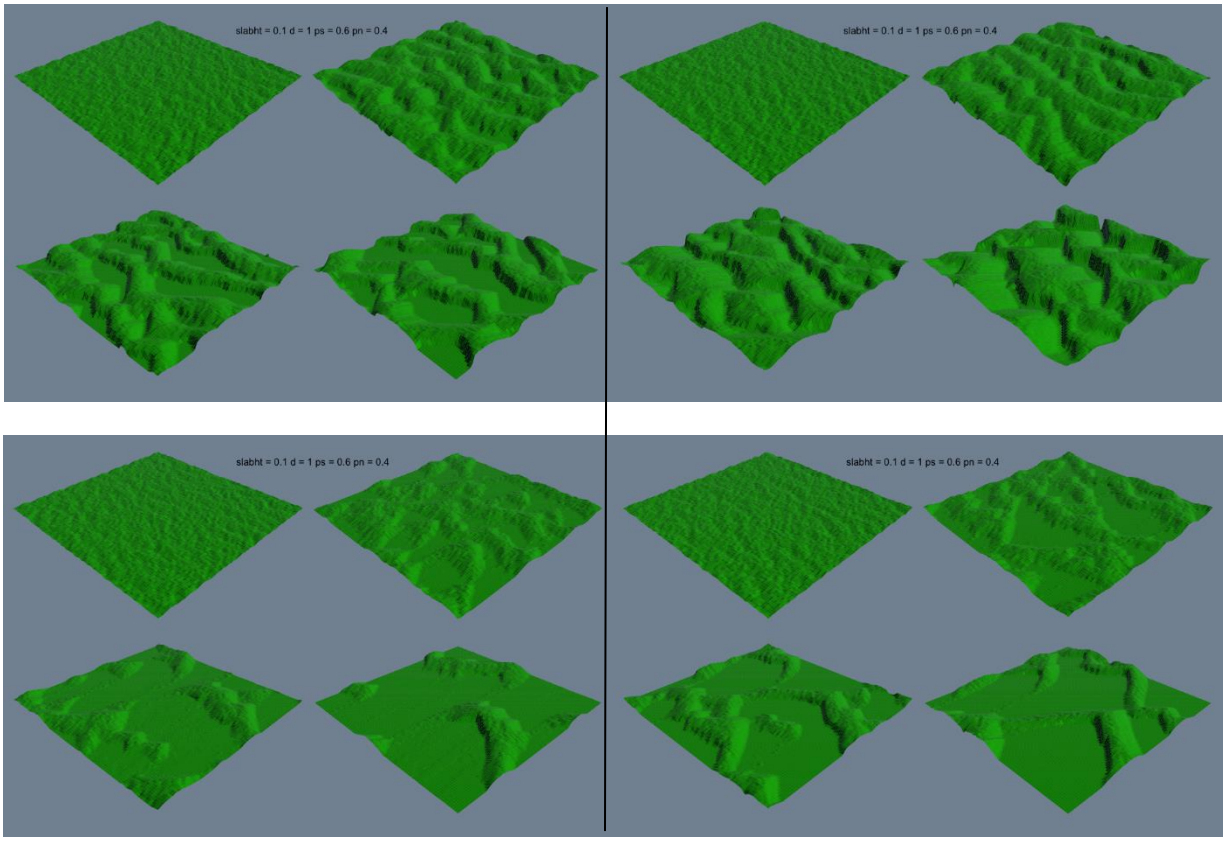

Figure 25 Sand dune development starting from flat surface after 2, 8, 14, and 20 years

(Top panel: Initial sand thickness= 2m, 5m; Bottom panel: initial sand thickness= 0.5m, 0.75m)

c. Modeling wind speed change in the Mu Us dune field

Following Fryberger and Dean (1979), I used wind velocity at 10m above ground for estimating rate of sand transport q:

$$q \propto V^2 (V - V_t)$$

Where V is the wind velocity at 10m height, and V_t is the impact threshold wind velocity at 10m. Q = q*t refers to DP.

The threshold wind velocity V_t can be determined using the following equation (Bagnold, 1941)

$$V_{(10\,m)} = 5.75\ V_t^* \log \frac{Z}{Z'} + V_t'$$

Where the surface roughness factor Z' is 0.3048cm. The threshold wind velocity at height Z' is 2.74m/s (V_t'), and V_t* is 0.16m/s. Using these values, $V_{(10m)}$ is estimated to be 11.6 knots.

An accurate estimate of the recent change in wind transport capacity in the Mu Us dune field should be based on hourly wind data. However, a rough estimate can be based on change in average wind speeds. Around 1980, average wind speed in Mu Us dune field measured at 10m was as high as 14.41knot (v_1). This value dropped down to 12.63 knot (v_2) in 1995 and remained relatively stable afterwards.

$q_1/q_2 = [14.41^2*(14.41 - 11.6)]/[12.63^2*(12.63-11.6)] = 3.55$

This value can be compared to DP values for individual stations shown by Mason et al. (2008) and Xu et al. (2015), in which DP around 1980 is four times or more greater than around 1995.

Given that the sand flux of a field can be calculated as the sum of sand flux of each sand slab, we have:

$q = n * q_0$

Where n is the average number of sand slabs that pass a cross section in one simulation, and q_0 is the average slab transport flux that are the same value in these two different wind schemes.

From Section 3.4.b, number of sand slabs that cross the border (n) can be predicted by p_e using a linear model:

$N = -111.33 + 3333.41 * p_e$

Assuming $p_{e1} = 1$ as the erosion probability during when average wind speed was 14.41 in 1980s,

$(-111.33 + 3333.41*p_{e1})/(-111.33 + 3333.41*p_{e2}) = 3.55$

then $p_{e2} = 0.305$

p_e is chosen as the parameter for modeling wind speed drop, because of its linear correlation with resultant sand transport rate.

The Mu Us dunes formed around 1995 after most of the decrease in wind power can be simulated using the following setup:

$p_e = 0.305$; p_s / p_n = 0.6/0.4; h0 = 1; d = 1

Starting with an established barchan dune field (101 year) developed with the original settings (p_e = 1), I ran 60 simulations with $p_e = 0.305$. As results show (Figure 26), dunes migrate much slower when $p_e = 0.305$ compared with when $p_e = 1$. Moreover, dune forms remain the same after 60 years' simulation. In comparison, small barchan dunes merged into one single transverse dune after 60 years in the original $p_e = 1$ scenario. Using this, we can control wind effects in the CA model and compare it with vegetation influences on dune forms and migration speed.

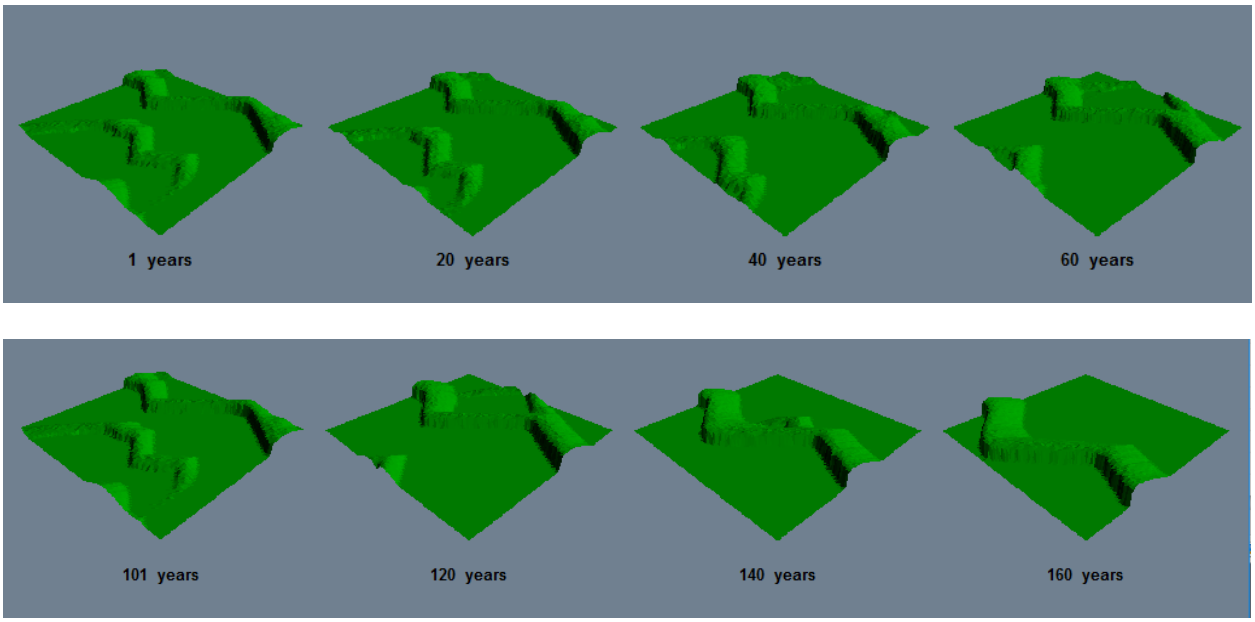

Figure 26 Simulation showing the effect of dropped wind speed (top panel, $p_e = 0.305$) in comparison to original setting (bottom panel, $p_e = 1$)

5. Web application

Improving the access and availability of geomorphology models is beneficial to the earth surface science community (Murray et al., 2009). Previous dune models were built in Turbo 2.0 (Baas, 2002), Python (Barchyn and Hugenholtz, 2012b) or Matlab (Nield and Baas, 2007). In this work, a web based application of dune CA model is developed through Rshiny. It provides an intuitive way of exploring dune form changes under different scenarios for both researchers and educators. I also released an R package for dune geomorphology modeling, which not only improves the accessibility of the model, but also allows for easy distribution and reproduction of research results. Through the interactive web interface and the R package, users can test hypothesis by modifying parameters and visualizing resultant dune forms. The web app can be found at:

https://feima.shinyapps.io/dune/

The advantage of using R for simulation and analysis is that R is equipped with numerous packages allowing for satellite image analysis (e.g. package 'raster'), visualization (e.g. package 'ggplot2', 'plotly') as well as numerical modeling. On the other hand, the web application can be limited by its slow processing speed since R is a single-thread computing language. Some R packages (such as 'parallel') allows the computation to be done at multi-CPU or multi-Core level, but these packages are not applicable in this research since they require the paralleled computation blocks to be unrelated. [3] That is, each iteration is dependent upon the surface formed in the previous iteration, and therefore cannot be computed simultaneously through multi-cores or CPUs.

Conclusions and Discussion

The CA model developed for this research, based on the work on Werner (1995), successfully reproduces the form and behavior of crescentic dunes formed by unidirectional winds. Dunes in the model evolve toward a stable form over a timescale of decades. Plots of maximum dune height, avalanche frequency, and number of slabs crossing the model domain boundary over time are useful in analyzing this evolution. A timescale can be estimated for the model to calibrate it to an actual dune field, although there are unresolved problems in doing this with the Mu Us dune field.

To use this type of model to help understand and predict change in dune fields affected by environmental change, I extended previous work to identify the best approach for representing changes in wind strength, the most important new contribution of this chapter. While a few parameters can potentially be adjusted for this purpose, most of them lead to model behavior that appears to be unrealistic, based on previous research and on observed response to a decrease in wind strength in the Mu Us dune field.

[3] https://stat.ethz.ch/R-manual/R-devel/library/parallel/doc/parallel.pdf

The downwind jump unit (d) cannot be increased above 2m without causing unrealistic flattening of the dunes, so it is effectively limited to two values (1m or 2m). The slab thickness (h) is also constrained to a narrow range of 0.06 to 0.13m, otherwise dunes do not form. This is consistent with the theoretical argument by Nield and Baas (2007) that h should fall in the range 0.077-0.13m. When deposition probability (p_s and p_n) is reduced (representing high wind strength), dunes take longer to stabilize than with the original settings. When p_s and p_n are increased to 0.8 and 0.6, representing weaker winds, dune forms undergo change that appears to be unrealistic; therefore deposition probability is not an ideal parameter for simulating response to changed wind strength. On the other hand, when erosion probability (p_e) is adjusted to higher or lower values, the size and spacing of dunes changes, but not their basic form. This is the most realistic response based on prior research, so adjustment of p_e is the best approach in simulating effects of changed wind strength. While many of the same factors influence both sediment erosion and deposition in actual dune fields, in this modeling approach, p_e and p_d are apparently not interchangeable as parameters that can be adjusted to represent changed environmental conditions.

Changing equivalent sand thickness (EST) cannot be used to represent lower or higher wind speed but can represent variation in sand supply. Higher EST results in larger and more closely spaced dunes, as expected for increased sand supply.

A change of p_e from the initial value of 1 to 0.305, representing the decline in DP in the Mu Us dune field in recent decades, produces somewhat different dune forms and behavior. With the lower value of p_e, barchans that initially formed do not merge into higher crescentic ridges as they do with the original setting. The dunes also migrate slower with a smaller p_e value as are expected from lower wind speed. The research in this chapter demonstrates that through modifying the value of p_e we can effectively map the model space to real world wind scenarios, and use the model to predict how dune forms evolve with time. As the next step, this link between p_e and wind speed can be built into the web app for testing dune response to varied wind speed in different fields of the world.

Chapter 4. Vegetation integrated dune stabilization model

The degree of dune activity or stability can be framed as the competition between sediment transport and vegetation growth. While sand dunes can merge and grow in size with increasing sand supply and wind drift, the threshold shear velocity of wind can be lowered by vegetation. Vegetation provides a positive feedback to dune stabilization: once a pioneer species is established, it protects the sand surface from further wind erosion and provides nutrient and shade for underlying plants, which contributes to vegetation growth and dune stabilization (Reynolds et al., 1999; Maestre and Cortina, 2005). While sand erosion and deposition are affected by vegetation cover, vegetation growth is also affected by both sand burial and erosion. Shallow burial is advantageous to plant growth and reproduction through increased water use efficiency, chlorophyll content, transpiration rate and net photosynthetic rates; deeper burial, however, can be harmful to plants (Qu et al., 2014). Erosion causes stress includes water and nutrition loss and elevated temperatures in the root system after exposure (Maun, 1998). Severe denudation can threaten most desert plants. The complex relationship between surface roughness and sediment flux makes numerical models challenging.

The vegetation that stabilizes the Mu Us dune field consists mainly of two types of shrubs (*Artemisia ordosica* and *Caragana microphylla*, Figure 27a), small trees such as willows (*Salix* spp., Figure 27b), sedges (*Carex* spp.), and tall grasses. *Artemisia ordosica* is the primary vegetation species in Mu Us dune field. Its reproduction is realized mainly through seed (sexual reproduction), and it can also split into clonal fragments occasionally (Schenk, 1999). Growth and reproduction of *Artemisia ordosica* are not affected by moderate denudation or burial, but severe denudation can reduce both its reproduction and growth due to water and nutrition stress (Li et al., 2010).

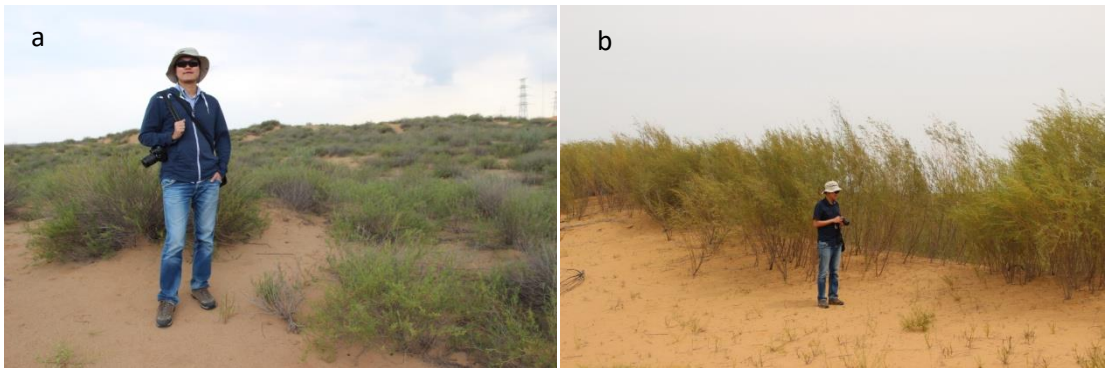

Figure 27 Typical dune vegetation a. Artemisia ordosica in interdune area; b. Willows (Salix spp.) on top of a large barchan dune

In this chapter, I aim to develop a CA model that simulates the stabilization process of barchan dunes with the presence of vegetation. I will first review current vegetation-integrated dune CA models and evaluate their capabilities in producing realistic dune forms, by implementing the same modeling approaches within the model framework I initially developed for bare dunes (Chapter 3). I then tune parameters to fit the model to Mu Us dune field and use it to test hypotheses.

Each simulation described in this chapter followed the modeling approach described in Chapter 3, but starting with a single barchan dune that developed from a single sand patch. That dune was then used to initialize a simulation using one of the vegetation models discussed here, with parameters the same as in the initial bare sand model except where they are modified to account for vegetation effects.

Due to the lack of long-term high-resolution data allowing reconstruction of dune-scale vegetation patterns and topography over the past few decades, these model results on dune form changes cannot be directly validated. In addition, the dune forms produced by models are not definitive. That is, random factors can cause model output to vary between runs. To cope with these challenge, I used features (such as dune shapes, dune migration speed, vegetation cover change rate, etc.) extracted from satellite images of the study areas (Chapter 1) to verify model outputs.

1. Current and proposed vegetation-integrated CA models

a. Elevation-based vegetation model

Chapter 1 and 2 showed that elevation can strongly influence the distribution of vegetation cover in some areas, possibly related with wind exposure or surface distance to water table. Vegetation cover can decrease with increasing dune height because of the lower probability of entrainment found in inter-dune areas (Pelletier et al., 2009). Pelletier et al. (2009) further proposed a power-law relationship between erosion probability, p_e, and elevation above the lowest interdune areas (relative elevation) to model vegetation effects on sediment flux.

In evaluating the possibility of incorporating elevation effects, I used height above base level (height = 0m) as a proxy for vegetation density in Mu Us dune field. Specifically, p_e is modified linearly according to the height of the cell:

$$p_e = (h_1/h_{max})*p_0$$

Where h_{max} is the maximum height of the barchan dune (typically 5 to 6m for the study area), and p_0 is set at 1. The form changes of the barchan dune are shown in Figure 28.

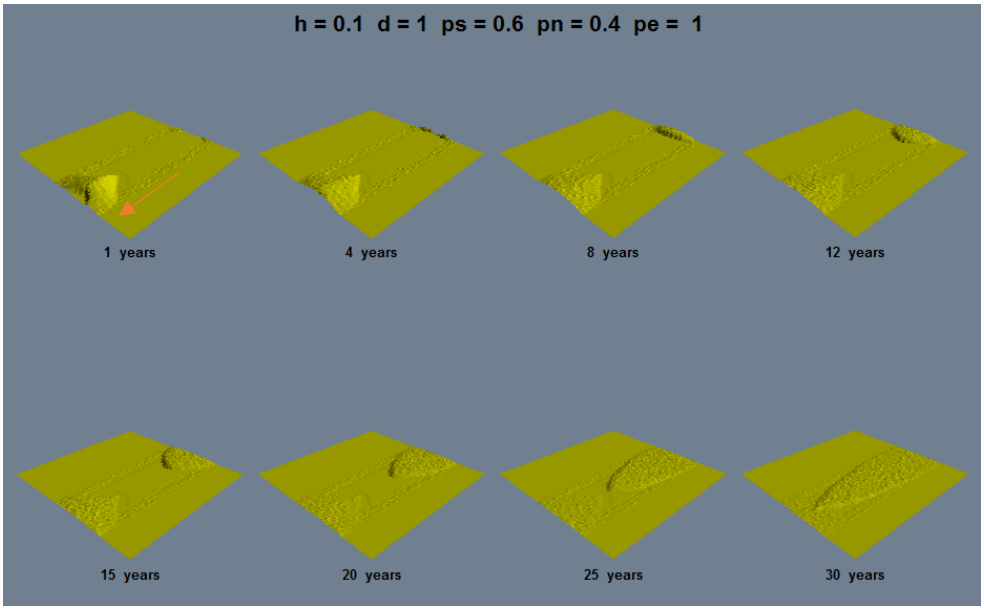

Figure 28 Barchan dune stabilized using vegetation elevation model

Wind direction is indicated by the red arrow

The experiment surface is initialized with one barchan dune. As shown in Figure 28, the barchan dune is gradually transformed into a parabolic shape, with the lower 'arms' pointing towards down-wind direction; the overall dune form is flattened as expected (Pelletier et al., 2009). This matches with field observations that on barchan dunes, vegetation typically anchors the lower 'horns' that are pointing downwind first; with the rest of the dune continue moving forward, barchan dune morphology transforms into parabolic forms, with 'arms' trailing upwind (Barchyn and Hugenholtz, 2015; Xu et al., 2015). However, unlike most actual parabolic dunes in this region, the dunes formed by the model did not develop distinctive 'arms' in the end.

b. Growth function model

Sand transport varies with height, roughness, species and density of plants (e.g. Wolfe and Nickling, 1993). To simulate the dune stabilization process with the presence of vegetation, Baas (2002) proposed a vegetation growth function model that extends the original Werner (1998) model. It

simulates parabolic dunes that develop from barchan dunes under the effect of two types of vegetation, a pioneer grass and a woody shrub. A pioneer species such as marram grass (*Ammophila*) requires sediment input for optimum vitality (Chadwick and Dalke, 1965; Moore, 1996; Van der Stoel et al., 2002), while neutral or negative balances lead to decline due to the impact of soil pathogens and parasites (Maun, 1998). Shrubs, on the other hand, reach their peak growth rate when sediment input and erosion are roughly balanced.

In the vegetation growth function model (Baas, 2002; Baas and Nield, 2007), erosion and deposition probability are modified to reflect vegetation stabilizing effects:

$$p_e(\text{veg}) = p_e(\text{bare}) - p_0$$

$$p_d(\text{veg}) = p_d(\text{bare}) + p_0(1-p_d(\text{bare}))$$

Where p_0 is vegetation effectiveness that ranges between 0 and 1, and its value varies depending on the vegetation species and sediment balance (Baas, 2002; Nield and Baas, 2007). If a randomly generated value between zero and one is less than entrainment probability (p_e) then the chosen sand unit will be entrained; otherwise the entrainment does not happen.

I tested this approach, in the full form proposed by Baas (2002), and with various modifications. In the full form, where vegetation exists, the deposition probability tends to be higher. However, a comparison between the results using p_d(veg) and p_d(bare) showed that deposition probability has minimal effect on the formed sand dunes: dune forms developed under these two deposition probabilities are very similar, with more small dunes formed with p_d(bare) (Figure 29). This is possibly due to the accumulation of sand on locations with a lower height (such as the end of 'arms'), where new parabolic forms start to develop with time. This result suggests that the modification of entrainment probability is more significant in driving the formation of parabolic shapes in the growth function method, echoing with Chapter 3 where modification of erosion probability was found to be an effective way to reflect wind regime changes.

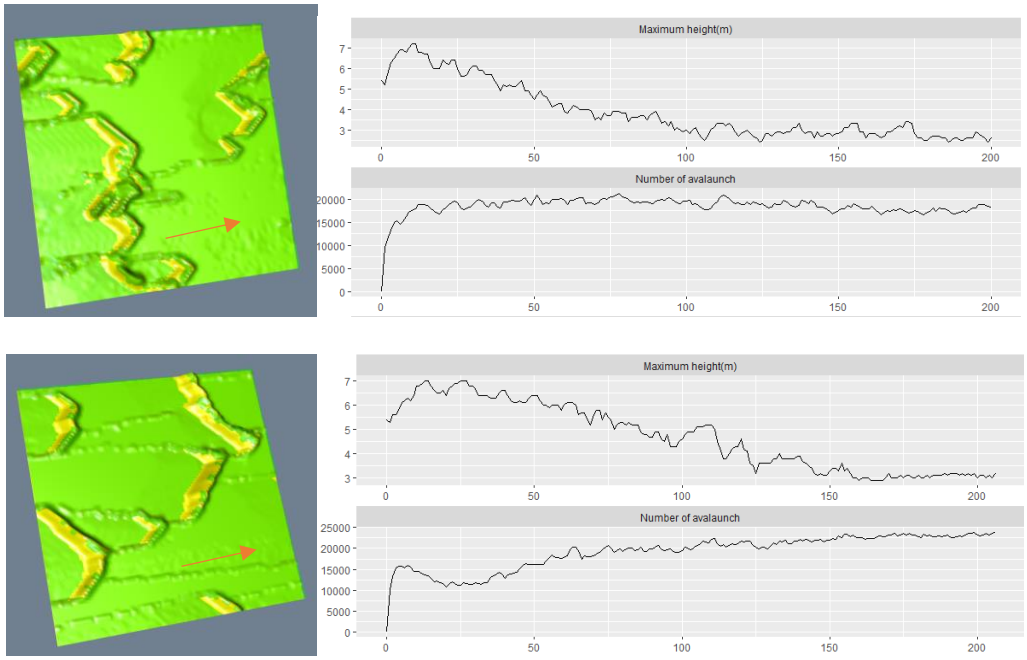

Figure 29 Parabolic dunes formed using p_d(bare) and p_d(veg)

Parabolic dune forms shaped by vegetation growth after 200 iterations (top: without vegetation modification on p_d; bottom: with vegetation modification on p_d). Green color represents vegetation, and yellow represents sand. Wind direction is indicated by the red arrow

I also considered the effects of including both plant types (pioneer species and shrubs), or only one of them. Model simulations with both vegetation types show that after 50 model years, the parabolic shape eventually emerges (Figure 30c). With the presence of only pioneer species (Figure 30a) or only shrub (Figure 30b) however, the parabolic shape doesn't develop in the end.

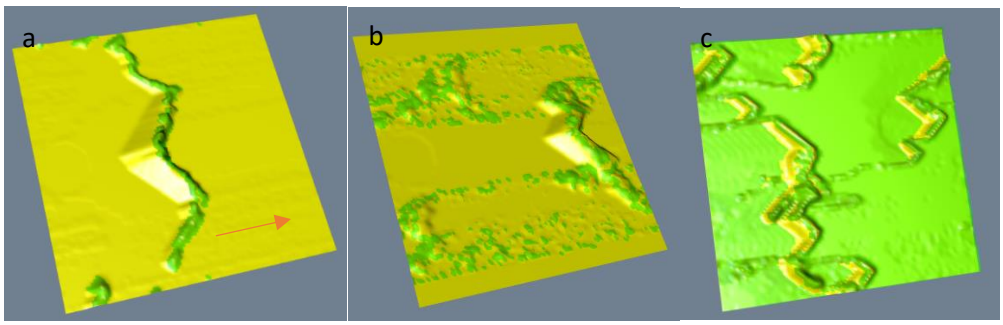

Figure 30 Dune forms after 50 years of model run with different vegetation cover

Starting with one barchan dune in the middle of model space (a: pioneer species only; b: shrub species only; c: with both species present); Wind direction is indicated by the red arrow

More specifically:

a. When only pioneer species is present, the original barchan dune extends along its crest and eventually develops a ridge of connected parabolic forms (Figure 31).

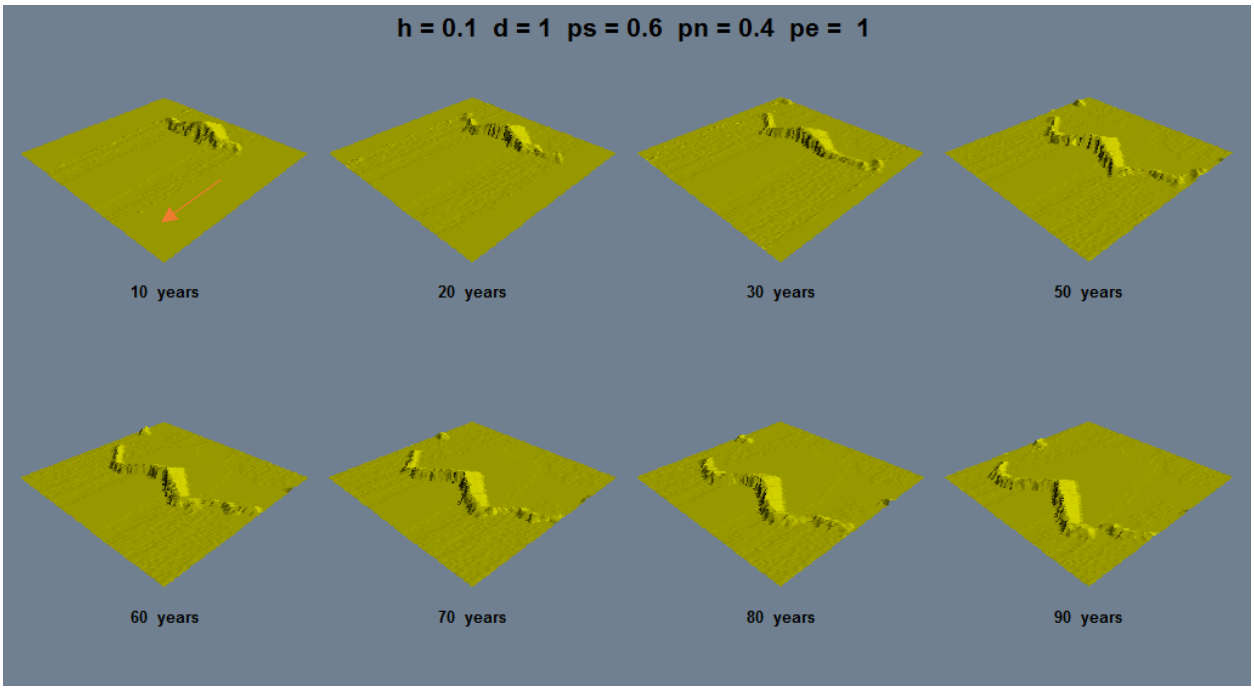

Figure 31 Dune form change with only pioneer species present

b. With shrub species alone, the original barchan dune extends its arms which then break down into smaller irregular forms. Clearly identifiable parabolic dunes do not develop. The dunes also move faster than the first scenario (Figure 32).

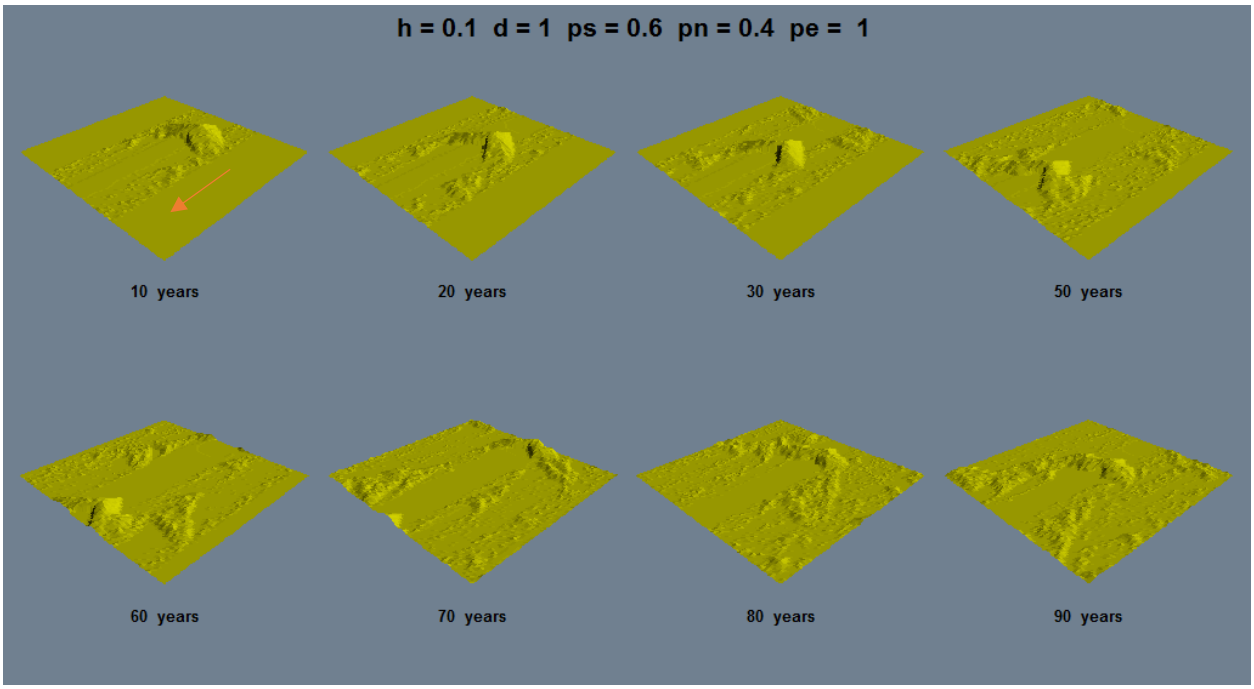

Figure 32 Dune form change with only shrubs present

c. When both species exist, the barchan dune first extends along its crest, then the lower portions break away from the main body of the original dune to form parabolic shapes, with arms pointing towards the upwind direction. The original barchan dune transforms into smaller parabolic dunes, which eventually merge into large, connected parabolic dunes. After 90 model years, two distinctive parabolic dunes are formed (Figure 33). This result is consistent with findings by Baas and Nield (2007) that both pioneer species and shrubs need to be present in the model in order for parabolic dune forms to develop.

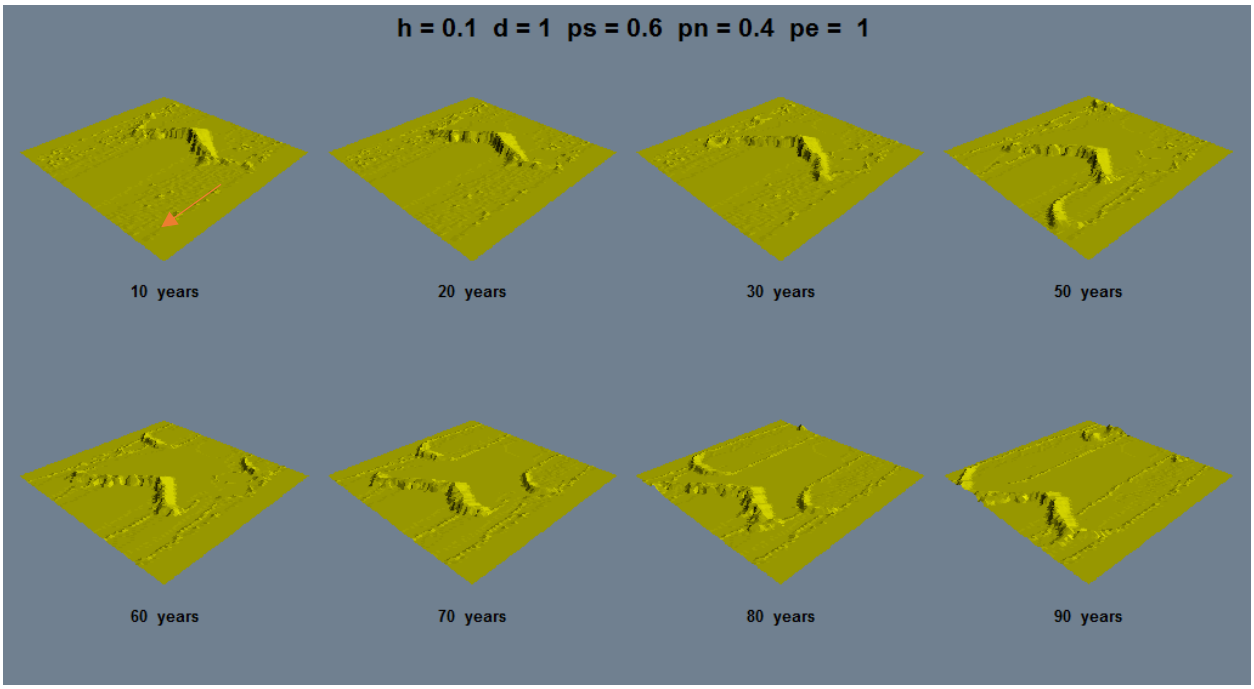

Figure 33 Dune form change with both pioneer species and shrubs present

The growth function method appears to have captured the different responses to sediment balance of various vegetation types and the transition from barchan to parabolic shapes, but in fact it does not. The drawbacks to this method are summarized below:

1) Vegetation growth function is derived through trial and error, making it difficult to apply the model to actual dune fields (Baas and Nield, 2010; Nield and Baas, 2007).

2) The physical process of parabolic dune formation generated by the model is different from other model simulations (Duran and Herrmann, 2006; Barchyn and Hugenholtz, 2015) or field observations, where the 'arms' get stabilized first while the central part keeps migrating down wind, thereby changing the shape from barchan to parabolic. In this model, the morphological change of barchan dunes starts with arms breaking from the main body while taking on parabolic shapes directly.

3) A closer look at vegetation growth shows that with time, vegetation cover first increases while the dune form stays the same, then it decreases as parabolic shapes develop (Figure 34). This is opposite to field observations that vegetation cover increases as parabolic dunes form.

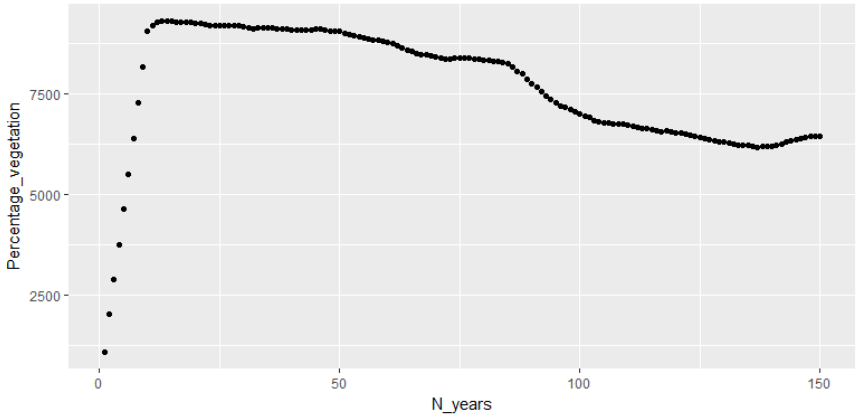

Figure 34 Change in vegetation cover with the increase in number of iterations

Using scenario c as example

4) The verification of such models requires multi-spectral satellite images. While different vegetation types can sometimes be distinguished using infrared bands, they often appear the same in optical imagery (Hugenholtz et al., 2012) . Multi-spectral imagery has enabled investigation on vegetation density, structure and species using spectral reflectance curves (Pinker and Karnieli, 1995). The infrared bands can be used to identify trees and certain shrub species (Nield and Baas, 2007). With only optical images, therefore, we cannot distinguish vegetation structure and obtain species information that is necessary for constructing growth curves.

c. Dune slice-height model

Barchyn and Hugenholtz (2015) predicted whether a sand dune will host vegetation and be immobilized using a dune slice (wind-parallel segment) analysis. Their work involved interpretation of actual vegetated and active dunes, rather than a CA model. They calculated

slipface deposition rate (δh/δt) on many dunes in several study areas, using DTMs developed from LiDAR images and estimates or measurements of sand flux. That deposition rate is then compared to vegetation growth tolerance (v_{peak}) of the study area. If their ratio is larger than 1, then it is predicted that the dune will continue to advance downwind; otherwise primary (pioneer) species start to colonize the dune crest. After this process, secondary species will grow and lead the dune to full stabilization. This criterion for stabilization successfully distinguished active and stable dunes in several study areas. Barchyn and Hugenholtz made two important assumptions: (i) environmental conditions (such as v_{peak} and wind direction) remained the same throughout the period of study; and (ii) the basic geometry of the slipface has remained relatively constant through stabilization.

The identification of the slipface is key to the analysis by Barchyn and Hugenholtz (2015). The slipfaces they identified closely resemble areas identified by the top 25% most deposited cells using Werner's model (1995) (Figure 35). In this section, I will adopt the dune slice concept of Barchyn and Hugenholtz (2015) as well as an elevation effect to construct a vegetation-integrated CA model. This dune slice-height CA model does not directly simulate the interaction of vegetation and deposition on the slipface, which would require information on vegetation tolerance and assumptions on environmental conditions or slipface geometry. Instead, it makes assumptions about the likelihood of stabilization of dune slices of various size and position within the dune in an environment generally favoring vegetation expansion.

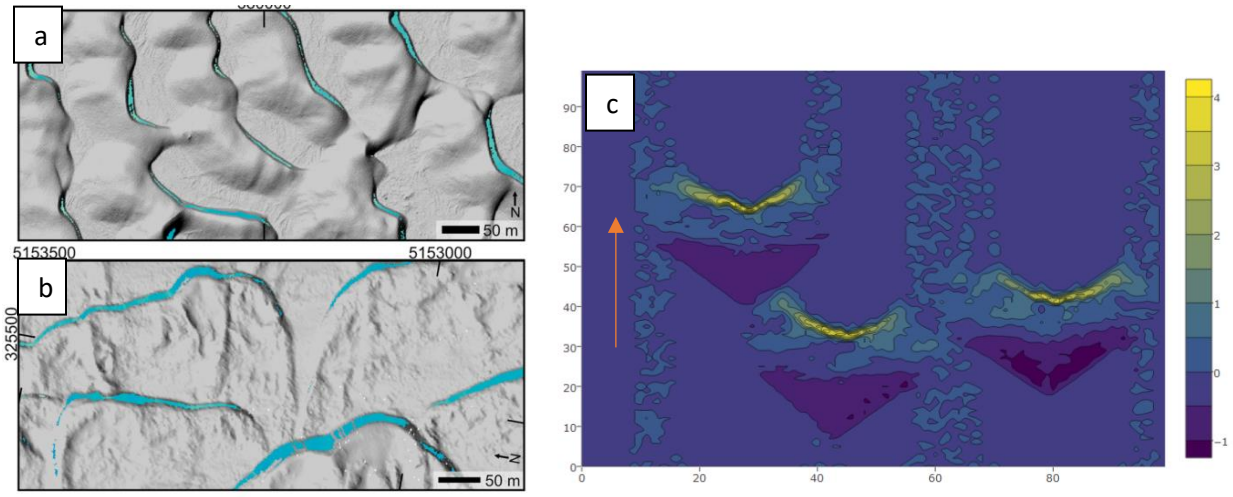

Figure 35 Areas of slipface

Slipfaces are identified by blue area in a and b (Barchan and Hugenholtz, 2015) and yellow/green area in c, which generated using Werner 1998 model, characterized by sand deposition. Wind direction is indicated by the red arrow

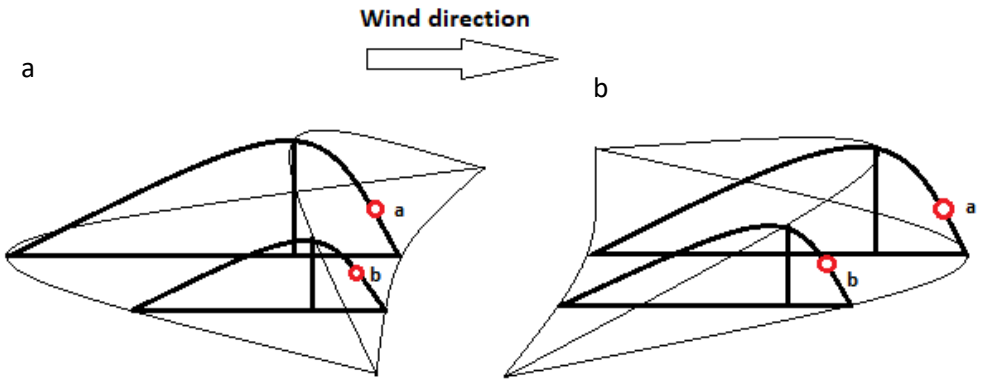

Figure 36 Dune slices in a barchan dune (a) and parabolic dune (b)

The conceptual basis of this modeling approach is as follows: Without vegetation, the rate at which the dune advances is controlled by the rate of sand deposition on the slipface, which is related to the sand flux from upwind but also to the height of the slipface. For the same sand flux, a lower slipface will advance faster because deposition is spread over a smaller area. Sand flux per unit width of the dune crest is greatest across a slipface that is perpendicular to the wind, and lower

where the slipface is oblique to the wind. As a barchan dune develops without the presence of vegetation, it will have a slipface that is higher in the middle (position of slice a in Figure 36a). This middle slice of the slipface will advance more slowly than the slice labeled b in Figure 36a), with a lower slipface. That is, the lower 'arms' of the dune move faster and migrate downwind to form the characteristic crescent shape of barchan dunes. Eventually, the oblique angle of the arms reduces sand flux per unit width of the crest, and the advance of the arms slows down to the same rate as the center of the dune, creating a stable form.

With the presence of expanding vegetation, migration speed again differs between locations on the dune. Assuming vegetation spreads onto the slipface from the interdune, and also assuming effects like those discussed in Chapter 2, such as a greater depth to the water table and greater wind exposure higher on the dune, vegetation will cover the lowest slipfaces of the barchan arms and reach the crests there first. When vegetation reaches the crest of a particular dune slice, burial of vegetation on the slipface of that slice will cease and it will no longer advance. At the same time, sand moving up the stoss (windward) slope is trapped and the whole slice is quickly vegetated and immobilized. Meanwhile, the higher dune slices closer to the center (a in Figure 36a) still experience active deposition and burial by avalanching, slowing advance of vegetation up the dune. As a result, the arms are progressively immobilized and the center of the dune advances past them, forming a parabolic dune form. As the center advances, the curvature of the part of the dune that is still active makes the crest more oblique to the wind on either side of the center of the parabola, reducing sand flux and enhancing stabilization of the arms (Figure 36b).

These effects can be integrated into a dune slice-height CA model in a simple way: slices that are closer to the maximum height are assigned a larger p_e value, and vice versa. The p_e of a dune slice is defined as:

$$p_e = p_{e0} * max_{height0} / max_{height}$$

where $p_{e0} = 1$, max_{height} is the maximum height of the entire model space, and $max_{height0}$ is maximum height of a given dune slice. In effect, the lower, smaller dune slices are assumed to be more likely to have been fully stabilized by vegetation (i.e. vegetation growth has exceeded slipface deposition and has reached the dune crest) in an environment favoring vegetation expansion. Therefore, the probability of erosion on the stoss slope and crest of that slice is lower. This slows down deposition on the slipface and therefore slows the advance of the lower, smaller slices. This effect involving the entire dune slice is not addressed in the original dune height model (Chapter 4.1.a; Pelletier et al., 2009), which simply varies erosion probability by elevation, regardless of position on the dune. This can explain the unformed 'arms' of parabolic dunes using the original dune height model (Figure 28).

Although it represents vegetation effects in a much simpler manner than a growth function model, the dune slice-height model better reflects the physical changes observed during actual dune stabilization (Figure 37a), because the output closely resembles parabolic dune forms observed in the field (Figure 37b).

a

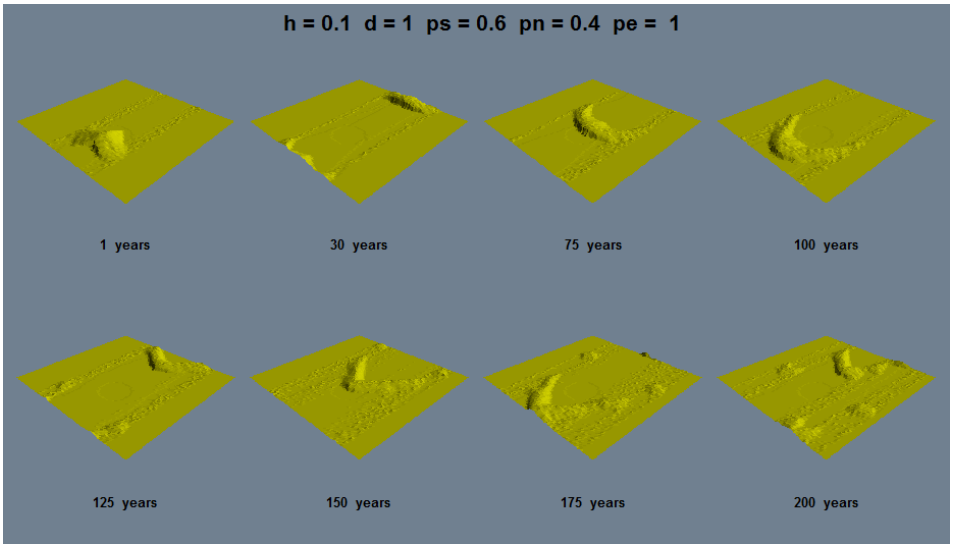

b

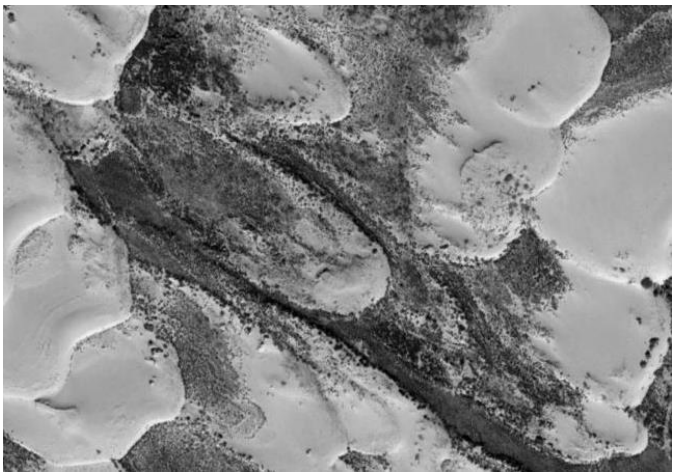

Figure 37 Stabilization of a barchan dune with slice-height model (a) and actual parabolic dunes in Area I6 (b)

North is toward top. Image source: Google™ Earth

Different stabilization scenarios can also be simulated by modifying model parameters. For example, when p_e varies, the maximum height of formed parabolic dunes also changes: the higher p_e is, the lower formed dunes are (Figure 38a). As shown in Figure 38a, parabolic dunes reach a stable height at around year 65 when $p_e = 1$, and afterwards they kept migrating downwind since p_e is not 0 (Figure 37a). It also takes longer for dunes to reach a stable height when p_e decreases (Figure 38a); for example, maximum height of dunes is still decreasing at year 100 when p_e is 0.5.

Figure 37a also shows that small sand piles that drift apart from the main dunes formed parabolic shapes, which is coherent with observations from the field (Figure 38b; Fig 3 in Duran and Herrmann, 2006). These smaller sand dunes migrate more slowly than bigger ones.

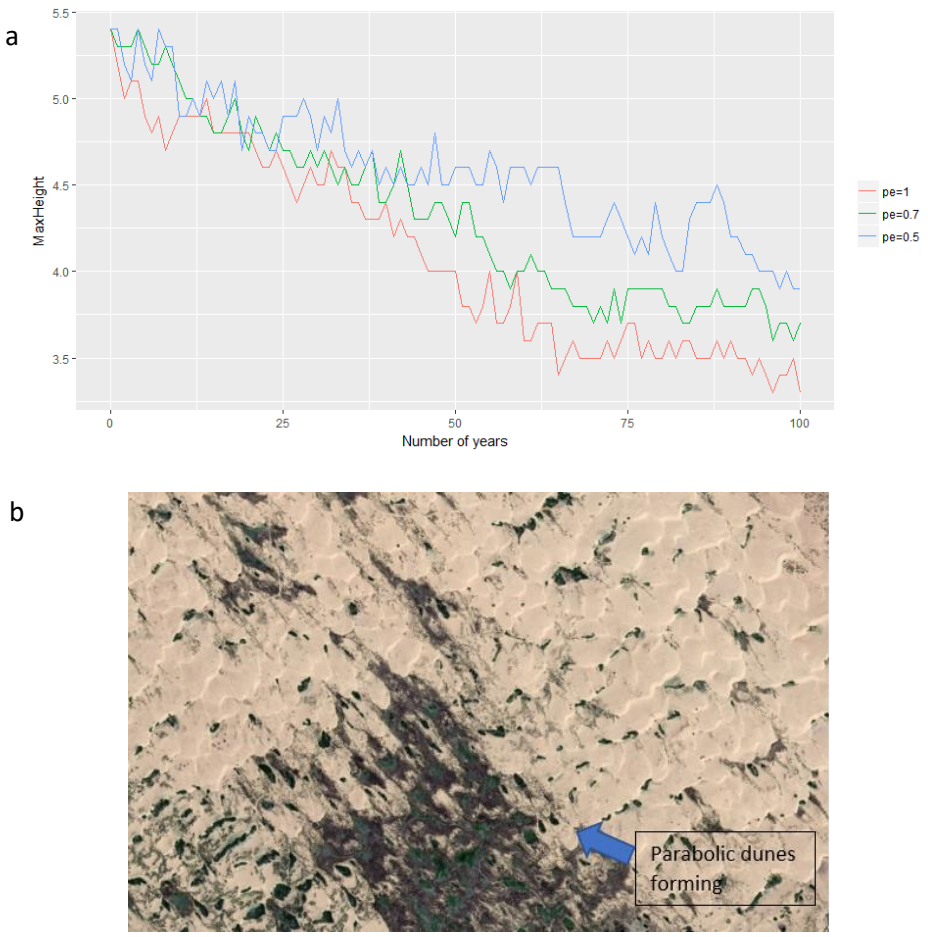

Figure 38 Experiment on p_e (a) and parabolic dunes forming near large, continuous dune field in Mu Us (b) North is toward top. Image source: Google™ Earth

Figure 38b also reflects that the proximity to vegetation patches can be an important factor contributing to dune stabilization speed, echoing with the findings in Chapter 2.

Fitting model to dune field

Dune stabilization often happens on a time scale that is longer than most remote sensing or scientific records, so numerical modeling is used to simulate the partially unobservable process of dune stabilization (Duran and Herrmann, 2006; Nield and Baas, 2007). As a result, model

simulations on dune dynamics are advancing ahead of available observational evidence, posing a challenge for model validation efforts (Hugenholtz et al., 2012).

The model by Baas (2002) is governed by 'growth curves' that are developed through 'trial-and-error' and lack real-world validation. Pelletier et al. (2009) directly applied their model to Jockey's Ridge, but their study subject is a small single dune (about 70m by 30m in size) instead of an actual dune field. The model of Barchyn and Hugenholtz (2015) can predict the potential for stabilization of various parts of actual dune fields, but it requires high resolution dune surface measurements.

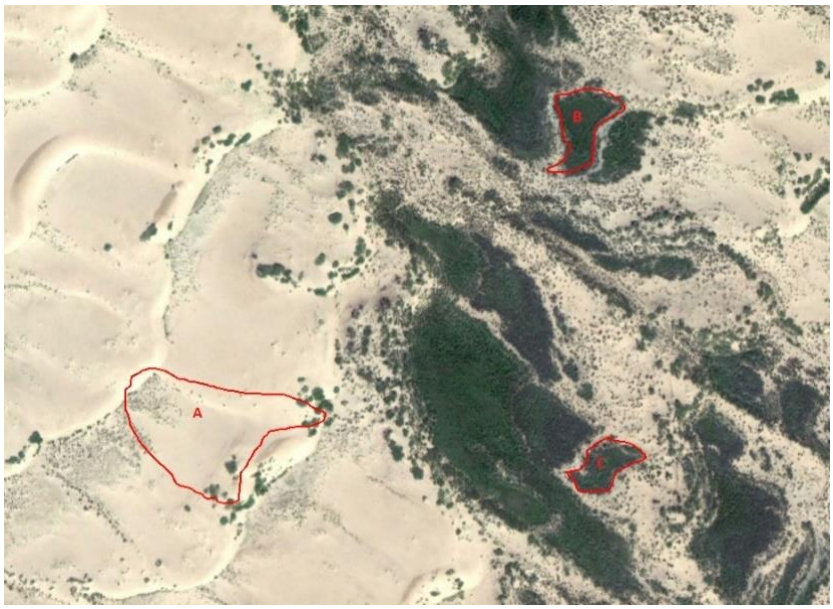

Figure 39 Sample dunes in Area I7.1 in 2010.8

(A: contour of a barchan dune in 2002.8; B and C: contour of stabilized dunes in 2010) North is toward top. Image source: Google™ Earth

With the dune slice-height model, we can use dune migration speed and change in vegetation cover obtained from satellite images of an actual dune field to simulate different scenarios. Similar to Chapter 3, dune migration speed is used for setting spatial and time scales. Users of the model can manually set the area-average erosion probability that declines with time (reflecting vegetation cover increase) and observe dune form changes. Taking dune A in Area I7 (Figure 39) as an example, bare sand dunes migrate at 3m/year according to Chapter 3.1. In the late 1990s, precipitation

reversed its declining trend and started to increase (Figure 2), while drift potential stayed roughly the same since then. In 8 years, vegetation cover increased by 20%; therefore we can make the somewhat simplistic assumption that vegetation will expand to cover the entire dune area by year 40. That is, erosion probability is set to decline linearly to 0 in 40 years starting from the year 2002. And in year i,

$$p_e(i) = 1 - i/40$$

Surface bareness is calculated by averaging p_e value of a year over the whole area (Figure 40d). Instead of keeping p_e the same value (Figure 37), p_e is set to be linearly declining, which slows down the dune migration with time (Figure 40e). As vegetation cover reaches 86% by year 28, dunes are migrating sufficiently slow that they can be considered stabilized (Figure 40 a and e). Vegetation growth was fast enough that parabolic dunes like the ones in Figure 37b did not form in the end. However, the resultant dune forms closely resemble that of stabilized dunes found in the field (Figure 39 dune B and C), with horns starting to shift to point upwind direction and the stoss face still discernible.

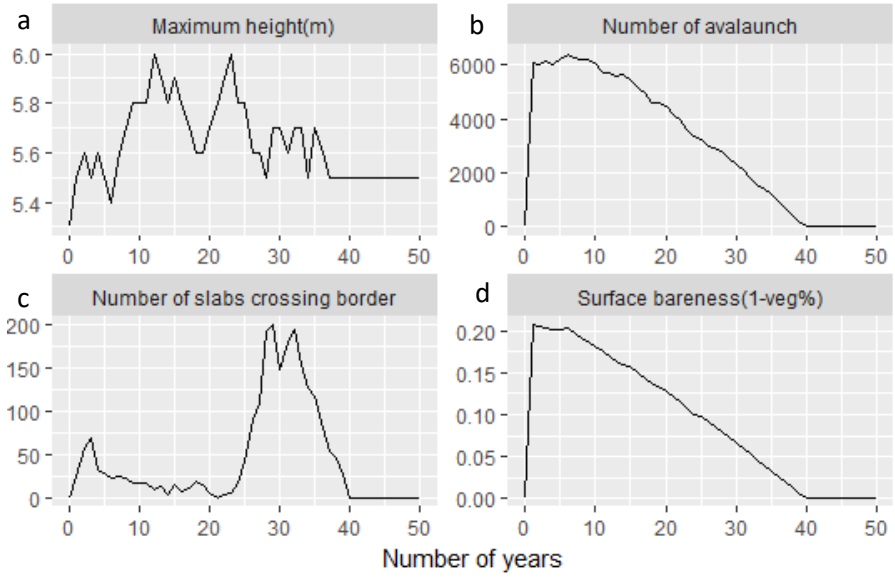

e

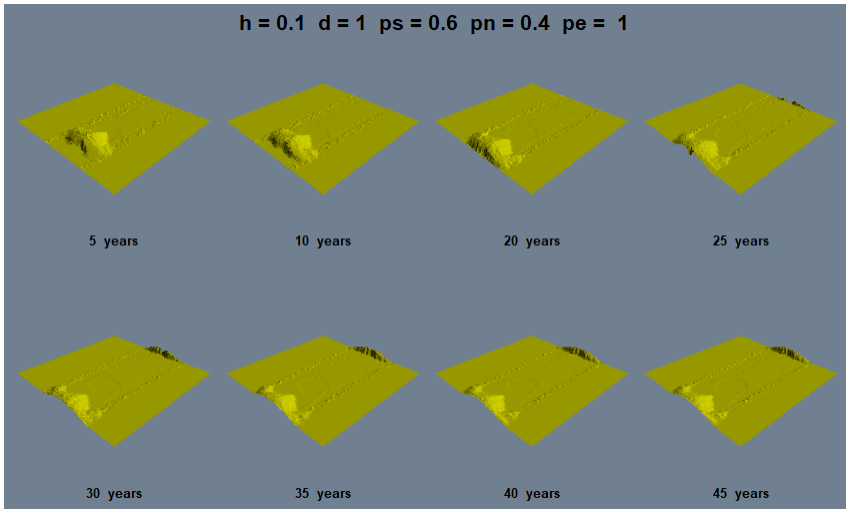

Figure 40 Parameters (a-d) and dune form change (e) with linearly increasing vegetation cover for Area I7

The above scenario reflects dune stabilization in this study area since the 1990s, when precipitation started increasing and DP (and therefore, sand drift) has been stable since its significant drop in the early 1990s. The modification in p_e only reflects the increased moisture level that caused vegetation cover to increase. A more complex adjustment in p_e is necessary for areas that experienced changes in wind drift or human activities in addition to vegetation growth.

2. Testing hypotheses on factors influencing vegetation stabilization of the dunes

a. Nearest neighbor effect

Research in the Mu Us dune field has suggested that plants often sprawl from nearby patches instead of establishing new colonies (Xu et al., 2015). Vegetation expansion and reproduction are heavily influenced not only by dune activities, but also by spatial interactions between plants. In active dune fields with *A. ordosica*, the spatial associations of the seedlings with the adults are mostly positive when they are at close distances (0-5m) with a clustered distribution (Zhang et al., 2015). The clustering pattern reflects the sheltering effect of adult plants on seedlings on active dunes, reducing wind erosion and forming a positive feedback loop favoring plant growth. This

spatial association declines with distance, and is weak or even neutral in semi-fixed dunes. In fixed dunes, water and nutrient stress resulting from competition between individual plants can exceed the advantages of sheltering, which then reduces the growth of seedlings (Zhang et al., 2015).

Using the dune slice model, we can test the nearest neighbor effect. Specifically, I assigned cells closer to a vegetation patch (a 3 by 3 grid with low p_e values) a smaller p_e value, and those that are farther the original value as defined in the dune slice-height model. The simulation starts with a number of barchan dunes generated using Werner's CA model (1995) on a lattice covered by one sand layer. This way we can test how vegetation distribution affects a dune field instead of a single dune. If vegetation nearest neighbor effect exists, parabolic dunes should form more quickly than the original setup without such effect. However, the resultant landscape demonstrates that the expected parabolic dunes did not form (Figure 41). In fact, the final 'dunes' have sharp edges and maintained their barchan forms, which is not observed in the field.

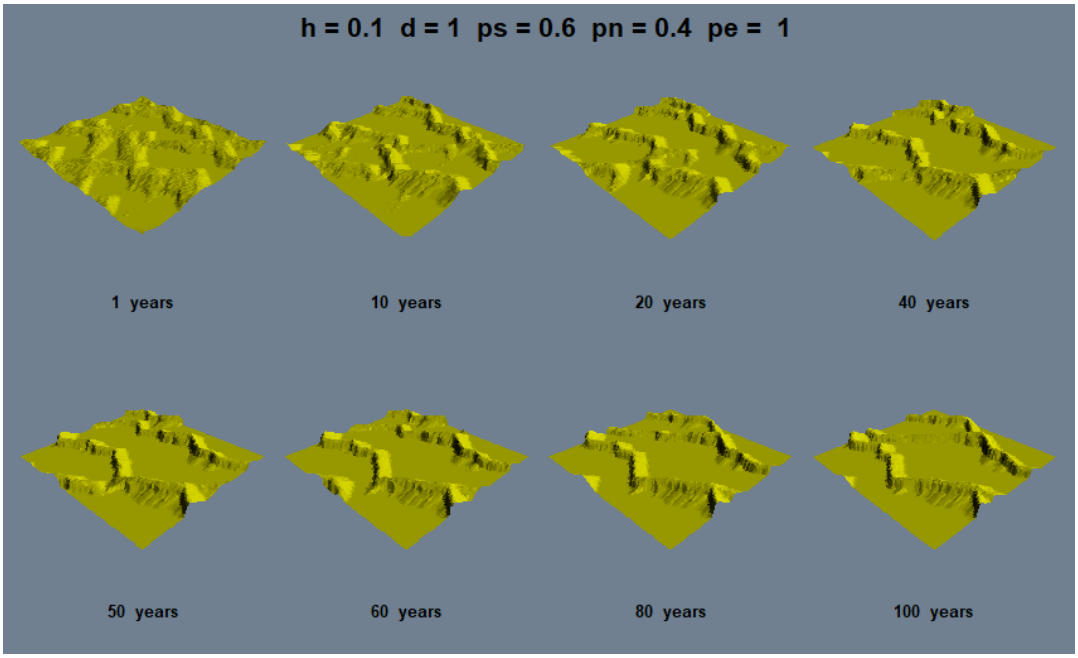

Figure 41 Output of dune slice-height model integrated with nearest neighbor effect

b. Effectiveness of windbreaking grids on top of dunes

Planting windbreaking grids of shrubs on dunes has been a common practice in Mu Us area as an effort to prevent farmlands or roads from being encroached by sand (Figure 42 a and b). As shown in Chapter 2, grid density is one of the leading factors in vegetation cover increase. In some areas, grids are implemented on a slope, while in others they are found on the crest of dunes. Researchers have shown that the vegetation feedback on dune crests is critical in dune stabilization process (Barchyn and Hugenholtz, 2015). Using the dune slice CA model we can test whether dunes can be stabilized by windbreaking grids planted on top of dunes.

To simulate this scenario, I assigned cells at dune crests with $p_e = 0.8$ without presence of vegetation. The model space starts with three barchan dunes generated using Werner's CA model (1995).

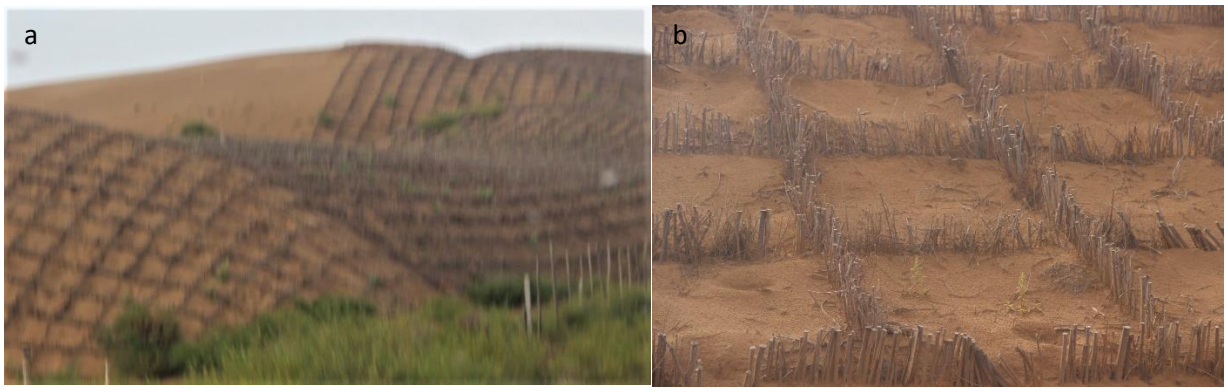

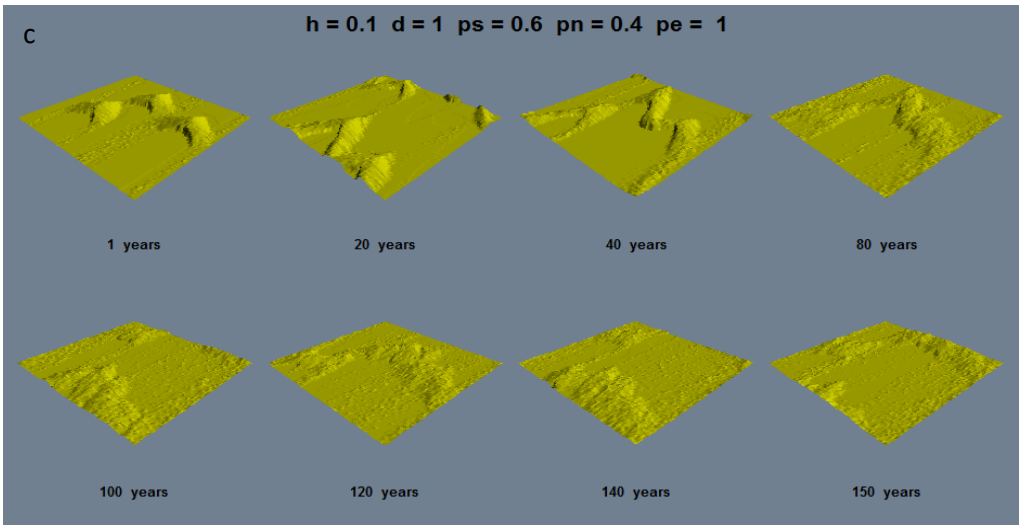

Figure 42 Wind breaking grids (a-b) and simulation results using dune slice-height model integrated with vegetation on dune crests (c)

As seen from the results (Figure 42c), colonizing only the top of dunes does not stabilize them or slow them down. Instead, the dune forms simply get flattened without forming parabolic shape. In fact, wind-breaking grids are often planted on slipfaces in Mu Us dune field where vegetation naturally occurs, which is more effective than grids set up at other locations. In addition, vegetation growth is not implemented in the test, which could explain the continued fast migration of the dunes.

Conclusions and Discussion

Field studies have shown that vegetation growth is the key process of dune stabilization (Maestre and Cortina, 2005), but previous work on integrating vegetation into the original CA model (Werner, 1995) proved to be ineffective or unrealistic. For example, Pelletier et al. (2009) proposed using a power law relationship between p_e and elevation above interdune area (relative elevation) to simulate vegetation effect, but 'arms' did not develop in the generated dune forms; the growth function method proposed by Baas (2002) is capable of creating parabolic forms, but the transition

process from barchan dunes does not match with field observations. For example, in their model arms of barchan dunes break off from the main body while taking on parabolic shapes directly; also, vegetation cover decreases as parabolic shapes develop.

In this chapter, I propose and test a new approach to representing effects of vegetation growth on dune forms, adapting the dune slice-height model proposed by Barchyn and Hugenholtz, (2015) and modifying p_e to reflect vegetation growth. Specifically, p_e of a cell is set to be proportional to its relative elevation as well as the maximum height of the dune slice the cell is located. Lower dune slices are stabilized faster than center, taller slices. As the center slices advance, the 'arms' portion of the dune are fixed and positioned towards upwind, thereby forming parabolic shapes. The model result and parabolic dune forming process are consistent with field observations, and represent improvements on previous vegetation integrated CA models (e.g. Baas, 2002; Pelletier et al., 2009). By setting p_e value to change with time, we can simulate actual dune stabilization process where vegetation cover increases or decreases. For example, when p_e is set to linearly decrease to 0 in 40 years, the model generates dune forms (in a 'transition' phase between barchan and parabolic form) that match with the actual stabilized dunes found in the study areas of Mu Us dune field. This observation suggests that this dune slice-height model can be an effective and simple tool for simulating dune morphodynamics without needing detailed information on dune geometry, vegetation growth and vegetation tolerance to sand burial, which is required in Barchyn and Hugenholtz (2015). However, more research is needed on characteristics of dune field plants and how they affect dune stabilization process in order to create realistic models.

Researchers suggested that plants are found to sprawl from nearby patches more often than establishing new colonies (nearest neighbor effect) (Zhang et al., 2015). I used the dune slice-height model to test this effect by assigning cells closer vegetation patches a smaller p_e value. Parabolic dunes did not form as expected, however, probably because of the size discrepancy: vegetation nearest neighbor effect can take place at scales smaller than 1/5 to 1/3 of the dune size as in the

simulation. To improve the test, cell size needs to be adjusted to smaller values; but then the size of formed dunes would also decrease. As such, this particular vegetation effect is probably untestable by the CA model.

Barchyn and Hugenholtz (2015) showed that vegetation feedback on dune crests is critical in dune stabilization processes. Therefore I tested the hypothesis that implanting windbreaking grids on top of dunes is effective for stabilizing barchan dunes. However, fast stabilization did not happen as expected; instead, formed dunes were flattened and continued migrating. This can be attributed to the absence of vegetation, which could start colonizing the slipface and stoss slope of the dune because of the reduced wind drift on the crest by the grids. In addition, we can test the effect of implementing grids at other locations, such as slipfaces or stoss slopes.

Conclusions

Dune field systems are subject to 21st century changes in atmospheric circulation and vegetation cover due to global warming, as well as human activities ranging from grazing to planting wind breaking grids. Research on identifying the leading drivers in dune activity among the many possible climatic and anthropogenic factors has been the focus of many workers studying multiple dune fields (e.g. Great Plains, US: Muhs and Maat, 1993; North-central China: Lu et al., 2005). I approached this problem through both simple correlation analysis and machine learning methods, utilizing information from satellite images, DEMs, and weather observations in Mu Us dune field of northern China, where there is a general trend toward greater vegetation cover and dune stabilization in recent years. A preliminary univariate analysis shows some correlation between vegetation cover and relative elevation for one study area, but only very weak relationships in others. Analyses of vegetation spatial patterns reveal evidence of patchiness and spatial autocorrelation, probably related to processes such as seed dispersal and more favorable environments for plant establishment near existing vegetation.

Through machine learning models (Random Forest, Support Vector Machine, Multivariate Regression) I evaluated the relative importance of climate, environmental and human-related variables as predictors of dune migration rate, and concluded that elevation is the most important of the 17 features considered. Size of nearest town and variables representing vegetation distribution near the dunes are also important in some cases. Similarly, elevation and wind-breaking grid density are identified to be the most important variables amongst a total of 15 features considered as predictors of vegetation cover change rate. Climate features are not found to be important in contributing to these two response variables. The importance of elevation as a factor in both dune migration rate and vegetation change is an interesting and potentially important finding, and may be explained by greater wind exposure and/or greater distance above

the water table at higher elevations. Other important predictor variables are related to vegetation dynamics and human activity. Apparently, the variation of climate across the dune field is not a significant factor in the varying rates of current dune migration and vegetation change observed in the study areas. The models simulate the spatial aspects of climate variables, but this analysis can potentially provide insight on response to climate change over time as well. The small range of spatial variation in these variables, however, limits the applicability of the model in simulating significant climate changes, such as the drop in DP in the 1990s. Despite the limitations in the methodology presented in Chapter 2 (e.g. the subjective factors in the process of data collection), the combination of machine learning methods and Google Earth images represents a new direction in exploring environmental variables in desert environments.

To investigate dune morphodynamics in response to external forcings (climate, vegetation, human activities, etc.), I modified the well-known Werner (1995) CA model and fit it to the Mu Us dune field using information obtained from satellite images. Barchan dunes formed with realistic shape and size without the presence of vegetation. As an extension of previous work with the Werner modelling approach, I demonstrated that the effect of changing wind speed and potential sand transport, as observed in the Mu Us dune field in recent decades, can be most effectively simulated by changing erosion probabilities. The link between wind speed and the CA model as demonstrated in Chapter 3 can be applied to the simulation of dune activities in response to various wind scenarios.

To better understand the linkage between dune form evolution and vegetation cover changes, I adapted the Werner (1995) model to account for the stabilizing effects of vegetation. Previously proposed approaches for doing this (e.g. Baas, 2002; Pelletier et al., 2009) were tested but found to produce results that are unrealistic in comparison to actual changes observed in dune fields, including the Mu Us. More realistic simulation of dune form change in response to increasing vegetation cover was produced using a dune slice-height model. Specifically, the erosion probability

of a cell is tuned to reflect its relative height to base level as well as the location of the dune slice it is located on. This model successfully produced a transition from barchan to parabolic dune forms as seen in the Mu Us dune field. The erosion probability can be further adjusted to reflect response of sand dunes to climate- or human-related vegetation change. More broadly, this modeling approach may be useful in simulating changes caused by other growth regime shifting factors, such as fire or invasive species introduction or removal (e.g., Zarnetske et al., 2012).

Reference

Adamatzky, A., 1994, Identification of Cellular Automata. Taylor and Francis, London

Anthonsen, K.L., Clemmensen, L.B., Jensen, J.H., 1996. Evolution of a dune from crescentic to parabolic form in response to short-term climatic changes: Råbjerg Mile, Skagen Odde, Denmark. Geomorphology 17, 63–77. https://doi.org/10.1016/0169-555X(95)00091-I

Ardon, K., Tsoar, H., Blumberg, D.G., 2009. Dynamics of nebkhas superimposed on a parabolic dune and their effect on the dune dynamics. J. Arid Environ. 73, 1014–1022. https://doi.org/10.1016/j.jaridenv.2009.04.021

Baas, A.C.W., 2002. Chaos, fractals and self-organization in coastal geomorphology: simulating dune landscapes in vegetated environments. Geomorphology 48, 309–328. https://doi.org/10.1016/S0169-555X(02)00187-3

Baas, A.C.W., Nield, J.M., 2010. Ecogeomorphic state variables and phase-space construction for quantifying the evolution of vegetated aeolian landscapes. Earth Surf. Process. Landforms 35, 717–731. https://doi.org/10.1002/esp.1990

Baas, a. C.W., Nield, J.M., 2007. Modelling vegetated dune landscapes. Geophys. Res. Lett. 34, L06405. https://doi.org/10.1029/2006GL029152

Bailey, S.D., Bristow, C.S., 2004. Migration of parabolic dunes at Aberffraw, Anglesey, north Wales. Geomorphology 59, 165–174. https://doi.org/10.1016/j.geomorph.2003.09.013

Bandeira, L., Marques, J.S., Saraiva, J., Pina, P., 2011. Automated detection of Martian dune fields. IEEE Geosci. Remote Sens. Lett. 8, 626–630. https://doi.org/10.1109/LGRS.2010.2098390

Barchyn, T.E., Hugenholtz, C.H., 2015. Predictability of dune activity in real dune fields under unidirectional wind regimes. J. Geophys. Res. Earth Surf. 120, 159–182. https://doi.org/10.1002/2014JF003248.Received

Barchyn, T.E., Hugenholtz, C.H., 2012a. Aeolian dune field geomorphology modulates the stabilization rate imposed by climate. J. Geophys. Res. Earth Surf. 117, 1–17. https://doi.org/10.1029/2011JF002274

Barchyn, T.E., Hugenholtz, C.H., 2012b. A new tool for modeling dune field evolution based on an accessible, GUI version of the Werner dune model. Geomorphology 138, 415–419. https://doi.org/10.1016/j.geomorph.2011.09.021

Barchyn, T.E., Hugenholtz, C.H., 2012. Aeolian dune field geomorphology modulates the stabilization rate imposed by climate. J. Geophys. Res. 117, 1–16. https://doi.org/10.1029/2011JF002274

Bishop, S.R., Momiji, H., Carretero-Gonz??lez, R., Warren, A., 2002. Modelling desert dune fields based on discrete dynamics. Discret. Dyn. Nat. Soc. 7, 7–17. https://doi.org/10.1080/10260220290013462

Breiman, L., 2001. Random forests. Mach. Learn. 45, 5–32. https://doi.org/10.1023/A:1010933404324

Brown, J.F., 1997. Effects of experimental burial on survival, growth and resource allocation of three species of dune plants. J. Ecol. 85, 151–158. https://doi.org/10.2307/2960647

Bullard, J.E., Thomas, D.S.G., Livingstone, I., Wiggs, G.F.S., 1995. Analysis of linear sand dune morphological variability , southwestem Kalahari Desert 11, 189–203.

Chadwick, H., Dalke, P., 1965. Plant Succession on Dune Sands in Fremont County, Idaho. Ecology 46, 766–780.

Duran, O., Herrmann, H.J., 2006. Vegetation against dune mobility 1–4.

Durán, O., Moore, L.J., 2013. Vegetation controls on the maximum size of coastal dunes. Proc. Natl.

Acad. Sci. 110, 17217–17222. https://doi.org/10.1073/pnas.1307580110

Eastwood, E., Nield, J., Baas, A., Kocurek, G., 2011. Modelling controls on aeolian dune-field pattern evolution. Sedimentology 58, 1391–1406. https://doi.org/10.1111/j.1365-3091.2010.01216.x

Ewing, R.C., Kocurek, G., 2010. Aeolian dune-field pattern boundary conditions. Geomorphology 114, 175–187. https://doi.org/10.1016/j.geomorph.2009.06.015

Fonstad, M.A., 2006. Cellular automata as analysis and synthesis engines at the geomorphology-ecology interface. Geomorphology 77, 217–234. https://doi.org/10.1016/j.geomorph.2006.01.006

Franklin, J., 1995. Predictive vegetation mapping: geographic modelling of biospatial patterns in relation to environmental gradients. Prog. Phys. Geogr. 19, 474–499. https://doi.org/10.1177/030913339501900403

Fryberger, S.G., Dean, gary, 1979. A study of Global Sand Seas.

Gaylord, D.R., Stetler, L.D., 1994. Aeolian-climatic thresholds and sand dunes at the Hanford site, south-central Washington, U.S.A. J. Arid Environ. 28, 95–116. https://doi.org/10.1016/S0140-1963(05)80041-2

Guisan, A., Theurillat, J.-P., 2000. Equilibrium modeling of alpine plant distribution: how far can we go? Phytocoenologia 30, 353–384. https://doi.org/10.1127/phyto/30/2000/353

Halfen, A.F., Johnson, W.C., 2013. A review of Great Plains dune field chronologies. Aeolian Res. 10, 135–160. https://doi.org/10.1016/j.aeolia.2013.03.001

Hatano, Y., Kanda, Y., Udo, K., Takewaka, S., Ueki, R., Hatano, N., Mouri, H., Chiba, M., Kurihara, K., Nishimura, H., 2004. A wind tunnel experiment of sand transport and its comparison with the Werner model. J. Geophys. Res. Surf. 109. https://doi.org/ARTN F01001\rDOI

10.1029/2002JF000015

Hugenholtz, C.H., Barchyn, T.E., 2010. Spatial analysis of sand dunes with a new global topographic dataset : new approaches and opportunities 992, 986–992. https://doi.org/10.1002/esp.2013

Hugenholtz, C.H., Levin, N., Barchyn, T.E., Baddock, M.C., 2012. Remote sensing and spatial analysis of aeolian sand dunes: A review and outlook. Earth-Science Rev. 111, 319–334. https://doi.org/10.1016/j.earscirev.2011.11.006

Hugenholtz, C.H., Wolfe, S. a., 2005. Recent stabilization of active sand dunes on the Canadian prairies and relation to recent climate variations. Geomorphology 68, 131–147. https://doi.org/10.1016/j.geomorph.2004.04.009

Hunter, R.E., Richmond, B.M., Alpha, T.R., 1983. Storm-controlled oblique dunes of the Oregon coast. GSA Bull. 94, 1450–1465.

Jimenez, J.A., Maia, L.P., Serra, J., Morais, J., 1999. Aeolian dune migration along the Cear?? coast, north-eastern Brazil. Sedimentology 46, 689–701. https://doi.org/10.1046/j.1365-3091.1999.00240.x

Kéfi, S., Rietkerk, M., Alados, C.L., Pueyo, Y., Papanastasis, V.P., ElAich, A., de Ruiter, P.C., Kefi, S., Rietkerk, M., Alados, C.L., Pueyo, Y., Papanastasis, V.P., ElAich, A., de Ruiter, P.C., 2007. Spatial vegetation patterns and imminent desertification in Mediterranean arid ecosystems. Nature 449, 213–7. https://doi.org/10.1038/nature06111

Kocurek, G., Ewing, R.C., 2005. Aeolian dune field self-organization – implications for the formation of simple versus complex dune-field patterns. Geomorphology 72, 94–105. https://doi.org/10.1016/j.geomorph.2005.05.005

Kuriyama, Y., Mochizuki, N., Nakashima, T., 2005. Influence of vegetation on aeolian sand transport rate from a backshore to a foredune at Hasaki, Japan. Sedimentology 52, 1123–1132.

https://doi.org/10.1111/j.1365-3091.2005.00734.x

Lancaster, N., 1988a. Development of linear dunes in the southwestern Kalahari, Southern Africa. J. Arid Environ. 14, 233–244. https://doi.org/10.1306/212f8927-2b24-11d7-8648000102c1865d

Lancaster, N., 1988b. Controls of eolian dune size and spacing. Geology 16, 972–975.

Lancaster, N., Baas, A., 1998. Influence of vegetation cover on sand transport by wind: field studies at Owens Lake, California. Earth Surf. Process. Landforms 23, 69–82. https://doi.org/10.1002/(SICI)1096-9837(199801)23:1<69::AID-ESP823>3.0.CO;2-G

Lancaster, N., Helm, P., 2000. A test of a climatic index of dune mobility using measurements from the southwestern United States. Earth Surf. Process. Landforms 25, 197–207. https://doi.org/10.1002/(SICI)1096-9837(200002)25:2<197::AID-ESP82>3.0.CO;2-H

Levin, N., Ben-Dor, E., Karnieli, A., 2004. Topographic information of sand dunes as extracted from shading effects using Landsat images. Remote Sens. Environ. 90, 190–209. https://doi.org/10.1016/j.rse.2003.12.008

Levin, N., Tsoar, H., Herrmann, H.J., Maia, L.P., Claudino-Sales, V., 2009. Modelling the formation of residual dune ridges behind barchan dunes in north-east Brazil. Sedimentology 56, 1623–1641. https://doi.org/10.1111/j.1365-3091.2009.01048.x

Li, S.L., Zuidema, P.A., Yu, F.H., Werger, M.J.A., Dong, M., 2010. Effects of denudation and burial on growth and reproduction of Artemisia ordosica in Mu Us sandland. Ecol. Res. 25, 655–661. https://doi.org/10.1007/s11284-010-0699-x

Livingstone, I., Wiggs, G.F.S., Weaver, C.M., 2007. Geomorphology of desert sand dunes: A review of recent progress. Earth-Science Rev. 80, 239–257. https://doi.org/10.1016/j.earscirev.2006.09.004

Lu, H., Miao, X., Zhou, Y., Mason, J., Swinheart, J., Zhang, J., Zhou, L., Yi, S., 2005. Late Quaternary aeolian activity in the Mu Us and Otindag dune fields (north China) and lagged response to insolation forcing. Geophys. Res. Lett. 32, 1–4. https://doi.org/10.1029/2005GL024560

Maestre, F.T., Cortina, J., 2005. Remnant shrubs in Mediterranean semi-arid steppes : effects of shrub size , abiotic factors and species identity on understorey richness and occurrence 27, 161–169. https://doi.org/10.1016/j.actao.2004.11.003

Mahowald, N., Jickells, T.D., Baker, A.R., Artaxo, P., Benitez-Nelson, C.R., Bergametti, G., Bond, T.C., Chen, Y., Cohen, D.D., Herut, B., Kubilay, N., Losno, R., Luo, C., Maenhaut, W., McGee, K.A., Okin, G.S., Siefert, R.L., Tsukuda, S., 2008. Global distribution of atmospheric phosphorus sources, concentrations and deposition rates, and anthropogenic impacts. Global Biogeochem. Cycles 22, 19 PP. https://doi.org/200810.1029/2008GB003240

Mason, J.A., Swinehart, J.B., Lu, H., Miao, X., Cha, P., Zhou, Y., 2008. Limited change in dune mobility in response to a large decrease in wind power in semi-arid northern China since the 1970s. Geomorphology 102, 351–363. https://doi.org/10.1016/j.geomorph.2008.04.004

Mason, J. a., Swinehart, J.B., Goble, R.J., Loope, D.B., 2004. Late-Holocene dune activity linked to hydrological drought, Nebraska Sand Hills, USA. The Holocene 14, 209–217. https://doi.org/10.1191/0959683604hl677rp

Maun, M.A., 1998. Adaptations of plants to burial in coastal sand dunes. Can. J. Bot. 76, 713–738. https://doi.org/10.1139/b98-058

Miao, X., Mason, J.A., Swinehart, J.B., Loope, D.B., Hanson, P.R., Goble, R.J., Liu, X., 2007. A 10,000 year record of dune activity, dust storms, and severe drought in the central Great Plains. Geology 35, 119–122. https://doi.org/10.1130/G23133A.1

Miller, J., Franklin, J., 2002. Modeling the distribution of four vegetation alliances using generalized

linear models and classification trees with spatial dependence. Ecol. Modell. 157, 227–247.

Mitasova, H., Overton, M., Harmon, R.S., 2005. Geospatial analysis of a coastal sand dune field evolution: Jockey's Ridge, North Carolina. Geomorphology 72, 204–221. https://doi.org/10.1016/j.geomorph.2005.06.001

Moore, P.D., 1996. Mystery of moribund marram. Nature 380, 285–286. https://doi.org/10.1038/nmat1434

Mountrakis, G., Im, J., Ogole, C., 2011. Support vector machines in remote sensing: A review. ISPRS J. Photogramm. Remote Sens. 66, 247–259. https://doi.org/10.1016/j.isprsjprs.2010.11.001

Muhs, D., Muhs, D., Holliday, V.T., Holliday, V.T., 1995. Evidence of active dune sand on the great plains in teh 19th entury from accounts of early explorers.pdf. Quat. Res.

Muhs, D.R., Maat, P.B., 1993. the Potential Response of Eolian Sand To Greenhouse Warming and Precipitation Reduction on the Great Plains of the Usa.Pdf. J. Arid Environ.

Muhs S. A. Wolfe, D.R., 1999. Sand dunes of the northern Great Plains of Canada and the United States. Geol. Surv. Canada 534, 183–197.

Murray, a. B., Lazarus, E., Ashton, A., Baas, A., Coco, G., Coulthard, T., Fonstad, M., Haff, P., McNamara, D., Paola, C., Pelletier, J., Reinhardt, L., 2009. Geomorphology, complexity, and the emerging science of the Earth's surface. Geomorphology 103, 496–505. https://doi.org/10.1016/j.geomorph.2008.08.013

Narteau, C., Zhang, D., Rozier, O., Claudin, P., 2009. Setting the length and time scales of a cellular automaton dune model from the analysis of superimposed bed forms. J. Geophys. Res. 114, F03006. https://doi.org/10.1029/2008JF001127

Nield, J.M., Baas, A.C.W., 2007. Investigating parabolic and nebkha dune formation using a cellular

automaton modelling approach. Earth Surf. Process. Landforms. https://doi.org/10.1002/esp

Parker Gay, S., 1999. Observations regarding the movement of barchan sand dunes in the Nazca to Tanaca area of southern Peru. Geomorphology 27, 279–293. https://doi.org/10.1016/S0169-555X(98)00084-1

Pelletier, J., Mitasova, H., Harmon, R., Overton, M., 2009. The effects of interdune vegetation changes on eolian dune field evolution: a numerical- modeling case study at Jockey's Ridge, North Carolina, USA. Earth Surf. Process. Landforms 34, 1245–1254. https://doi.org/10.1002/esp

Pelletier, J.D., 2009. Controls on the height and spacing of eolian ripples and transverse dunes: A numerical modeling investigation. Geomorphology 105, 322–333. https://doi.org/10.1016/j.geomorph.2008.10.010

Pinker, R.T., Karnieli, A., 1995. Characteristic spectral reflectance of a semi-arid environment. Int. J. Remote Sens. 16, 1341–1363. https://doi.org/10.1080/01431169508954480

Prasad, A.M., Iverson, L.R., Liaw, A., 2006. Newer classification and regression tree techniques: Bagging and random forests for ecological prediction. Ecosystems 9, 181–199. https://doi.org/10.1007/s10021-005-0054-1

Qian, W., Quan, L., Shi, S., 2002. Variations of the Dust Storm in China and its Climatic Control. J. Clim. 15, 1216–1229.

Qu, H., Zhao, H., Zhou, R., 2014. Effects of sand burial on dune plants : a review. Sci. Cold Arid Reg. 6, 201–208. https://doi.org/10.3724/SP.J.1226.2014.00201.Effects

Reynolds, J.F., Virginia, R.A., Kemp, P.R., de Soyza, A.G., Tremmel, D.C., 1999. Impact of Drought on Desert Shrubs: Effects of Seasonality and Degree of Resource Island Development. Ecol. Monogr. 69, 69–106. https://doi.org/10.1890/0012-9615(1999)069[0069:IODODS]2.0.CO;2

Rodriguez-Galiano, V.F., Ghimire, B., Rogan, J., Chica-Olmo, M., Rigol-Sanchez, J.P., 2012. An assessment of the effectiveness of a random forest classifier for land-cover classification. ISPRS J. Photogramm. Remote Sens. 67, 93–104. https://doi.org/10.1016/j.isprsjprs.2011.11.002

Runnström, M.C., 2003. Rangeland development of the Mu Us Sandy Land in semiarid China: An analysis using landsat and NOAA remote sensing data. L. Degrad. Dev. 14, 189–202. https://doi.org/10.1002/ldr.545

Schenk, H.J., 1999. Clonal splitting in desert shrubs. Plant Ecol. 141, 41–52. https://doi.org/10.1023/A:1009895603783

Stout, J.E., Lee, J.A., 2003. Indirect evidence of wind erosion trends on the Southern High Plains of North America. J. Arid Environ. 55, 43–61. https://doi.org/10.1016/S0140-1963(02)00266-5

Strobl, C., Boulesteix, A.-L., Kneib, T., Augustin, T., Zeileis, A., 2008. Conditional Variable Importance for Random Forests. BMC Bioinformatics 9, 307. https://doi.org/10.1186/1471-2105-9-307

Szuster, B.W., Chen, Q., Borger, M., 2011. A comparison of classification techniques to support land cover and land use analysis in tropical coastal zones. Appl. Geogr. 31, 525–532. https://doi.org/10.1016/j.apgeog.2010.11.007

Thomas, D.S.G., Knight, M., Wiggs, G.F.S., 2005. Remobilization of southern African desert dune systems by twenty-first century global warming. Nature 435, 1218–21. https://doi.org/10.1038/nature03717

Thomas, D.S.G., Leason, H.C., 2005. Dunefield activity response to climate variability in the southwest Kalahari. Geomorphology 64, 117–132. https://doi.org/10.1016/j.geomorph.2004.06.004

Thornthwaite, C.W., 1948. An approach toward a rational classification of climate. Geogr. Rev. 38,

55–94.

Tsoar, H., 2005. Sand dune mobility and stability in relation to climate. Physica A 357, 50–56.

Tsoar, H., Blumberg, D.G., 2002. Formation of parabolic dunes from barchan and transverse dunes along Israel's Mediterranean coast. Earth Surf. Process. Landforms 27, 1147–1161. https://doi.org/10.1002/esp.417

Van der Stoel, C.D., Van der Putten, W.H., Duyts, H., 2002. Development of a negative plant-soil feedback in the expansion zone of the clonal grass Ammophila arenaria following root formation and nematode colonization. J. Ecol. 90, 978–988. https://doi.org/10.1046/j.1365-2745.2002.00727.x

Vandewalle, N., Galam, S., 1999. Ripples versus giant dunes in a saltation-avalanche model. Int. J. Mod. Phys. C 10, 1071–1076. https://doi.org/10.1142/S0129183199000875

Wang, H., Yang, F., Luo, Z., 2016. An experimental study of the intrinsic stability of random forest variable importance measures. BMC Bioinformatics 1–18. https://doi.org/10.1186/s12859-016-0900-5

Wang, X., Chen, F.-H., Dong, Z., Xia, D., 2005. Evolution of the Southern Mu Us Desert in North China Activity and Climate Parameters. L. Degrad. Dev. 16, 351–366. https://doi.org/DOI: 10.1002/ldr.663

Wang, X., Zhou, Z., Dong, Z., 2006. Control of dust emissions by geomorphic conditions, wind environments and land use in northern China: An examination based on dust storm frequency from 1960 to 2003. Geomorphology 81, 292–308. https://doi.org/10.1016/j.geomorph.2006.04.015

Wasson, R.J., Hyde, R., 1983. Factors determining desert dune type.

Werner, B.T., 1995. Eolian dunes: Computer simulations and attractor interpretation. Geology 23, 1107. https://doi.org/10.1130/0091-7613(1995)023<1107:EDCSAA>2.3.CO;2

Werner, B.T., Kocurek, G., 1999. Bedform spacing from defect dynamics. https://doi.org/10.1130/0091-7613(1999)027<0727

Wiesmeier, M., Barthold, F., Blank, B., Kögel-Knabner, I., 2011. Digital mapping of soil organic matter stocks using Random Forest modeling in a semi-arid steppe ecosystem. Plant Soil 340, 7–24. https://doi.org/10.1007/s11104-010-0425-z

Wiggs, G.F.S., Livingstone, I., Thomas, D.S.G., Bullard, J.E.C.N.-253, 1994. The effect of vegetation removal on airflow structure and dune mobility in the southwest Kalahari. L. Degrad. Rehabil. 5, 13–24 ST–The effect of vegetation removal on ai.

Wilson, I.G., 1972. Aeolian Bedforms: Their Development and Origins. Sedimentology 19, 173–210. https://doi.org/10.1111/j.1365-3091.1972.tb00020.x

Wolfe, S. a., Nickling, W.G., 1993. The protective role of sparse vegetation in wind erosion. Prog. Phys. Geogr. 17, 50–68. https://doi.org/10.1177/030913339301700104

Wu, B., Ci, L.J., 2002. Landscape change and desertification development in the Mu Us Sandland, Northern China. J. Arid Environ. 50, 429–444. https://doi.org/10.1006/jare.2001.0847

Xu, Z., Mason, J. a., Lu, H., 2015. Vegetated dune morphodynamics during recent stabilization of the Mu Us dune field, north-central China. Geomorphology 228, 486–503. https://doi.org/10.1016/j.geomorph.2014.10.001

Yao, Z.Y., Wang, T., Han, Z.W., Zhang, W.M., Zhao, A.G., 2007. Migration of sand dunes on the northern Alxa Plateau, Inner Mongolia, China. J. Arid Environ. 70, 80–93. https://doi.org/10.1016/j.jaridenv.2006.12.012

Yizhaq, H., Ashkenazy, Y., Tsoar, H., 2009. Sand dune dynamics and climate change: A modeling approach. J. Geophys. Res. 114, 1–11. https://doi.org/10.1029/2008JF001138

Yizhaq, H., Ashkenazy, Y., Tsoar, H., 2007. Why Do Active and Stabilized Dunes Coexist under the Same Climatic Conditions? Phys. Rev. Lett. 98, 188001. https://doi.org/10.1103/PhysRevLett.98.188001

Zarnetske, P.L., Hacker, S.D., Seabloom, E.W., Ruggiero, P., Jason, R., Maddux, T.B., Cox, D., Zarnetske, L., 2012. Biophysical feedback mediates effects of invasive grasses on coastal dune shape. Ecol. Soc. Am. Biophys. 93, 1439–1450.

Zhang, J., Zhang, Y., Fan, D., Qin, S., Jia, X., Wu, B., Chen, D., Gao, H., Zhu, L., 2015. Effects of sand dune stabilization on the spatial pattern of artemisia ordosica population in Mu Us desert, Northwest China. PLoS One 10, 1–14. https://doi.org/10.1371/journal.pone.0129728